

5-2017

MATHEMATICAL MODELING REVEALS THAT G2/M CHECKPOINT OVERRIDE CREATES A THERAPEUTIC VULNERABILITY IN TSC2-NULL TUMORS

Hui Ju Hsieh

Follow this and additional works at: https://digitalcommons.library.tmc.edu/utgsbs_dissertations



Part of the [Medicine and Health Sciences Commons](#)

Recommended Citation

Hsieh, Hui Ju, "MATHEMATICAL MODELING REVEALS THAT G2/M CHECKPOINT OVERRIDE CREATES A THERAPEUTIC VULNERABILITY IN TSC2-NULL TUMORS" (2017). *The University of Texas MD Anderson Cancer Center UTHealth Graduate School of Biomedical Sciences Dissertations and Theses (Open Access)*. 808.

https://digitalcommons.library.tmc.edu/utgsbs_dissertations/808

This Dissertation (PhD) is brought to you for free and open access by the The University of Texas MD Anderson Cancer Center UTHealth Graduate School of Biomedical Sciences at DigitalCommons@TMC. It has been accepted for inclusion in The University of Texas MD Anderson Cancer Center UTHealth Graduate School of Biomedical Sciences Dissertations and Theses (Open Access) by an authorized administrator of DigitalCommons@TMC. For more information, please contact digitalcommons@library.tmc.edu.

**MATHEMATICAL MODELING REVEALS THAT G2/M CHECKPOINT OVERRIDE
CREATES A THERAPEUTIC VULNERABILITY IN TSC2-NULL TUMORS**

by

Hui-Ju Hsieh, M.D.

APPROVED:

Guang Peng, M.D., Ph.D., Supervisor

Xiongbín Lu, Ph.D.

Shiaw-Yih Lin, Ph.D.

Dos Sarbassov, Ph.D.

Kenneth Y. Tsai, M.D., Ph.D.

APPROVED:

Dean, The University of Texas

MD Anderson Cancer Center UTHHealth Graduate School of Biomedical Sciences

**MATHEMATICAL MODELING REVEALS THAT G2/M CHECKPOINT OVERRIDE
CREATES A THERAPEUTIC VULNERABILITY IN TSC2-NULL TUMORS**

A

DISSERTATION

Presented to the Faculty of

The University of Texas

MD Anderson Cancer Center UTHealth

Graduate School of Biomedical Sciences

In Partial Fulfillment of the Requirements

For the Degree of

DOCTOR OF PHILOSOPHY

by

Hui-Ju Hsieh, M.D.

Houston, Texas

May, 2017

DEDICATION

This Ph.D. dissertation is dedicated to

my families, friends, and mentors

who give me help, support and love

ABSTRACT

Cell cycle checkpoints determine whether cells meet requirements to progress through the next stage. In response to DNA damage, how cells activate checkpoints have been well studied, but little is known about checkpoint deactivation (recovery), which directly impacts on cell fate. In tumor cells, the signaling network has been rewired due to epigenetic and genetic alterations, which result in resistance to the cell cycle control, and thus resistance to chemotherapy or radiation therapy. Therefore, it is critical to identify molecules required for checkpoint recovery or adaptation after DNA damage.

To achieve this goal, we performed a multidisciplinary study combining reverse phase protein array (RPPA) data, molecular biology and mathematical modeling to systematically identify molecules required for DNA damage checkpoint recovery. The mTOR complex 1 (mTORC1) plays an essential role to regulate mitotic entry after irradiation. Inhibition of the mTOR pathway delayed G2/M checkpoint recovery, while TSC2-null cells with hyperactivity of mTORC1 exhibited the opposite results. Furthermore, our mechanistic study revealed that mTOR signaling pathway controls a transcriptional program of mitotic entry through regulating histone lysine demethylase KDM4B, which is required for the epigenetic regulation of key mitosis-related genes including *CCNB1* and *PLK1*.

Given accelerated G2/M checkpoint recovery in TSC2-null cells with mTORC1 hyperactivity, we postulated that further abrogation of the G2/M checkpoint may facilitate mitotic catastrophe and selectively kill cells. As we expected, TSC2-null cells

were more sensitive to the WEE1 inhibitor, a negative regulator of mitotic entry, compared to wild-type cells.

In summary, we reported a novel mechanism of the mTORC1 signaling in regulating a transcriptional program required for G2/M checkpoint recovery after DNA damage. This mechanism provided a therapeutic strategy for TSC patients with mTORC1 hyperactivity using the WEE1 inhibitor, which has a potential to be translated into clinical trials.

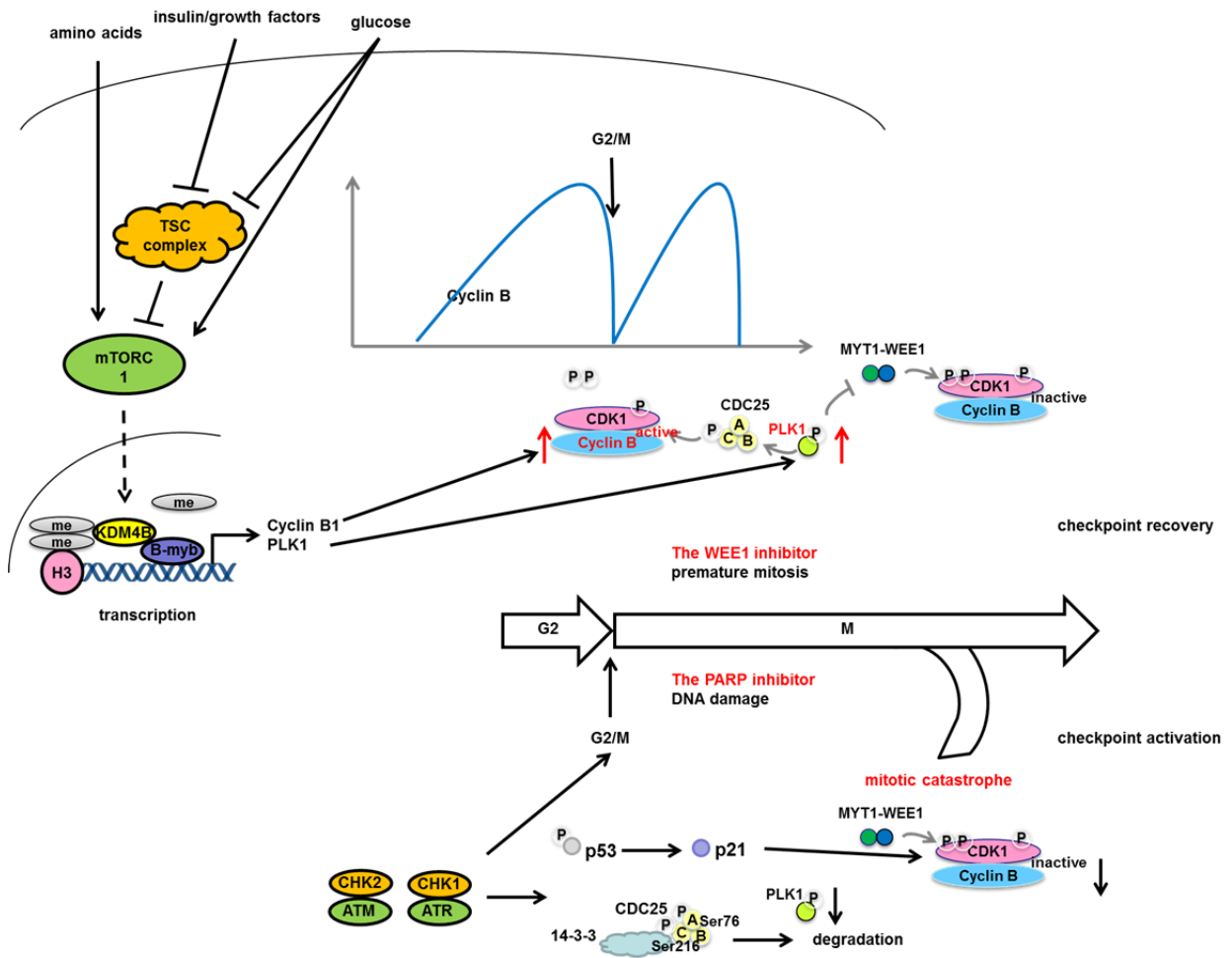


TABLE OF CONTENTS

Approval Form	I
Title Page	II
Dedication	III
Abstract	IV
Table of Contents	VI
List of Abbreviations	XI
List of Figures	XIV
List of Tables	XVII
CHAPTER 1: Introduction	1
1.1 The PIKK family	1
1.2 mTOR and the molecular composition of mTOR complexes	4
1.2.1 The signaling pathways of mTORC1	5
1.2.2 The summary of mTOR inhibitors	8
1.3 Cell cycle regulation	9
1.4 DNA damage checkpoints: activation, recovery and adaptation	12
1.4.1 Activation	12
1.4.2 Recovery	16
1.4.3 Adaptation	17
1.5 Mitotic catastrophe as a mechanism to maintain genomic stability	18
1.6 Drugs related to DNA damage response	20
1.6.1 PARP inhibitors	20

1.6.2 WEE1 inhibitors	21
SIGNIFICANCE OF THE STUDY	22
CHAPTER 2: Materials and Methods	23
2.1 Cell lines and culture	23
2.2 Ionizing radiation	24
2.3 Antibodies, plasmids and reagents	24
2.4 Cell viability, cell proliferation assay, apoptosis assay and 3D culture	25
2.5 Cell cycle analysis and mitotic entry by flow cytometry	26
2.6 Western blotting	27
2.7 Immunofluorescence staining	27
2.8 Single-cell gel electrophoresis (comet assay)	28
2.9 RNA isolation and qRT-PCR	28
2.10 Chromatin immunoprecipitation (ChIP)-qPCR assay	30
2.11 Dual-luciferase reporter assay	31
2.12 Reverse phase protein array (RPPA)	31
2.13 Animal studies	32
2.14 Statistics	35
CHAPTER 3: The Role of mTORC1 in Checkpoint Recovery	36
3.1 mTOR is the candidate to mediate DNA damage checkpoint recovery	36
3.2 mTOR regulates mitotic entry during recovery from IR-induced G2 arrest	45
3.3 The mTORC1 kinase activity is required for mitotic entry after irradiation	50
3.4 mTORC1 functions as positive transcription regulator of <i>CCNB1</i> and <i>PLK1</i>	57
3.5 mTOR controls transcription of <i>CCNB1</i> and <i>PLK1</i> through KDM4B	62
3.6 The high mTOR kinase activity in TSC2-depleted cells promotes recovery	74

from irradiation-induced G2 arrest	
3.7 WEE1 inhibition is a therapeutic strategy for tuberous sclerosis complex	79
CHAPTER 4: Discussion, Conclusions and Perspectives	92
BIBLIOGRAPHY	101
VITA	107

LIST OF ABBREVIATIONS

4EBPx	eukaryotic translation initiation factor 4E-binding protein x
53BP1	P53-binding protein 1
5'-UTR	5'-untranslated region
9-1-1	RAD9-RAD1-HUS1
AAs	amino acids
AMPK	AMP-dependent kinase
APC	anaphase-promoting complex
ATG13	autophagy related 13
ATM	ataxia telangiectasia mutated
ATR	ATM and Rad3-related
ATRIP	ATR interacting protein
BSA	bovine serum albumin
BUB	budding uninhibited by benzimidazole
BUBR1	BUB-related protein kinase 1
CDCx	cell-division cycle protein x
CDKx	cyclin-dependent kinase x
ChIP	chromatin immunoprecipitation
DAPI	4',6-diamidino-2-phenylindole
DDR	DNA damage response
DEPTOR	Dep-domain mTOR interacting protein
DMEM	Dulbecco's modified Eagle's medium

DMSO	dimethyl sulfoxide
DNA	
ssDNA	single-stranded DNA
dsDNA	double-stranded DNA
DNA2	helicase/nuclease
DNA-PKcs	DNA protein kinase catalytic subunit
DSB(s)	double strand break(s)
ECL	enhanced chemiluminescence
EDTA	ethylenediaminetetraacetic acid
eIF4E/G	eukaryotic translation initiation factor 4E/G
FAD	flavin adenine dinucleotide
FBS	fetal bovine serum
FDA	Food and Drug Administration
FKBP12	FK506 binding protein 12
FOXM1	forkhead box M1
FRB	FKBP12-rapamycin binding
GAP	GTPase-activating protein
GFP	green fluorescent protein
H3Kx	histone H3 lysine x
HCl	hydrochloric acid
HEPES	N-2-hydroxyethylpiperazine-N'-2-ethanesulfonic acid
HR	homologous recombination
HRP	horseradish peroxidase
IGF	insulin-like growth factor

IGG	immunoglobulin G
IP	immunoprecipitation
IR	ionizing radiation
JmjC	Jumonji C
JMJD	Jumonji C domain demethylase
KCl	potassium chloride
KDMx	lysine (K) demethylase x
LSD	lysine-specific demethylase
MCC	mitotic checkpoint complex
MCMx	minichromosome maintenance complex component x
MDM2	mouse double minute 2
MEF	mouse embryonic fibroblast
MEM	minimum essential medium
MgCl ₂	magnesium chloride
mLST8	mammalian lethal with sec-13 protein 8
MRN	MRE11-RAD50-NBS1
MRE11	meiotic recombination 11
NBS1	Nijmegen breakage syndrome 1
mSIN1	mammalian stress-activated protein kinase interacting protein
mTOR	mammalian/mechanistic target of rapamycin
mTORC1/2	mTOR complex 1/2
MTT	3-(4,5-dimethylthiazol-2-yl)-2,5-diphenyltetrazolium bromide
MYT1	myelin transcription factor 1
PBS	phosphate-buffered saline

PI	propidium iodide
PI3K	phosphoinositide 3-kinase/phosphatidylinositide 3 kinase
PIKK	PI3K-related kinase
PKB	protein kinase B
PKC	protein kinase C
PLK1	polo-like kinase 1
PP2A	protein phosphatase 2A
PRAS40	proline-rich AKT/PKB substrate 49kDa
PROTOR1	protein observed with RICTOR 1
qPCR	quantitative polymerase chain reaction
qRT-PCR	quantitative reverse transcription polymerase chain reaction
RAG	RAS-related GTP-binding protein
RAPTOR	regulatory-associated protein of mTOR
RB	retinoblastoma protein
RHEB	RAS homolog enriched in brain
RICTOR	rapamycin-insensitive companion of mTOR
RPA32	replication protein A 32
RPMI-1640	Roswell Park Memorial Institute-1640
S6K	ribosomal protein S6 kinase
SAC	spindle assembly checkpoint
SCF	Skp1/Cullin/F-box protein
SDS-PAGE	sodium dodecyl sulfate polyacrylamide gel electrophoresis
SSB(s)	single strand break(s)
TBC1D7	TBC1 domain family member 7

TOPBP1	topoisomerase II β binding protein 1
TRRAP	transformation/transcription associated protein
TSC	tuberous sclerosis complex
TSC1	tuberous sclerosis complex 1, hamartin
TSC2	tuberous sclerosis complex 2, tuberin
ULK1	unc-51 like autophagy activating kinase 1
WIP1	wild-type P53-induced phosphatase 1

LIST OF FIGURES

Figure 1 The domain structure of PIKKs	3
Figure 2 The signaling pathways related to mTORC1	6
Figure 3 The cell cycle transition	13
Figure 4 The Ford-Fulkerson algorithm and breadth-first search in MATLAB	33
Figure 5 The flow chart for the main program written in MATLAB	34
Figure 6 The flow chart for RPPA data analysis	39
Figure 7 The first step for RPPA data analysis-cell cycle alignment	40
Figure 8 The second step for RPPA data analysis-linear regression and correlation	41
Figure 9 Top ten canonical pathways identified from IPA	43
Figure 10 The final step for RPPA data analysis-the IPA network and the Ford-Fulkerson algorithm	44
Figure 11 mTOR regulated G2/M checkpoint recovery-cell cycle analysis	46
Figure 12 mTOR regulated G2/M checkpoint recovery-mitotic entry analysis	47
Figure 13 mTOR regulated G2/M checkpoint recovery-western blot	48
Figure 14 The function of mTOR in G2/M checkpoint recovery is not cell-type specific	49
Figure 15 The mTOR activity is required for recovery from IR-induced G2 arrest	52
Figure 16 The structure and the test of mTOR conditional knock-in cell line	53
Figure 17 The mTOR kinase activity is required for the recovery from IR-induced G2 arrest	54

Figure 18 The mTORC1 kinase activity is required for the recovery from IR-induced G2 arrest	55
Figure 19 The amino acid withdrawal experiment confirmed that mTORC1 is required for G2/M checkpoint recovery	56
Figure 20 The mTOR expression level was associated with <i>CCNB1</i> and <i>PLK1</i> transcription	58
Figure 21 The Raptor expression level was associated with <i>CCNB1</i> and <i>PLK1</i> transcription	59
Figure 22 The dual luciferase assay showed the requirement of mTOR in <i>CCNB1</i> and <i>PLK1</i> transcription regulation.	60
Figure 23 The dual luciferase assay confirmed the function of mTOR in <i>CCNB1</i> and <i>PLK1</i> transcription regulation through mTOR over-expression.	61
Figure 24 KDM4B linked mTOR to Cyclin B expression	64
Figure 25 Regulation of KDM4B expression by mTOR was not U2OS cell-specific	65
Figure 26 KDM4B expression was not affected by the AKT inhibitor	66
Figure 27 KDM4B was required for mitotic entry after irradiation	67
Figure 28 KDM4B was associated with <i>CCNB1</i> gene	68
Figure 29 KDM4B links mTORC1 to transcriptional control of <i>CCNB1</i>	69
Figure 30 Regulation of KDM4B expression by mTOR was probably through proteasome degradation	70
Figure 31 mTOR depletion did not affect IR-induced DNA breaks and repairs	71
Figure 32 mTOR depletion did not affect IR-induced DNA damage response	72
Figure 33 ATM depletion did not change expression of mitosis-related proteins	73
Figure 34 TSC2 depletion facilitates G2/M checkpoint recovery-mitotic entry	75

analysis

Figure 35 TSC2 depletion facilitates G2/M checkpoint recovery-western blot	76
Figure 36 The change of KDM4B expression was mainly in nuclei	77
Figure 37 TSC2 depletion promotes mitotic entry after IR-induced G2 arrest	78
Figure 38 TSC2-null cells were more sensitive to the WEE1 inhibitor-MTT assay	81
Figure 39 TSC2-null cells were more sensitive to the WEE1 inhibitor-3D culture	82
Figure 40 TSC2-null cells with WEE1 inhibition showed faster cell cycle progression into mitosis	83
Figure 41 Prolonged WEE1 inhibition induced persistent DNA damage in TSC2-null cells	84
Figure 42 TSC2-null cells were more sensitive to the WEE1 inhibitor combined with the PARP inhibitor BMN 673-MTT assay	85
Figure 43 TSC2-null cells were more sensitive to the WEE1 inhibitor combined with the PARP inhibitor BMN 673-apoptosis assay	86
Figure 44 TSC2-null cells were more sensitive to the WEE1 inhibitor combined with the PARP inhibitor BMN 673-Cytochrome c staining	87
Figure 45 TSC2-null cells were more sensitive to the WEE1 inhibitor combined with the PARP inhibitor olaparib-apoptosis assay	88
Figure 46 The WEE1 inhibitor MK1775 combined with the PARP inhibitor BMN 673 induced stronger mitotic catastrophe in TSC2-null cells	89
Figure 47 The combination effect was relatively similar in rapamycin-sensitive and rapamycin-resistant TSC2-null cells	90
Figure 48 TSC2-null tumors were more sensitive to the WEE1 inhibitor <i>in vivo</i>	91
Figure 49 The summary of the study	100

LIST OF TABLES

Table 1 Oligonucleotides used for qPCR and ChIP-qPCR	29
Table 2: Top two network functions and their molecules identified from IPA	42

CHAPTER 1

Introduction

The mechanistic (or mammalian) target of rapamycin (mTOR) has been studied for decades as a serine/threonine kinase with multiple functions. As part of the mTORC1 and mTORC2 complexes, mTOR serves as a central regulator of cell metabolism, cell growth, proliferation and survival in response to nutrients, growth factors, energy levels and cellular stress (1). Recent studies provide insights into the role of mTOR in signaling pathways involved in human diseases, stimulating interest in mTOR as the target for disease treatment (2). In this study, a multidisciplinary approach identified that the mTOR signaling network is associated with checkpoint recovery after DNA damage which affects genomic instability, the major cause of many diseases, including cancer. The link between nutritional status and genome integrity may provide a comprehensive approach to biomedical science and clinical applications.

1.1 The PIKK family

mTOR belongs to the phosphatidylinositol 3-kinase (PI3K)-related kinase (PIKK) family, which also comprises DNA protein kinase catalytic subunit (DNA-PKcs), ataxia telangiectasia mutated (ATM), ATM and Rad3-related (ATR), suppressor of morphogenesis in genitalia (SMG1), and transformation/transcription associated protein (TRRAP) (3-5). The functions of PIKK family include DNA damage response (DDR),

nutrient-dependent signaling, nonsense-mediated mRNA decay and transcription. They share sequence similarity in the FRAP-ATM-TRRAP (FAT) domain, the PIKK domain and the FAT C-terminal (FATC) domain in their C terminus. The region for protein-protein interactions in the N terminus is poorly conserved, which controls the protein activity and causes functional diversity (Fig. 1). The activity of DNK-PKcs in DNA double strands breaks (DSBs) is regulated by KU70/80. ATM is also involved in the cellular response to DSBs with the help of the MRE11-RAD50-NBS1 (MRN) complex. ATR is activated by ATR-interacting protein (ATRIP), topoisomerase II β binding protein 1 (TOPBP1), and Claspin at ssDNA sites, such as resected DSBs and stalled replication forks, and ATR is associated with ssDNA damage repair and replication origin firing. The functions of mTOR mainly rely on interactions with many proteins to form different complexes (4, 6). Although PIKK family members interact with their own partners, the members still have the possibility to collaborate with each other in response to common environmental cues.

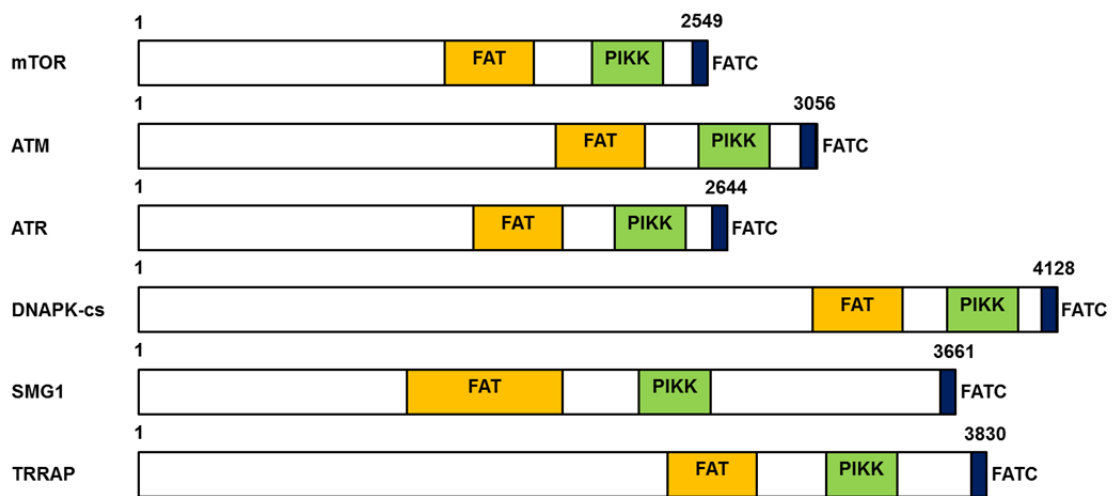


Figure 1 The domain structure of PIKKs

The diagram only shows the locations of the FRAP-ATM-TRRAP (FAT) domain, the PI3K-related kinase (PIKK) domain, and the FAT C-terminal domain (FATC) in PIKK family members, which share sequence similarity within these three domains.

1.2 mTOR and the molecular composition of mTOR complexes

mTOR forms at least two protein complexes called mTOR complex 1 (mTORC1) and mTOR complex 2 (mTORC2). mTORC1 and mTORC2 share three components including mTOR, mammalian lethal with Sec13 protein 8 (mLST8) and DEP-domain-containing mTOR-interacting protein (DEPTOR). The kinase activity of mTOR is enhanced by mLST8 which directly stabilizes the active site of mTOR (7) and is negatively regulated by DEPTOR (8). The complex mTORC1 also contains regulatory-associated protein of mTOR (Raptor) and another inhibitory regulator proline-rich AKT substrate 40 kDa (PRAS40) (9-10). mTORC2 comprises rapamycin-insensitive companion of mTOR (Rictor), mammalian stress-activated protein kinase interacting protein (mSIN1) and protein observed with Rictor1 (PROTOR1) (1). Different compositions of both complexes affect their activation and function. In general, mTORC1 regulates cell growth in response of growth factor, nutrients, and stress through downstream effectors ribosomal protein S6 kinase (S6K) and eukaryotic translation initiation factor 4E-binding protein 1 (4E-BP1). mTORC2 controls cytoskeleton rearrangement, cell proliferation and survival by phosphorylating and activating AKT (known as protein kinase B, PKB), protein kinase C (PKC) and serum/glucocorticoid regulated kinase 1 (SGK1) (11-12). Although mTORC1 and mTORC2 have their downstream targets, crosstalk exists between two complexes. mTORC1 inhibits mTORC2 through S6K-mediated phosphorylation of Rictor at Thr1135 and inhibition of S6K causes an increase of AKT phosphorylation at Ser473 by mTORC2 (13); mTORC2 activates mTORC1 through AKT activation (14). It is difficult to completely separate the connections between two complexes but in this study the focus is still on mTORC1.

1.2.1 The signaling pathways of mTORC1

The activation of mTORC1 is in response to different upstream cues through different pathways (Fig. 2). Insulin/growth factors activate mTORC1 via the PI3K/AKT pathway and the mitogen-activated protein kinases (MAPK) pathway. Both pathways control the upstream negative regulator of mTORC1, a trimeric complex (in this thesis, the term “the TSC complex” will be used) composing of tuberous sclerosis complex 1 (TSC1, hamartin), TSC2 (tuberin), and TBC1 domain family member 7 (TBC1D7) (15). AKT and MAPK phosphorylate TSC2 and inhibit the function of TSC2 as a GTPase-activating protein (GAP), thus inhibiting GTP hydrolysis and promoting GTP-bound RAS homolog enriched in brain (RHEB) GTPase to activate mTORC1 (16). AKT also phosphorylates PRAS40, resulting in PRAS40 dissociation from mTORC1 and mTORC1 activation (17).

Amino acids (AAs), particularly leucine and arginine, are crucial for mTORC1 activation. Even with sufficient growth factors, amino acids withdrawal still inhibits mTORC1 signaling. AAs activate mTORC1 through another GTPase called the RAS-related GTP-binding protein (Rag) family of GTPase, a heterodimer of RAGA/RAGB with RAGC/RAGD. With accumulation of amino acids in the lysosomal lumen, the Ragulator complex anchors the Rag GTPase to the lysosome and activates the Rag GTPase (RAGA/RAGB^{GTP}-RAGC/RAGD^{GDP}). The activated GTPase then recruits mTORC1 to the lysosome through direct interaction with Raptor (18-19). Meanwhile, AKT-mediated dissociation of the TSC complex from the lysosomal surface places activated RHEB^{GTP} and mTORC1 in the close proximity at the lysosome for mTORC1 activation (20-21).

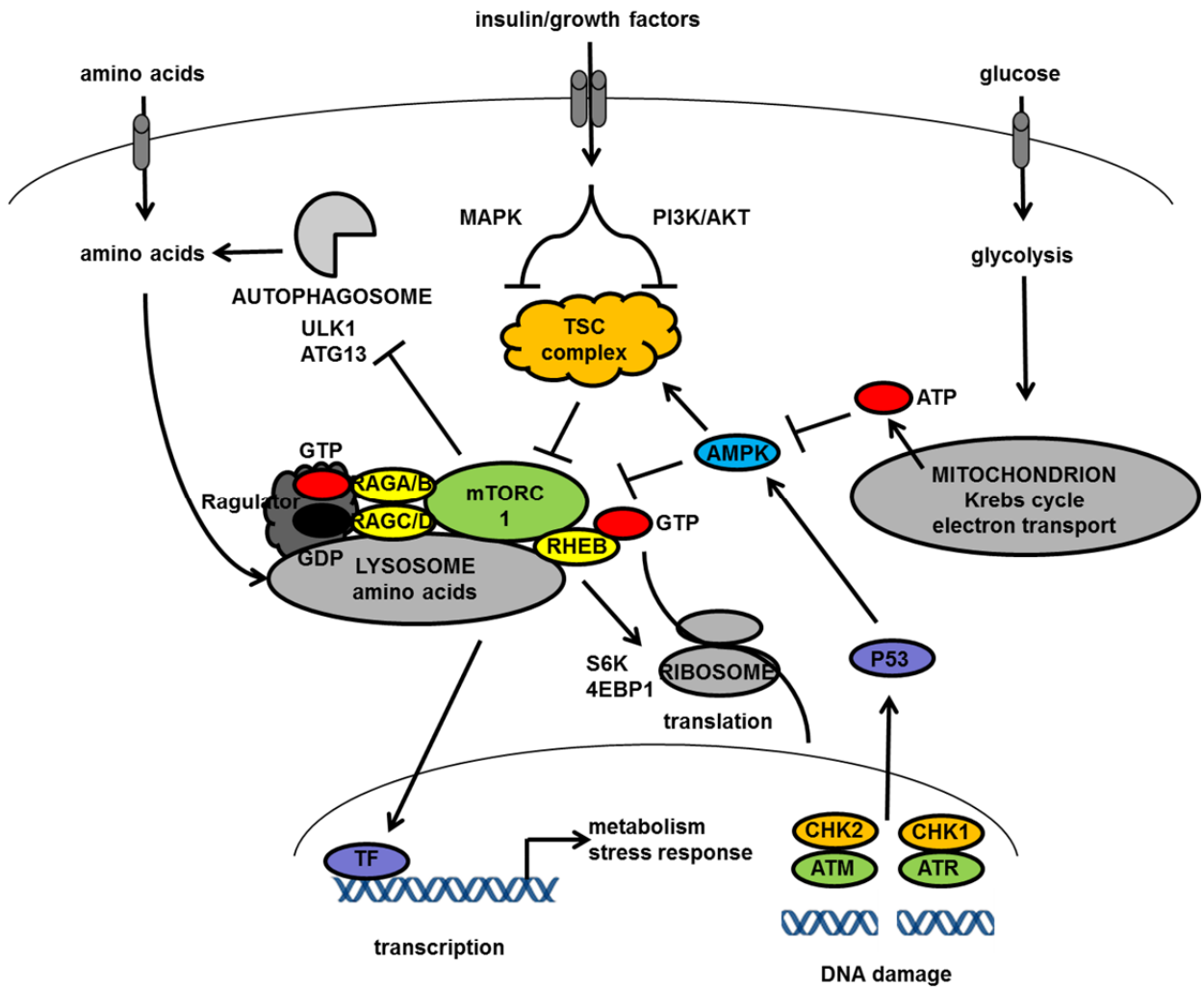


Figure 2 The signaling pathways related to mTORC1

The diagram briefly shows how mTORC1 responds to upstream cues through different pathways. TF: transcription factor

Different types of stress can negatively regulate mTORC1 activity. Cellular respiration, including glycolysis, Krebs circle and electron transport, is the process to generate ATP from glucose. When cellular ATP levels drop due to nutrient deprivation, AMP-activated kinase (AMPK) senses the increased ratios of AMP/ATP and inhibits mTORC1 through phosphorylating TSC2 and Raptor. DNA damage also regulates mTORC1 activity through P53-dependent upregulation of AMPK. P53 downstream transcriptional targets Sestrin 1 and 2 activate AMPK, thus suppressing mTORC1 activity (17).

Activated mTORC1 phosphorylates downstream targets and regulates many cellular processes, including transcription, translation, mRNA splicing, and autophagy. The phosphorylated targets are involved in cell growth, cell proliferation, cell cycle, metabolism, and stress response (22). For example, mTORC1 is the direct mediator between nutritional condition and autophagy. In the presence of nutrients and growth factors, PI3K/ATK, MAPK and AMPK are all upstream inhibitors of autophagy via mTORC1 activation. Activated mTORC1 shuts down autophagy by phosphorylating and inactivating unc-51 like autophagy activating kinase 1 (ULK1) and autophagy related 13 (ATG13), which are required for the phagophore formation (23). Two well-known mTORC1 targets, 4EBP1 and S6K, are translational regulators. 4EBP1 competes with eukaryotic translation initiation factor 4G (eIF4G) to form the complex with eIF4E and inhibits eIF4E-dependent translation. Phosphorylation of 4EBP1 by mTORC1 at Thr37/Thr46 decreases its binding affinity to eIF4E and activates eIF4E-dependent translation (24). Phosphorylation of S6K by mTORC1 at Thr389 promotes mRNA maturation and the synthesis of ribosomal mRNAs and proteins. They both promote many proteins related to cell growth, such as c-MYC and Cyclin D (25).

mTORC1 also indirectly controls transcription factors related to metabolism and stress response, which makes the role of mTORC1 even broader (26).

1.2.2 The summary of mTOR inhibitors

Rapamycin is the first generation of mTOR inhibitors. It inhibits the ability of mTORC1, but not mTORC2, to phosphorylate substrates. Rapamycin binds FK506-Binding Protein 1A (FKBP1A) and dissociates Raptor from mTOR, thus preventing the access of mTOR to some substrates (27). Prolonged treatment with rapamycin may also inhibit mTORC2 in some tissues and cell lines. This effect may involve progressive sequestration of the mTOR pool in a complex with rapamycin-FKBP12, thus making it unavailable for mTORC2 (17). Rapamycin analogs (rapalogs), such as temsirolimus (intravenous) and everolimus (oral), have been approved for advanced renal cell carcinoma treatment, but not for the majority of cancer therapy (28). For example, a prospective, randomized phase III study shows that everolimus is associated with a survival benefit of 6.3 months in patients with advanced pancreatic neuroendocrine tumors, but the finding is not statistically significant (29). One reason why it is more cytostatic-like is that rapalogs do not directly cause cell death. The other reason is that inhibition of mTORC1 alone suppresses negative feedback of PI3K/AKT and promotes cell survival (30).

In order to improve the clinical application of mTOR inhibition, PI3K/mTOR dual kinase inhibitors target the ATP binding pockets in the kinase domain of PI3K and mTOR. The prototype compounds are ATP competitive PI3K inhibitors because PI3K and mTOR share sequence similarities. Due to the potential high toxicity of PI3K/mTOR dual inhibitors, inhibitors that are more specific to mTOR, such as

KU0063794 and AZD8055, have been developed. Some of them are in either phase I or II clinical trials for cancer treatment (30).

1.3 Cell cycle regulation

The cell cycle is tightly controlled at multiple stages called cell cycle checkpoints (Fig.3). Generally there are three checkpoints: the G1, G2/M and mitotic checkpoints. At each checkpoint, cells determine whether the condition is optimal for the next phase. Proteins engaged in checkpoint regulation usually undergo a cycle of synthesis/degradation and phosphorylation/de-phosphorylation. Cell cycle-specific Cyclin-dependent kinases (CDKs) and Cyclins form complexes and are responsible for cell cycle transition. The activity of CDKs, the most important enzymes in cell cycle regulation, fluctuates during cell cycle. A set of kinases and phosphatases controls CDKs activities through protein phosphorylation and de-phosphorylation, and the expression levels of those kinases and phosphatases are usually regulated by different ubiquitin proteasome systems under different conditions. CDKs activities also depend on the dynamic changes of their partners Cyclins. Different Cyclins show their abundance in different cell cycle phases through mRNA transcription control and ubiquitin-mediated protein degradation. Here the whole cell cycle process will be described shortly.

The G1 phase is a critical stage to decide whether a cell stays in the cell cycle or enters a quiescent stage called the G0 phase. This point is known as the restriction point (R) and it separates the G1 phase into two parts: the G1-pm (post-mitotic) and the G1-ps (pre-S) phase. The restriction point is growth factor-dependent and a steady rate

of mRNA and protein synthesis keeps the cell moving forward. Another G1 checkpoint close to the S phase (the G1/S checkpoint) is a nutrient-sensing checkpoint. During normal conditions, the CDK4/6-Cyclin D complex (first) and the CDK2-Cyclin E complex (later) phosphorylate retinoblastoma protein (RB), which releases the E2F family of transcription factors and triggers E2F-dependent transcription of cyclin E and other genes required for S phase progression (31). Both Cyclin D and Cyclin E expression is regulated by mTORC1-mediated protein synthesis (32). Proteins such as PI3K and AMPK sense metabolic capability and mediate the mTORC1 activity. These proteins link the status of growth factors, nutrition, amino acids, and energy to the G1 checkpoint, especially the late G1/S checkpoint, via control of Cyclins expression.

The S phase stands for the synthesis phase. The whole DNA replication process is from the early G1phase to the end of the S phase. Before cells enter the S phase, replication-related proteins keep recruited to the origins. Cells enter the S phase only when everything is ready for DNA synthesis. Cells will not enter the G2/M phase if replication is not complete.

The G2 phase is the rapid stage where cells make sure the division will go smoothly in mitosis. The integrity of the genome will be checked and mitosis-related proteins will be synthesized. The CDK1-Cyclin B complex mainly regulates G2/M transition. The complex activity is controlled by the phosphorylation status of CDK1 and the abundance of nuclear Cyclin B. In normal cells, Cyclin B expression is relatively low in the G1 phase and reaches its peak in the end of the G2 phase. However, the CDK1-Cyclin B complex is still inactive due to inhibitory phosphorylation of CDK1 at Tyr15/Thr14 by WEE1/myelin transcription factor 1 (MYT1). Cells enter mitosis only when increased cell division cycle 25 phosphatases (CDC25A/B/C) de-phosphorylate

these residues. This step also activates a positive feedback loop to ensure rapid amplification of CDK1 activity: the CDK1-Cyclin B complex inhibits its inhibitors WEE1/MYT1 and activates its activators CDC25 phosphatases through a protein called polo-like kinase (PLK1) (33). In the late G2 phase, PLK1 is recruited to the centrosome and promotes the recruitment of aurora kinase A which is responsible for PLK1 activation. The CDK1-Cyclin B1 complex phosphorylates Bora, the cofactor of aurora kinase A, to facilitate PLK1 phosphorylation and activation by aurora kinase A at Thr210. PLK1 is a positive regulator of CDC25C (34), and also triggers WEE1 degradation via the ubiquitin proteasome pathway (35-36). Thus, G2/M transition is tightly controlled by the balance of CDC25 phosphatases and WEE1/MYT1 kinases that function in the CDK1 de-phosphorylation and phosphorylation (35).

Mitosis is the phase to produce two identical daughter cells and it contains five different stages. In prophase, chromatin condenses, nucleoli disappear and mitotic spindles form. The nuclear membrane then breaks down and microtubules extend from each end of the cell to the kinetochore, a protein around the centromere (prometaphase). In metaphase, all chromosomes are perfectly oriented and line up along the equator of the cell on the metaphase plate. Each pair of chromosomes (sister chromatid pair) is then pulled to the opposite poles of the cell and separated into two identical and independent chromosomes by mitotic spindles (anaphase). It is followed by nuclear membrane and nucleoli reappearance, chromosome unwinding, and cytokinesis that divides the cytoplasm into two identical cells (telophase).

The mitotic checkpoint, also known as the spindle assembly checkpoint (SAC), controls metaphase-anaphase transition. Any single unattached kinetochore or a lack of tension in the centromeric region during prometaphase can activate the checkpoint.

During prometaphase, all SAC proteins and CDC20 are localized at kinetochores. The checkpoint promotes assembly of the mitotic checkpoint complex, which contains mitotic arrest deficient 2 (MAD2), budding uninhibited by benzimidazole 3 (BUB3) and BUB1-related protein kinase (BUBR1), at the kinetochore and further inhibits the activity of CDC20. SAC proteins, including the mitotic checkpoint complex, remain active until the formation of kinetochore microtubules. After all chromosomes has aligned, SAC proteins are removed and the E3 ubiquitin ligase anaphase-promoting complex/cyclosome (APC/C) with its co-activator CDC20 degrades Cyclin B1 and promotes mitotic exit after cell division (37). Daughter cells then enter the G1 phase again.

1.4 DNA damage checkpoints: activation, recovery and adaptation

1.4.1 Activation

The cell cycle checkpoints in DNA damage response are not exactly the same as checkpoints during normal cell cycle progression. The purpose of DNA damage checkpoints is to ensure the competent state of DNA for duplication and division. It not only provides time for cell-cycle specific repair, such as homologous recombination (HR) repair in the S phase, but also prevents the transition that may interfere normal processing.

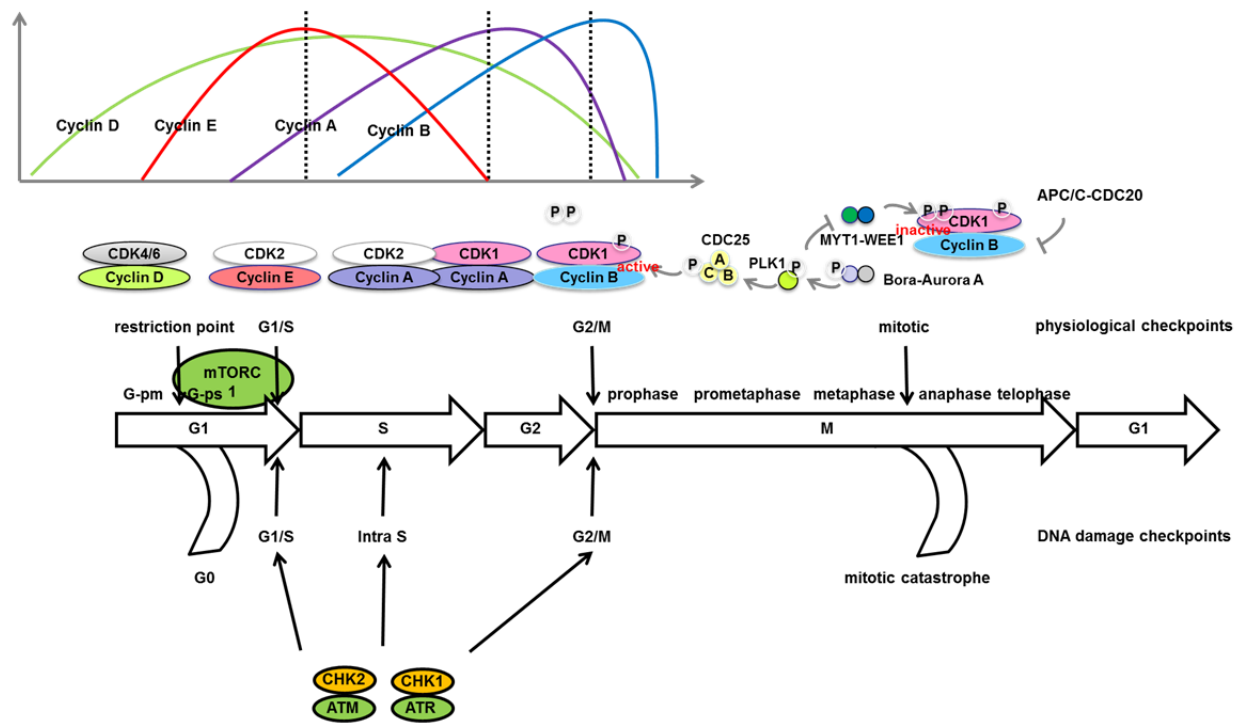


Figure 3 The cell cycle transition

The diagram simply shows the cell cycle, checkpoints, and dynamic changes of the CDK-Cyclin complexes.

ATM and ATR signaling pathways control DNA damage checkpoint activation. Different stimulants may activate different checkpoints and pathways. For example, IR induces G2 arrest significantly but also activates G1/S and intra-S phase checkpoints through ATM (first) and ATR (later) signaling pathways. Replication stress delays the intra-S phase and G2/M transition generally through ATR activation. Once ATM and ATR are activated, mainly ATM phosphorylates CHK2 at thy68 and ATR phosphorylates CHK1 at Ser317/345. The following signaling cascade targets the specific CDK-Cyclin complex and determines where cell cycle arrest.

ATM and ATR signaling pathways control DNA damage checkpoint activation. Different stimulants may activate different checkpoints and pathways. For example, IR induces G2 arrest significantly but also activates G1/S and intra-S phase checkpoints through ATM (first) and ATR (later) signaling pathways. Replication stress delays the intra-S phase and G2/M transition generally through ATR activation. Once ATM and ATR are activated, mainly ATM phosphorylates CHK2 at thy68 and ATR phosphorylates CHK1 at Ser317/345. The following signaling cascade targets the specific CDK-Cyclin complex and determines where cell cycle arrest.

To control the G1/S checkpoint, the CDK2-Cyclin E complex and the CDK4/6-Cyclin E complex are first locked in an inactive state through CDC25A degradation, and they stay inactive through P53 stabilization. Phosphorylation of CDC25A at Ser123 by CHK1 and CHK2 not only facilitates CDC25A degradation through the ubiquitin-mediated proteolysis, but also regulates CDC25A interaction with the CDK2-Cyclin E complex and the CDK4/6-Cyclin D complex (38). P53 is phosphorylated by ATM (at Ser15), ATR (at Ser15), and CHK2 (at Ser20), and the phosphorylation leads to P53 stabilization by preventing its binding to mouse double minute 2 (MDM2), an E3

ubiquitin-protein ligase. The stabilized P53 then drives gene transcription related to cell cycle progression and programmed cell death, such as P21. As a negative cell cycle regulator, P21 inhibits the CDK2-Cyclin E complex and the CDK4/6-Cyclin D complex, further activating the G1/S checkpoint (39-41).

G2 arrest is predominant in cells treated with IR and the CDK1-Cyclin B1 complex plays a critical role. One mechanism to activate the G2/M checkpoint is persistent inhibitory phosphorylation of CDK1. In response to DNA damage, WEE1 directly phosphorylates and inhibits CDK1 (42); meanwhile, nuclear CDC25A and CDC25C decrease and reduce removal of phosphorylation from CDK1. 14-3-3 mediated degradation and cytoplasmic sequestration of CDC25A and CDC25C are facilitated by their phosphorylation (Both CHK1 and CHK2 phosphorylate CDC25C at Ser216 and CDC25A at Ser76) (6, 43). P21 interaction with the CDK1-Cyclin B1 complex excludes CDC25C from CDK1 and also maintains the inhibitory phosphorylation of CDK1. Repression of *PLK1* gene transcription by BRCA1 and CHK1 indirectly inhibits CDK1 activity via WEE1 and CDC25C (44). The other mechanism to arrest cells in the G2 phase is the decrease of *CCNB1* (encoding Cyclin B1) mRNA level and 14-3-3 σ -mediated cytoplasmic localization of Cyclin B1 (34). Another factor aurora kinase B is phosphorylated by CHK1 at Ser311 and also contributes to premature mitosis when cells face replication stress (45).

Unlike G1 and G2 checkpoints, the intra-S phase checkpoint is transient and only affect part of the genome. In response to DNA damage, ATR and CHK1 directly inhibit assembly of replication proteins, such as CDC7, CDC45, TOPBP1 and the minichromosome maintenance complex component (MCM) complex, at the replication fork and delay normal DNA synthesis (46-48). Degradation of CDC25A through CHK1

and CHK2 phosphorylation inhibits the CDK2-Cyclin A complex, the main complex for S phase control (34). CHK1 also controls the activity of the CDK1-Cyclin A2 complex through CDC25A, which is related to abnormal origin firing (49).

1.4.2 Recovery

After DNA damage has been repaired, cells arrested in specific phases eventually restart their cell cycle progression. During checkpoint recovery, cells reactivate the CDK-Cyclin complexes and reverse the checkpoint actions mainly through inactivation of ATM and ATR signaling pathways and regulation of proteins independent to DNA damage pathways. The process is still controlled by protein synthesis/degradation and phosphorylation/dephosphorylation, but it is not exactly opposite to checkpoint activation. For example, a E3 ubiquitin ligase called the Skp1/Cullin/F-box protein (SCF) complex degrades different proteins during checkpoint activation and recovery (50). Here molecules involved in checkpoint recovery are briefly summarized here but the detail mechanisms are still not well known. Therefore, more systemic approaches may need to be done.

Protein phosphatases dephosphorylated proteins in DNA damage pathways. During the unperturbed S phase, CHK1 is continuously phosphorylated by ATR; meanwhile, CHK1 dephosphorylated by protein phosphatase 2A (PP2A) prevents phosphorylated CHK1 accumulation (38). Based on the function of PP2A in the balance of phosphorylated CHK1, PP2A is likely to be one of the factors that control checkpoint recovery. Another phosphatase called wild-type P53-induced phosphatase 1 (WIP1, PP2C δ) recognizes the p(S/T)Q motif which is specifically phosphorylated by ATM and ATR. Many ATM and ATR downstream targets can also be targets of WIP1 (51).

During G2/M checkpoint recovery, PLK1 seems to play an important role (51). PLK1 phosphorylates WEE1 and Claspin for their degradation. PLK1 also phosphorylates CHK2 and inhibits CHK2 kinase activity. Furthermore, during mitosis reentry, PLK1 directly interacts with P53-binding protein 1 (53BP1) to inactivate the checkpoint signaling (52). PLK1 promotes CDC25C translocation to nucleus to activate CDK1 activity. However, how PLK1 is regulated during checkpoint recovery is not well known. One possible regulation is through aurora kinase A, but more detail mechanisms should be studied.

Other proteins, such as Artemis (the phosphorylated form regulates the CDK-Cyclin complexes) and forkhead box M1 (FOXO1, a transcription factor required for G2/M checkpoint recovery), also involve in checkpoint recovery (53). In general, there is still a gap between checkpoint activation and checkpoint recovery, and the process is important for cell survival.

1.4.3 Adaptation

Checkpoint adaptation is first discovered in yeast. This is the phenomenon that cells escape from long-term cell cycle arrest in spite of the presence of DNA damage. Cells usually maintain a basal level of the CDK-Cyclin complexes during DNA damage-induced cell cycle arrest and it provides capabilities to recover or escape from cell cycle arrest. Similar to checkpoint recovery, the process is controlled by ATM and ATR signaling pathways and pathways independent to DNA damage signaling (54). The difference is persisted DNA damage in checkpoint adaptation but how cells ignore damage is still not clear. If checkpoint adaptation happens in cells with other checkpoint defects, cells will keep proliferation and it may result in genomic instability.

1.5 Mitotic catastrophe as a mechanism to maintain genomic stability

Genome integrity has a significant impact on cell survival. In order to maintain genomic stability, cells have developed a network, the DNA damage response, to detect and repair DNA damage with cell cycle arrest. Inhibition of proteins in the network affects normal cell cycle progression, including inappropriate DNA synthesis in the S phase and abnormal cell division in mitosis. For example, deregulated CDK activity increases late origins firing inappropriately in the S phase. WEE1 depletion induces DNA damage in newly replicated DNA (48). If those damages are not repaired, cells may undergo cell cycle arrest, programmed cell death, or keep moving to the next cell cycle phase with those damages. The persisted damages will further cause genomic instability, which may promote cancer formation.

Mitotic catastrophe results from premature or inappropriate entry of cells into mitosis. It occurs either during or shortly after dysregulated mitosis. The aberrant mitosis is usually induced by various agents in the presence of genetic defects, such as impaired DNA repair machineries, insufficient checkpoint functions, or mitosis defects. The consequence of mitotic catastrophe can be apoptosis, necrosis, or senescence. It depends on the molecular profiles of cells and the duration of mitotic arrest (55-56). For example, the absence of P53 in CHK2-depleted cells abrogates the availability of caspases and drives cells from mitotic catastrophe to necrosis, while the presence of functional P53 in CHK2-depleted cells facilitates apoptosis (57). Cells arrested in mitosis for a short period of time showed variable fates, while cells blocked in mitosis

for longer time died after exiting mitosis (58). The characteristics of mitotic catastrophe suggest that it is heterogeneous and involves several mechanisms.

Mitotic catastrophe is associated with chromosomal breaks, deficient nuclear division (karyokinesis), premature condensation of chromosome, and the formation of giant cells with multiple micronuclei, some of which are also shown in apoptosis and necrosis. The morphological changes of apoptosis include cell shrinkage, chromatin condensation (pyknosis), nuclear fragmentation (karyorrhexis), extensive membrane blebbing, formation of apoptotic bodies (budding) and phagocytosis (59). Necrosis involves cell and organelle swelling, cytoplasmic vacuoles formation, chromatin condensation and nuclear membrane dilatation, plasma membrane disruption and presence of inflammatory reaction (60). Given mitotic catastrophe as a prelude to apoptosis, necrosis, or senescence, it is difficult to define mitotic catastrophe simply based on the morphological criteria.

Many proteins have been identified to link aberrant mitosis, mitotic catastrophe and cell death together. They include SAC proteins, CDK1, P53, BCL-2 family members, and Death Domain (DD) super-family members, such as Caspases. The MCC component BUBR1 directly interacts and disrupts the formation of the Caspase 2-based platform at the kinetochore, and further inhibits apoptosis during mitosis (61). On the contrary, Caspases have been shown to cleave and inactivate BUBR1 (62). CDK1-mediated phosphorylation of the BCL-2 family, Caspase 2, 8 and 9 prevents apoptosis during mitosis (56, 63). Phosphorylation of P53 by SAC proteins, such as PLK1, regulates the transcriptional activity of P53 and controls cell death. Those molecules tightly work as a network to mediate mitosis and cell fates after mitotic entry.

The function of mitotic catastrophe links to genomic stability. Cells with mitotic catastrophe suppression may generate aneuploid cells through multipolar or abnormal bipolar divisions, or generate polyploid cells through mitotic slippage (cells exit mitosis without division through unspecific degradation of Cyclin B1 in spite of the SAC signaling (64)). Those abnormal cells are usually arrested in the G1 phase or undergo mitotic catastrophe in the next M phase. However, if cells bypass those barriers, cells may increase genomic instability, a driving force of certain human diseases such as cancer. Therefore, mitotic catastrophe can be a strategy to prevent or treat human diseases.

1.6 Drugs related to DNA damage response

The DNA damage response machinery is linked with human diseases. It forms a biological barrier against the development human diseases, and in the meanwhile, the high demand of the DDR machinery in certain types of cells provides a therapeutic window. Here two drugs in this study will be only briefly introduced.

1.6.1 PARP inhibitors

Poly(ADP-ribose) polymerase (PARP) involves in various repair machineries and fork reversal. In response to ssDNA breaks, PARP can directly bind DNA, and the polymerization of ADP-ribose usually occurs immediately to provide a platform for other damage response proteins. CHK1 activation is also enhanced by poly(ADP-ribose), which suggests that PARP inhibition may increase replication stress by diminishing the CHK1 activity. PARP inhibition causes synthetic lethality with HR repair defects, and the effect results from the increase of unrepaired primary lesions processed into DSBs

which require Rad51-dependent HR repair. The most famous example is PARP inhibitors in *Brca1*- or *Brca2*-mutated cancer treatment (65-66). Three randomized phase III trials of a PARP inhibitor olaparib in *Brca*-mutated breast cancer have been conducted and another PARP inhibitor, rucaparib, has been approved by US Food and Drug Administration (FDA) for advanced ovarian cancer treatment (46). BMN 673, one of the PARP inhibitors in my study, shares many biochemical profiles with early generations of PARP inhibitors, such as olaparib and rucaparib, but BMN 673 achieves its cytotoxic effect with much lower concentration. Recent studies have shown that the cytotoxicity of the PARP inhibitor is correlated with its ability to trap PARP-DNA complexes instead of the catalytic inhibitory property (67-69). It became the rationale to test BMN 673 in my study.

1.6.2 WEE1 inhibitors

Both WEE1 and CHK1 involve in the G2/M checkpoint control. WEE1 inhibition enhances the CDK activity and induces premature mitotic entry. Similar to CHK1 inhibition, drug-based WEE1 inhibition also leads to unscheduled origin firing, the shortage of nucleotides, the decrease of fork progression speed, massive DSBs and eventually cell death (46). Cells without functional P53 are usually more sensitive to the G2/M checkpoint abrogation because they lack the P53-dependent G1 checkpoint and therefore depend on the G2/M checkpoint for DNA damage repair (42). Several phase II clinical trials have tested MK-1775 (AZD-1775), a selective ATP-competitive WEE1 kinase inhibitor, in P53-mutant cancer patients and the trials are still ongoing (47).

SIGNIFICANCE OF THE STUDY

Developed a systematic approach to analyze RPPA data and simplified the complex biomedical question using a non-biased mathematical modeling

Identified that mTORC1 controlled a transcriptional program of mitotic entry through epigenetic regulation of mitosis-related genes during checkpoint recovery

Linked nutrient status to G2/M checkpoint recovery from irradiation

Provide a therapeutic strategy using the WEE1 inhibitor for TSC patients

CHAPTER 2

Materials and Methods

2.1 Cell lines and culture

Human U2OS cells were grown in McCoy's 5A medium with 10% fetal bovine serum (FBS, ThermoFisher Scientific). HEK 293T (human embryonic kidney epithelial) cells, HCT-116 (human colorectal carcinoma) cells, MEF (mouse embryonic fibroblast) cells and ELT3-V3/T3 (Eker rat uterine leiomyoma, from Dr. Jane Yu's lab) cells were in DMEM medium plus 10% FBS and 1x penicillin-streptomycin (15140-122, Gibco, Life technologies). HCT116 mTOR kinase-dead conditional knock-in (D2338A-cKI) cells were in RPMI-1640 medium with 2mM L-glutamine, 25mM sodium bicarbonate, and 10% FBS as Horizon suggested. Cells were all kept in the 37°C humid incubator with 5% CO₂.

To make AA⁺ medium, we added 1X MEM amino acids (Invitrogen), 1X MEM non-essential amino acids (Invitrogen) and 1X L-glutamine (Invitrogen) into amino-acid free (AA⁻) RPMI-1640 medium with 10% FBS. We then mixed AA⁻ medium (0%) with AA⁺ medium (100%) to make 0.01% to 10% AA medium.

To generate the rapamycin-resistant cell line ELT3-V3R, most of ELT3-V3 cells were killed with 10nM rapamycin and then the rest of cells were cultured with low-dose to high-dose rapamycin for a period of time.

2.2 Ionizing radiation

Ionizing radiation (IR) was induced by the high-voltage X-ray tubes (RS-2000 Biological Research Irradiator, Red Source Technologies). MEF cells were irradiated with 15Gy and the rest of the cells were irradiated with 7Gy. We treated cells with 2 μ M paclitaxel after IR to arrest cells in mitotic phase (HCT116: 2 hours after IR; U2OS: 6 hours after IR; TSC2: immediately after IR).

2.3 Antibodies, plasmids and reagents

The purpose of rapamycin (0.02nM or 20nM, Sigma-Aldrich), KU0063794 (1 μ M, Selleckchem) and AZD8055 (1 μ M, Selleckchem) is to inhibit mTOR activity. MK2206 (0.1 μ M, AKT inhibitor), MK1775 (10nM to 0.5 μ M, Wee1 inhibitor), BMN 673 (20nM or 50nM, PARP inhibitor), and olaparib (5 μ M, PARP inhibitor) were purchased from Selleckchem. Paclitaxel (2 μ M) was from Sigma-Aldrich.

Myc-tagged mTOR-WT (wild type) plasmid, Myc-tagged mTOR-KD (kinase dead) plasmid, mTOR, and control shRNA were provided by Dr. Dos Sarbassov (70). ATM, ATR, mTOR, and KDM4B smart-pool siRNA, and control siRNA (ON-TARGETplus Non-targeting control siRNAs #1) were purchased from GE Dharmacon. Individual mTOR (#1: 5'-GGCCAUAGCUAGCCUCAUA-3' and #2: 5'-CAAAGGACUUCGCCCAUAA-3'), Raptor (5'-GGACAACGGCCACAAGUAC-3'), Rictor (5'-ACUUGUGAAGAAUCGUAUC-3'), and control (Mission siRNA universal negative control #1) siRNAs were synthesized from Sigma-Aldrich (71-73).

Rabbit anti-mTOR antibody, rabbit anti-S6K antibody, rabbit anti-S6 antibody, rabbit anti-p-S6 (Ser235/236) antibody, rabbit anti-AKT antibody, rabbit anti-p-AKT (Ser473) antibody, rabbit anti-KDM4B antibody, rabbit anti-Cyclin B1 antibody, rabbit anti-p-H3 (Ser10), rabbit anti-ATM antibody, mouse anti-CHK1 antibody, rabbit anti-p-CHK1 (Ser345) antibody, mouse anti-CHK2 antibody, rabbit anti-p-CHK2 (Thr68) antibody, rabbit anti-H2AX antibody, and rabbit anti- γ -H2AX (Ser139) antibody were purchased from cell signaling technology. ChIP grade rabbit anti-mTOR antibody was from Abcam. Mouse anti- β -Actin antibody and mouse anti- α -Tubulin antibody were from Sigma-Aldrich. Mouse anti-Cytochrome c antibody was from BD Biosciences. Antibodies from Bethyl Laboratories were rabbit anti-Raptor antibody and rabbit anti-KDM4B antibody. Reagents from Santa Cruz Biotech include goat anti-Rictor antibody, mouse anti-PLK1 antibody, goat anti-ATR antibody, mouse anti-MYC antibody, mouse anti-GADPH antibody, all HRP-conjugated secondary antibodies, and normal IgG. Anti-annexin-V Alexa Fluor 647 conjugated antibody and Alexa Fluor fluorescent dyes were from Life Technologies.

2.4 Cell viability, cell proliferation assay, apoptosis assay and 3D culture

Cell viability was examined with MTT (3-(4, 5-dimethylthiazolyl-2)-2, 5-dephenyltetrazolium bromide) assay. First, we plated 250 or 500 cells/well in 96-well plates one day before drug treatment and incubated cells with drugs for at least four days. After treatment, cells were incubated with 20 μ l 2 μ g/ μ l MTT (Life technologies) at 37°C for 3 hours. DMSO (dimethyl sulfoxide, Fisher Scientific) was added to dissolve blue formazan crystals and the absorbance values were read in the plate reader (Bio-

Tek). To evaluate cell apoptosis after drug treatment, the percentage of apoptotic cells was determined by detection of annexin V-bound translocated membrane component by flow cytometry and the protocol was provided by the manufacturer (Life Technologies). For 3D cell culture, we coated 96-well plates with 30 μ l/well Matrigel (Fisher Scientific) and seeded 1000cells/100 μ l medium in each well. Two days after seeding cells, we changed new medium with/without drugs and incubated cells for another three days. 10 μ l of PrestoBlue cell viability reagent (Invitrogen) was directly added into each well for 10 minutes at 37°C. Fluorescent values were measured with 530/25 and 590/35 nm as excitation and emission wavelength in Synergy H1 Multi-Mode Reader (BioTek). For 3D culture representative photos, we seeded 4000 cells/400 μ l medium in each Matrigel pre-coated 8-well chamber slides and cultured cells for 10 days. 0.2 μ M MK1775 was added on Day 3 and the medium \pm 0.2 μ M MK1775 was changed every three days. The photos were taken with Olympus IX71 microscope (NORTH Campus Flow Cytometry and Cellular Imaging Core Facility, MD Anderson Cancer Center) and analyzed by Image J. To determine the percentage of apoptotic cells after drug treatment, we followed the protocol provided by the manufacturer (Life Technologies) and detected annexin V-Alexa Fluor 647-positive cells as apoptotic cells on Gallios Flow Cytometer.

2.5 Cell cycle analysis and mitotic entry by flow cytometry

Different biomarkers were used to measure cell populations in different cell cycle. Propidium iodide (PI, excitation source 488nm argon ion laser) is to assess cell cycle by quantitation of DNA content. Phosphorylated histone H3 on Ser10 is the

mitosis phase marker. Cells were harvested and fixed in 70% alcohol at -20°C for at least 2 hours before stained with PI, fluorophore-conjugated antibodies against phosphorylated histone H3. For PI staining, we incubated cells with PI solution (10µg/ml PI, 1.25µg/ml RNase A and 0.05% Triton X) for at least 10 minutes. To detect mitotic cells, cells were incubated in permeabilization buffer (0.25% Triton X100 in PBS) on ice for 10 minutes and stained with phosphorylated histone H3-Ser10-Alexa 647 antibody at room temperature for at least 3 hours. All cell cycle progression data were acquired on Gallios Flow Cytometer (Beckman Coulter, Inc.) at the University of Texas MD Anderson Cancer Center FACS core facility and were analyzed by FlowJo V10 software (FlowJo, LLC).

2.6 Western blotting

To detect total protein expression, cells were lysed in urea lysis buffer (8M urea, 50mM Tris-HCl pH 7.5 and 150mM β-mercaptoethanol). We separated nuclear and non-nuclear fractions using Dounce homogenizer with Nori buffer (20mM HEPES pH 7.0, 10mM KCl, 2mM MgCl₂, 0.5% NP-40 and 1X protease inhibitor cocktails) and urea buffer. Signals were detected with Amersham Enhanced Chemiluminescence (ECL) Prime Western Blotting Detection Reagent (GE Healthcare Life Sciences).

2.7 Immunofluorescence staining

Cells on cover slips were fixed with 4% paraformaldehyde solution (Santa Cruz Biotechnology) at room temperature for 10 minutes, and blocked with 3% BSA in 0.1%

Triton X-100-PBS for 30 minutes. Cells were incubated in primary antibody at room temperature for 2 hours and in secondary antibody at room temperature for 2 hours. Cells may be counterstained with DAPI (4', 6-diamidino-2-phenylindole) before mounting. Photos were taken with Olympus IX81 microscope or FV1000 laser confocal microscope (NORTH Campus Flow Cytometry and Cellular Imaging Core Facility, MD Anderson Cancer Center), and data was analyzed by Image J or FV10-ASW 4.2 Viewer (Olympus).

2.8 Single-cell gel electrophoresis (comet assay)

U2OS cells were treated with IR and DNA damage was detected by alkaline comet assay following the CometAssay Reagent Kit instruction (Trevigen). After cells were stained with SYBR Green, the photos were taken with Olympus IX81 microscope (NORTH Campus Flow Cytometry and Cellular Imaging Core Facility, MD Anderson Cancer Center) and data was analyzed by CometScore 1.6 (TriTek Corp.).

2.9 RNA isolation and qRT-PCR

Complementary DNA was generated from RNA using TRIzol reagent and the SuperScript III kit (Invitrogen). The quantitative polymerase chain reaction (qPCR) reactions were performed using Power SYBR Green PCR Master Mix kit on the ViiA7 Real-Time PCR System (Invitrogen). qPCR primers were designed to span exon–intron boundaries of respective genes, ensuring the results were not affected by genomic DNA contamination. The sequences of qPCR primers are listed in Table 1.

Oligonucleotides for qPCR

Gene name		Primer Sequence (5'-3')	Product
<i>PLK1</i>	F	GGCAACCTTTTCCTGAATGA	103 bp
	R	TCCCACACAGGGTCTTCTTC	
<i>CCNB1</i>	F	TTGGGGACATTGGTAACAAAGTC	226 bp
	R	ATAGGCTCAGGCGAAAGTTTTT	
<i>ACTB</i>	F	GAGCACAGAGCCTCGCCTTT	113 bp
	R	TCATCATCCATGGTGAGCTG	

Oligonucleotides for ChIP-qPCR

Gene name		Primer Sequence (5'-3')	Promoter region
<i>PLK1</i>	F	GTAACGTTCCCAGCGCCG	-60 ~ +63 bp
	R	CAGCTTCCCTGCAGTCACTG	
<i>CCNB1</i>	F	CCAATAAGGAGGGAGCAGTG	+86 ~ +187 bp
	R	GGACCTACACCCAGCAGAAA	

F: forward; R: reverse

Table 1 Oligonucleotides used for qPCR and ChIP-qPCR

2.10 Chromatin immunoprecipitation (ChIP)-qPCR assay

We performed ChIP-qPCR assay following the EZ-ChIP kit instruction (Millipore). U2OS cells were incubated in the growth medium with 1% formaldehyde for 10 minutes and the crosslink reaction was stopped with 0.125M Glycine for 5 minutes at RT. We suspended cells in SDS lysis buffer (1% SDS, 10mM EDTA, 50mM Tris pH 6.5, 1X protease inhibitor cocktail) and sheared DNA to around 600 base pairs in length by 60 Sonic Dismembrator (Fisher Scientific). For each ChIP reaction, we added 900ul Dilution Buffer into 100ul of chromatin and incubated chromatin with Protein G agarose beads at 4°C for 1 hour. After centrifugation, 10ul of the supernatant was removed as Input and the rest supernatant was incubated with 1-2µg antibodies overnight and Protein G agarose beads for 1 hour. The antibodies for ChIP-qPCR were rabbit anti-KDM4B (Cell Signaling), ChIP-Grade rabbit anti-H3-trimethyl K9 (H3K9me3, Abcam), rabbit anti-B-myb (Bethyl) antibodies and rabbit normal IgG (Santa Cruz).

After IP samples were washed by buffers containing different concentrations of salts, protein-DNA complexes were eluted and their crosslinks were reversed in IP samples and also Input. DNA was purified in 50ul Elution Buffer for subsequent qPCR analysis. We added 23ul of qPCR mix containing 400nM of primers and Power SYBR Green PCR Master Mix (Life Technologies) to 2µl of purified DNA for one reaction. The qPCR reactions were performed in the ViiA7 Real-Time PCR System (Invitrogen) and the results of ChIP-samples were normalized to Input individually in each set of samples. The sequences of ChIP-qPCR primers were listed in Table 1.

2.11 Dual-luciferase reporter assay

U2OS cells were cultured in 60 mm plates and siRNA oligonucleotides were transfected. One day after siRNA transfection, cells were transfected again with indicated luciferase (Luc) expressing plasmids and then were split into 6-well plates. One day after Luc transfection, cells were given 7Gy IR and cultured for indicated time points for the assay. We measured PLK1-Luc or Cyclin B1-Luc levels in 96-well plates using Dual-luciferase Reporter Assay kit (Promega) and the manufacturer's instructions in FLUOstar Omega microplate reader (BMG Labtech) were followed. All samples were normalized to Renilla-Luc activity.

2.12 Reverse phase protein array (RPPA)

We mainly followed the lysate preparation protocol provided by RPPA Core Facility in MD Anderson Cancer Center. U2OS and HCT116 cells were seeded in 6-well plates and the final cell amounts in each sample fitted the minimum requirement of RPPA. Cells were irradiated with 7Gy and then were incubated with 2 μ M paclitaxel at indicated time points. We washed the cells with PBS twice before lysed the cells with lysis buffer (1% Triton X-100, 50mM HEPES, pH 7.4, 150mM NaCl, 1.5mM MgCl₂, 1mM EGTA, 100mM NaF, 10mM sodium pyrophosphate, 1mM Na₃VO₄, 10% glycerol, protease and phosphatase inhibitors) on ice for 20 minutes. Cells were collected into tubes and spun down at 14,000 rpm at 4°C for 10 minutes. Protein concentration in supernatant was determined and was adjusted to 1-1.5 μ g/ μ l. Cell lysate was mixed with 4x SDS sample buffer without bromophenol blue and boiled for 5 minutes. Samples were stored in -80°C before RPPA processing. The RPPA data was

normalized by RPPA Core Facility and was further analyzed with the statistical programming language R, Ingenuity Pathway Analysis (IPA, QIAGEN) and MATLAB (MathWorks). The files “bfs_augmentpath.m” and “show_ff_max_flow.m” were written based on the Ford-Fulkerson algorithm and breadth-first search, but we don’t claim the authorship (Fig. 4). The files “output_data.m” and “save_data_build.m” were used to export and save data to Microsoft Excel (Microsoft). We used the file “main.m” to control all other MATLAB files and to generate the array for further calculation (Fig. 5).

2.13 Animal studies

All animal works were performed with protocols approved by the MD Anderson Animal Care and Use Committee. 2×10^6 ELT3-V3/T3-luciferase cells were injected subcutaneously into the bilateral posterior flanks of female CB17-SCID mice (Charles River Laboratories). Five weeks after cell injection, mice bearing 100-150mm³ tumors were randomized into different groups (n=6) (74). Mice were treated with MK1775 vehicle or 60mg/kg MK1775 (in 0.5% methylcellulose) once every two days plus BMN 673 vehicle or 0.33mg/kg BMN 673 (in 5% dimethylacetamide and 5% Solutol and 85% PBS) once daily until tumor size in any group reached 1500mm³ (three weeks in total) (67, 75). Body weight was measured once a week as the parameter of toxicity. Tumor volume using the formula $(\text{length} \times \text{width}^2)/2$ was measured twice a week. We also used bioluminescence imaging to follow tumor size (IVIS 200, MDACC Small Animal Imaging Facility). At the end point, tumor weight was measured when mice were sacrificed.

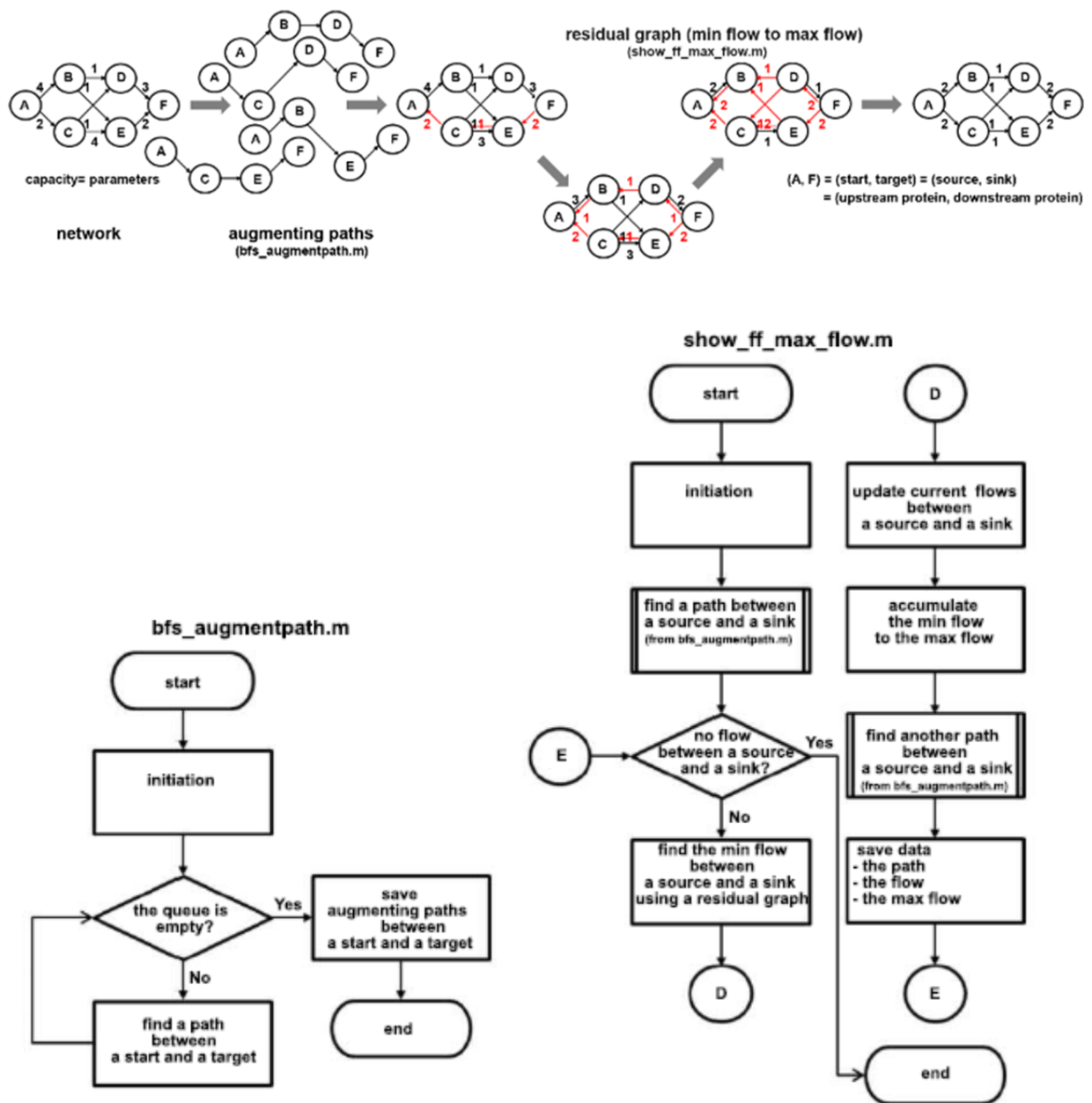


Figure 4 The Ford-Fulkerson algorithm and breadth-first search in MATLAB

The graph on the top was an example how the Ford-Fulkerson algorithm worked and how we defined the terms we used in our programs. The flow charts demonstrated how we found potential targets and pathways in MATLAB by the Ford-Fulkerson algorithm and breadth-first search.

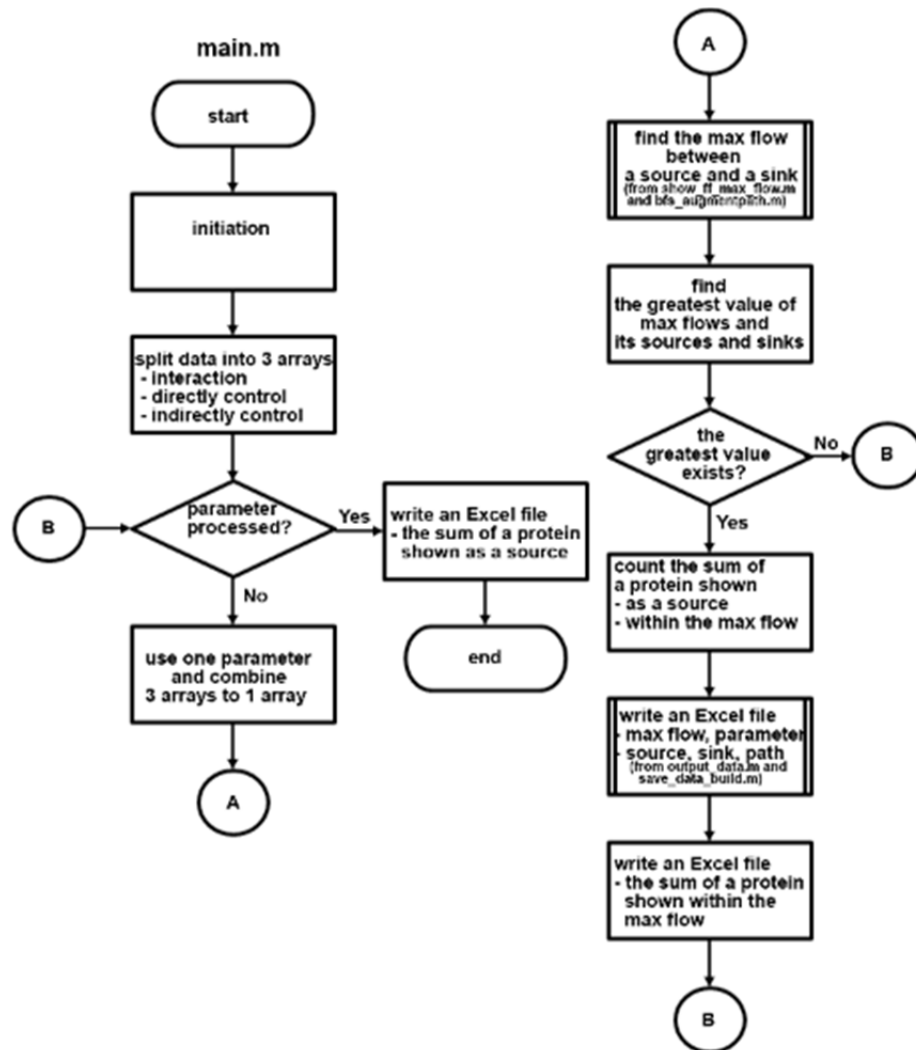


Figure 5 The flow chart for the main program written in MATLAB

The flow chart demonstrated how we used the main program “main.m” to control subroutines (all other “.m” files) in MATLAB.

2.14 Statistics

All graphs were shown as mean values \pm SD (standard deviation) or SEM (standard error of the mean). Statistical significant was determined by two-tailed, unpaired Student's *t*-test in software Graphpad Prism 6. The statistical significance was defined as *p* value under 0.05.

CHAPTER 3

The Role of mTORC1 in Checkpoint Recovery

DNA damage response has been studied for decades, but how cells recover from checkpoint activation is not well known. In order to systematically understand the molecular basis of checkpoint termination, we performed a multidisciplinary study by combining reverse phase protein array (RPPA) data, molecular biology and mathematical modeling to identify molecules required for DNA damage checkpoint recovery. mTORC1 played an essential role to regulate mitotic entry after irradiation. It controlled a transcriptional program of checkpoint recovery through regulating histone lysine demethylase KDM4B and further epigenetically regulated mitosis-related genes including *CCNB1* (encoding Cyclin B1) and *PLK1* (encoding PLK1). Given TSC2-depleted cells with faster checkpoint recovery, we tested the effect of the WEE1 inhibitor combined with the PARP inhibitor both *in vitro* and *in vivo*. The combination treatment induced stronger mitotic catastrophe in TSC2-depleted cells and the WEE1 inhibitor itself showed its effect in the mouse model. Thus, we provided a therapeutic approach for TSC patients with TSC2 mutation.

3.1 mTOR is the candidate to mediate DNA damage checkpoint recovery

In order to discover potential molecules which generally control G2/M checkpoint recovery after ionizing radiation (IR), we performed the reverse phase protein array

(RPPA) in two p53-proficient cell lines (U2OS and HCT116) and developed a series of methods to analyze data (Fig. 6). Basically, we treated cells with IR and then arrested cells in the mitosis phase with paclitaxel to ensure that each cell enter the mitosis phase only once. We aligned 6 time points in two cell lines during the process of checkpoint recovery based on cell cycle and mitotic entry analysis in order to compare protein expression in parallel later (Fig. 7). After we got RPPA data, the expression levels of each protein at different time points were first normalized by the level at time 0 for each cell line. Simple linear models were then constructed to predict normalized expression of each protein in U2OS by respective expression in HCT116. Regression equations with a false discovery rate (FDR) < 0.3 were considered significant and the correlation coefficients (r) between 0.7 and 1 were in terms of strong positive linear relationship. Based on the criteria above, we selected 84 molecules and the heat map showed that the protein expression trends during recovery in U2OS and HCT116 were similar (Fig. 8). We then uploaded 84 molecules in Ingenuity Pathway Analysis (IPA) for canonical pathway and network analysis (76). The top ten canonical pathways based on p-value included pathways related to cancers and the PI3K signaling network (Fig. 9). The top two networks with the score higher than 20 involved cellular response to IR, including cell death and survival, cellular growth and proliferation, and cancer (Table 2). To identify key molecules which regulate checkpoint recovery after IR, we merged those two IPA networks and applied the Ford-Fulkerson algorithm to calculate the maximum signals received by *CCNB1* or *CCND1* (the genes encoding Cyclin B1 or Cyclin D1, two proteins that control cell cycle progression). We chose ten sets of parameters to represent relationships between two molecules in the IPA network (interaction, direct control and indirect control) and calculated total numbers of each

protein shown as the upstream regulator (source) or in the pathways with maximum signals to *CCNB1* or *CCND1*. The scatter plot showed that *MTOR*, *EGFR*, and *AR* (the genes encoding mTOR, EGFR, and androgen receptor) were the top three candidates when we combined results of *CCNB1* and *CCND1* groups. We compared our results to the IPA upstream regulator analysis result which has no specific downstream target, *MTOR*, *EGFR*, and *AR* were the only three molecules shown in the three groups (Fig. 10). Given mTOR belonging to the same family as ATM and ATR, we chose mTOR as our target for further studies.

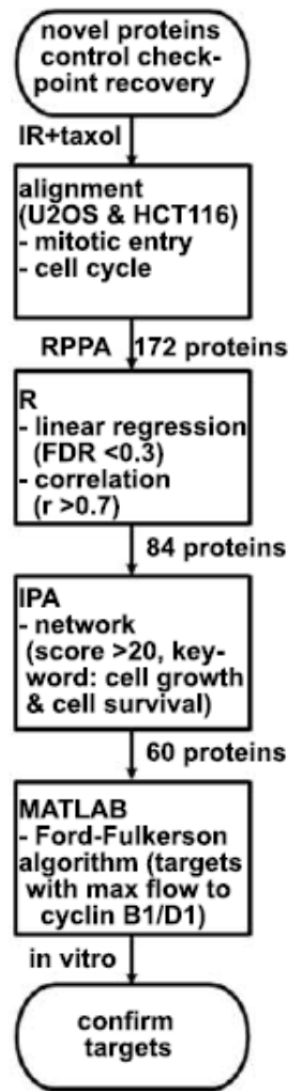


Figure 6 The flow chart for RPPA data analysis

The flow chart demonstrated the process how we identified candidates related to DNA damage recovery from RPPA results

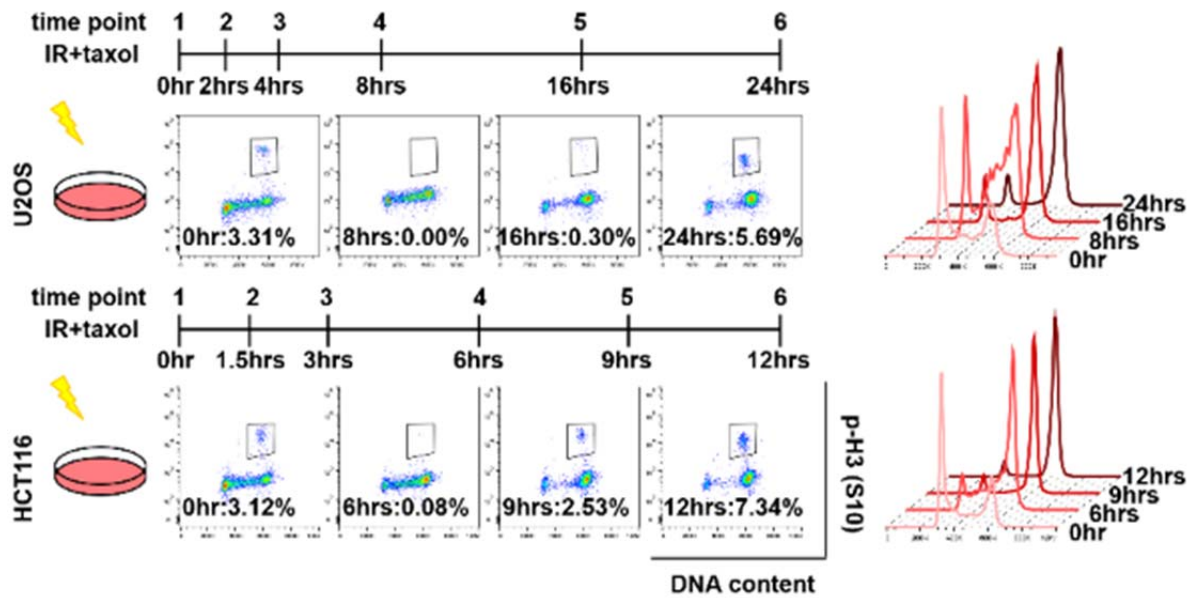


Figure 7 The first step for RPPA data analysis-cell cycle alignment

RPPA was performed in U2OS cells and HCT116 cells. Cells were irradiated with IR 7Gy and then were trapped in the mitotic phase using 2 μ M paclitaxel for a period of time. Six time points were chosen based on cell cycle patterns and mitotic entry analysis. The percentage of mitotic cells defined as phospho-Histone H3 (p-H3) positive cells was shown in each representative graph.

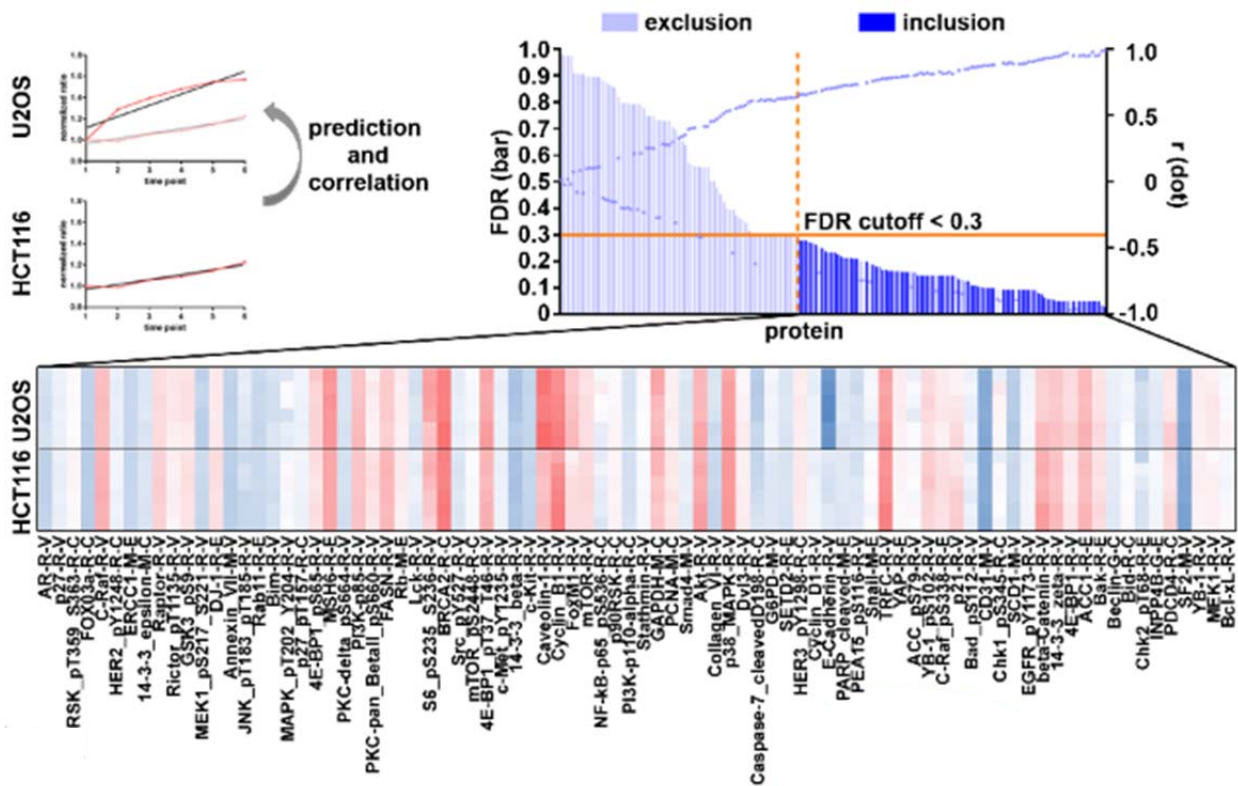


Figure 8 The second step for RPPA data analysis-linear regression and correlation

We used the linear regression slope of each protein in U2OS cells to predict the same protein expression in HCT116 cells and calculate correlations between two cell lines. Regression equations with a FDR value < 0.3 were considered significant in terms of linear relationship and within those proteins, we only chose proteins with correlation r value > +0.7 for IPA network analysis. The names in red were two proteins we used as the downstream targets for calculation.

Network functions	Molecules	Score	Molecules
Cell death and survival, cancer, organismal injury and abnormalities	AKT1,AR,BAD,BCL2L1,BCL2L11,BEC N1,CAV1,CDKN1A,CDKN1B,CHEK1, EGFR,ERBB2,ERBB3,FOXO3, FOXO3,MAP2K1,MET,MSH6,MTOR, PARP1,PCNA,PIK3CA,PIK3R1,RAF1, RB1,RICTOR,RPS6,RPS6KA1,Src, STMN1,YAP1,YBX1,YWHAB,YWHAZ, YWHAZ	79	35
Cell death and survival, cellular development, cellular growth and proliferation	BAK1,BID,BRCA2,CASP7,CCNB1, CCND1,CDH1,CTNNB1,DVL3, EIF4EBP1,FASN,GAPDH,LCK, MAPK1,MAPK8,MAPK14,NFKB1, PDCD4,PECAM1,PRKCD,RPTOR, SETD2,SMAD4,SNAI2,SRSF1	47	25

Table 2: Top two network functions and their molecules identified from IPA

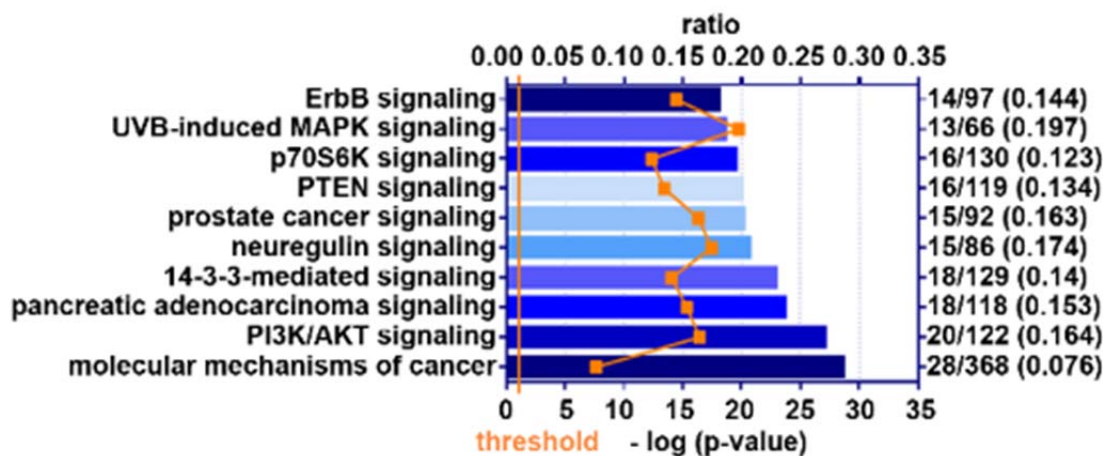


Figure 9 Top ten canonical pathways identified from IPA

Top ten significant canonical pathways enriched with molecules from our screened RPPA dataset were calculated in Ingenuity Pathway Analysis (IPA). The ratio indicated how many molecules in our RPPA dataset were associated with the specific pathway.

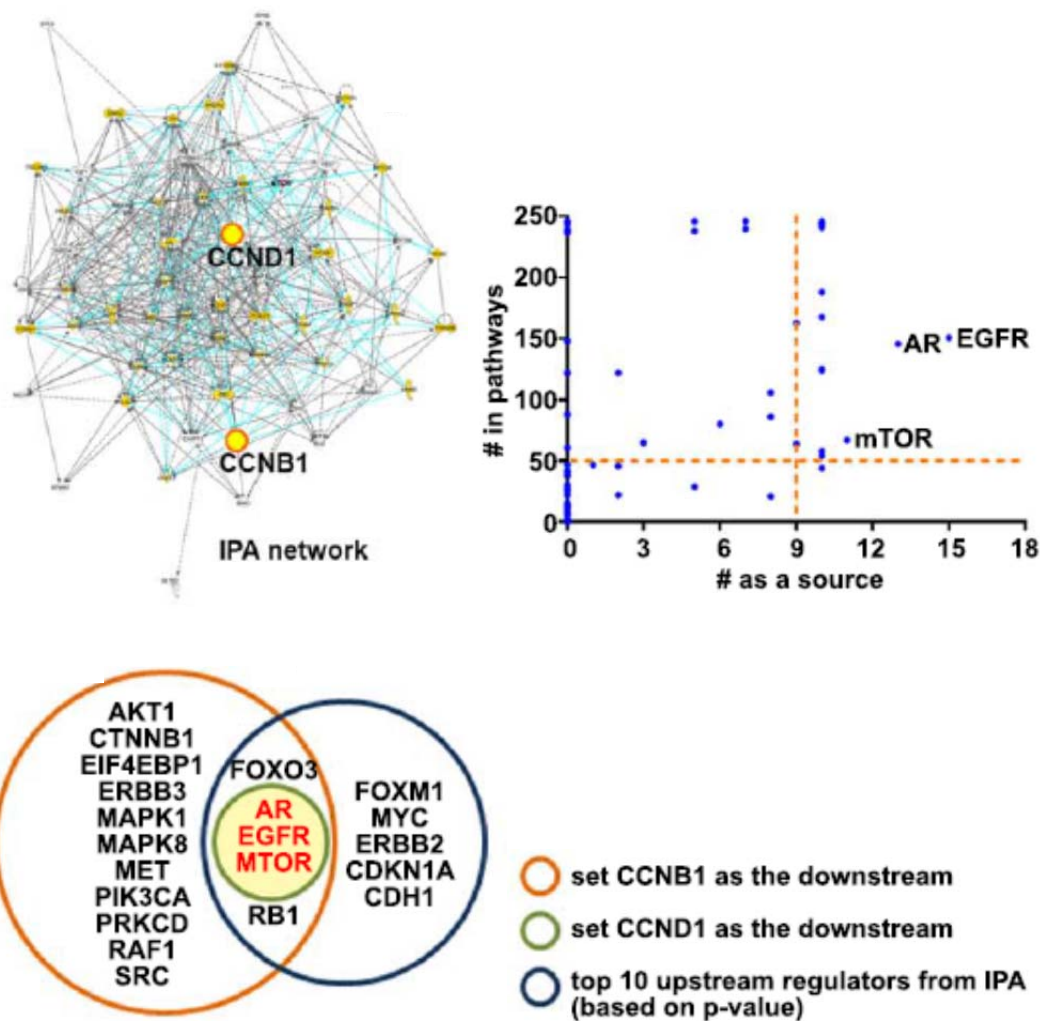


Figure 10 The final step for RPPA data analysis-the IPA network and the Ford-Fulkerson algorithm

We generated the network in IPA and the scatter plot represented the calculation result based on the Ford-Fulkerson algorithm. The potential upstream targets (words in red) came from comparison between our calculation results and IPA upstream regulator analysis. FDR: false discovery rate.

3.2 mTOR regulates mitotic entry during recovery from IR-induced G2 arrest

We depleted mTOR by siRNA oligos in U2OS cells and treated cells with ionizing radiation (IR, 7Gy). In control groups, cell cycle progression was arrested in the G2/M phase 16 hours after IR and was recovered gradually 40 hours after IR. Cells with mTOR depletion showed impairment of cell cycle recovery after IR and more than half of cells were still in the G2/M phase (Fig. 11). We further measured the accumulations of mitotic cells trapped by paclitaxel after IR using p-H3 (S10) staining (Fig. 12). Without IR treatment, the percentages of mitotic cells were relatively similar in both control and mTOR-depleted groups. During recovery from irradiation, the mitotic cells dropped to almost zero first and then increased. Cells with mTOR depletion showed the defect in mitotic entry and statistical analysis demonstrated the significance both 24 hours and 32 hours after IR. The similarity of mitotic cell percentages in both control and mTOR-depleted groups treated with paclitaxel alone indicated the delay of mitotic entry in mTOR-depleted cells was caused by IR but not paclitaxel. We also detected expression of cell cycle regulators, including Polo-Like Kinase 1 (PLK1), Cyclin B1 and p-H3, and those protein levels were lower in mTOR-depleted cells compared to control cells at each time point after IR (Fig. 13). The results suggested that mTOR played a role in G2/M checkpoint recovery after IR, and the phenomenon in U2OS cells also found in HCT116 cells (Fig. 14) indicated the function of mTOR was not cell-type specific.

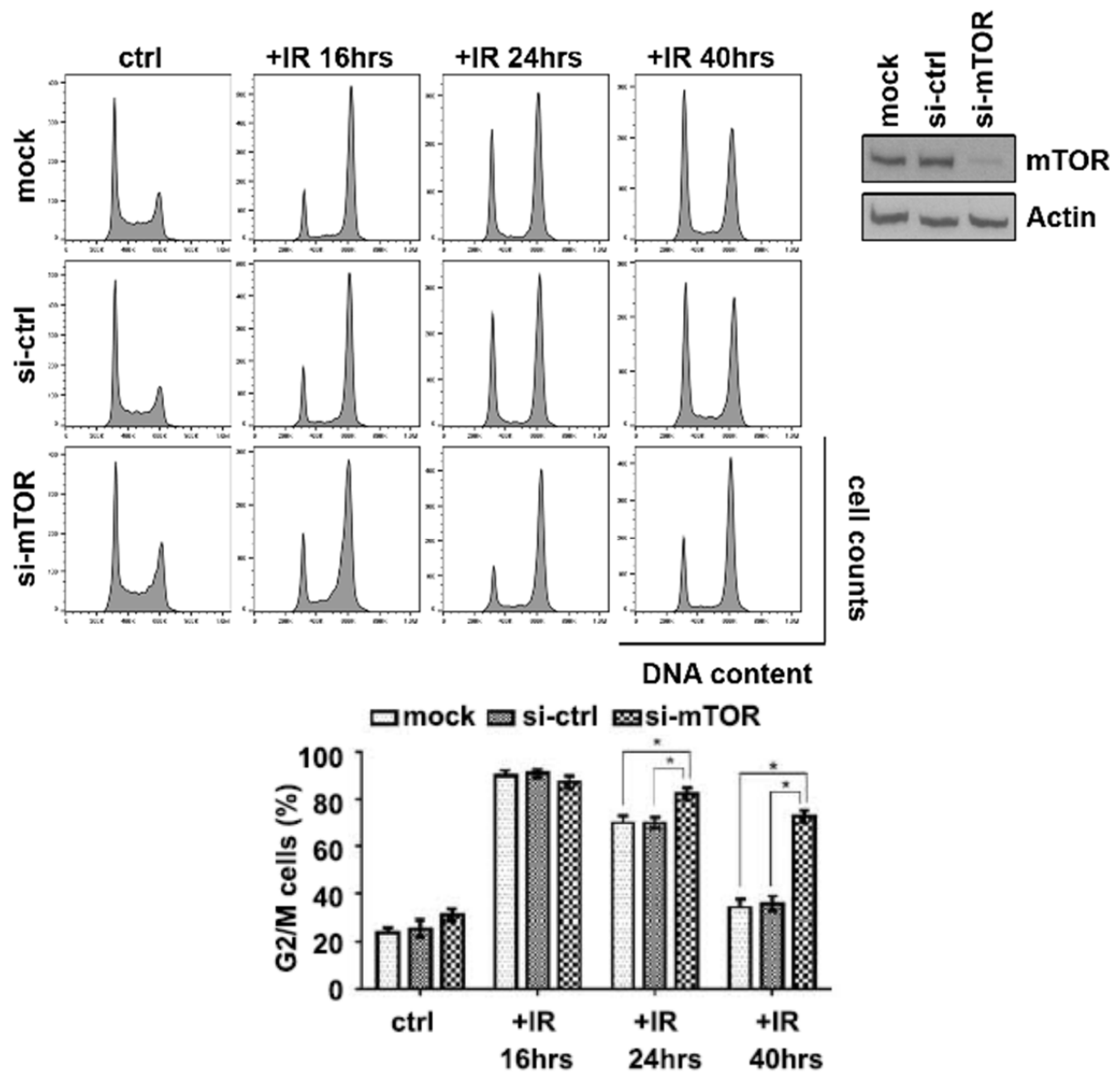


Figure 11 mTOR regulated G2/M checkpoint recovery-cell cycle analysis

U2OS cells with or without mTOR depletion were collected at different time points after IR (7Gy) for cell cycle analysis and the percentages of G2/M cells were presented in the bar graph. The depletion of mTOR was detected by western blot. Mock: cells incubated with only the transfection reagent; si-ctrl and si-mTOR: cells transfected with non-target control siRNA and mTOR siRNA; ctrl: control; error bars represent mean \pm SEM; n = 3 independent experiments; * p<0.05

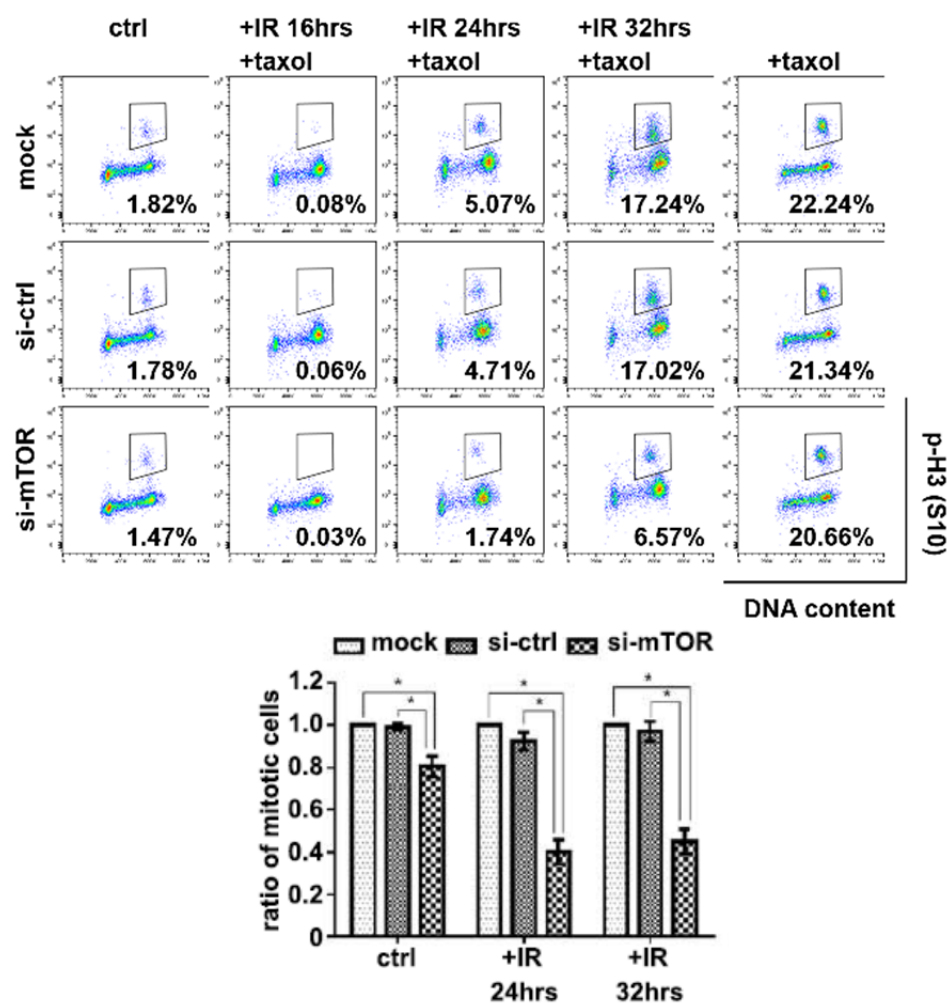


Figure 12 mTOR regulated G2/M checkpoint recovery-mitotic entry analysis

U2OS cells were treated with IR (7Gy) and 2 μ M paclitaxel following siRNA transfection. Cells were stained with PI and p-H3 for mitotic entry analysis. The numbers in representative figures indicated the percentages of mitotic cells, which were defined as positive phospho-Histone H3 (p-H3 (+)) cells with 4N DNA contents. The ratio of mitotic cells was presented as the percentage of mitotic cells in the si-ctrl or si-mTOR group relative to the percentage of mitotic cells in the mock group at each time point. Mock: cells incubated with only the transfection reagent; si-ctrl and si-mTOR: cells transfected with non-target control siRNA and mTOR siRNA; ctrl: control; error bars represent mean \pm SEM; n = 3 independent experiments; * p<0.05

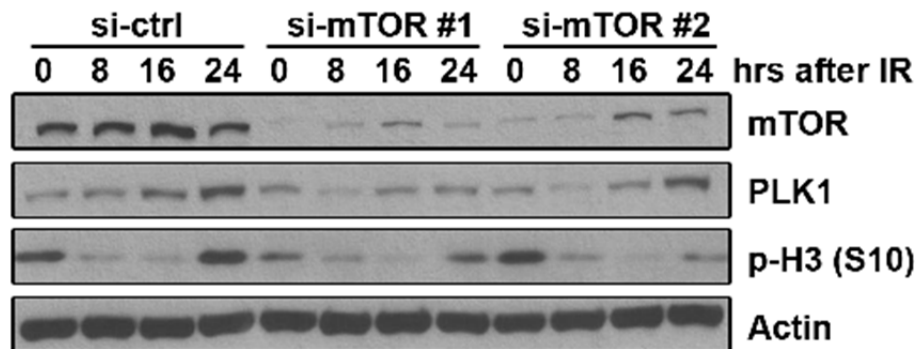
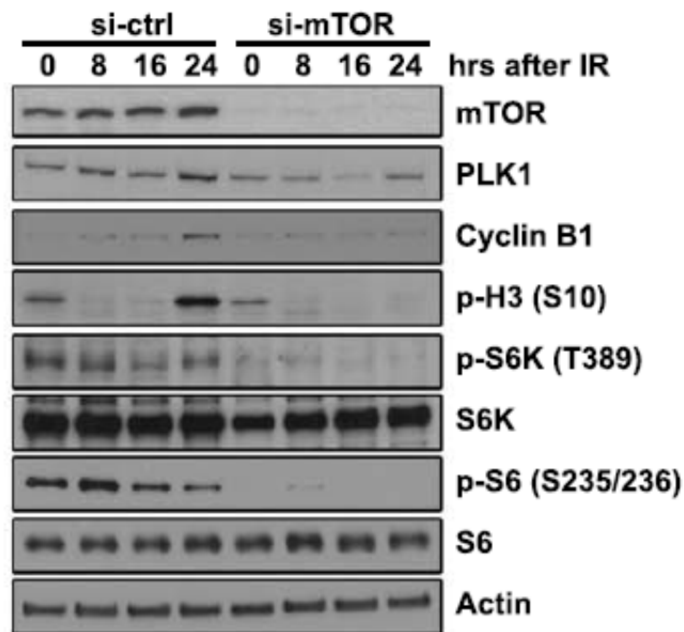


Figure 13 mTOR regulated G2/M checkpoint recovery-western blot

mTOR was depleted by either siRNA pool oligos (si-mTOR) or two individual siRNA oligos (si-mTOR #1 and #2) in U2OS cells. Protein samples at different time points were collected for immunoblot. Actin was an internal control.

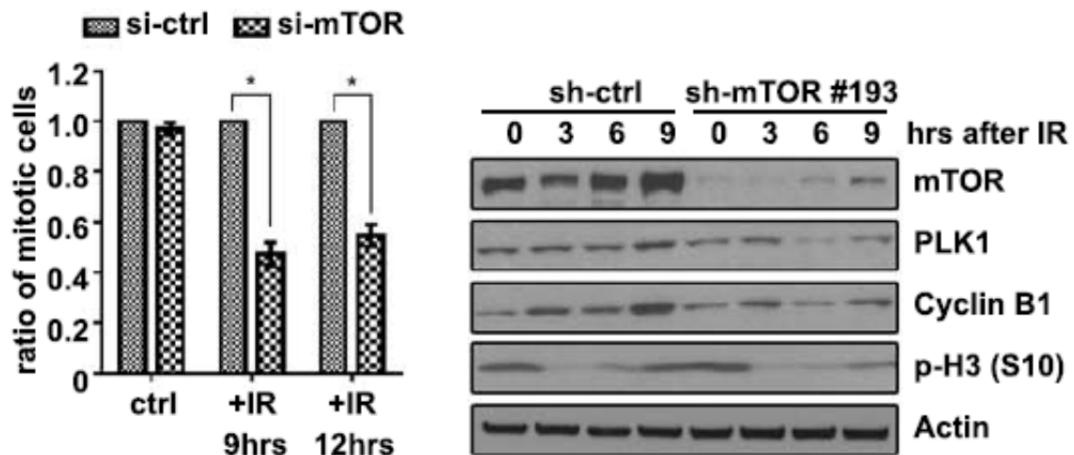
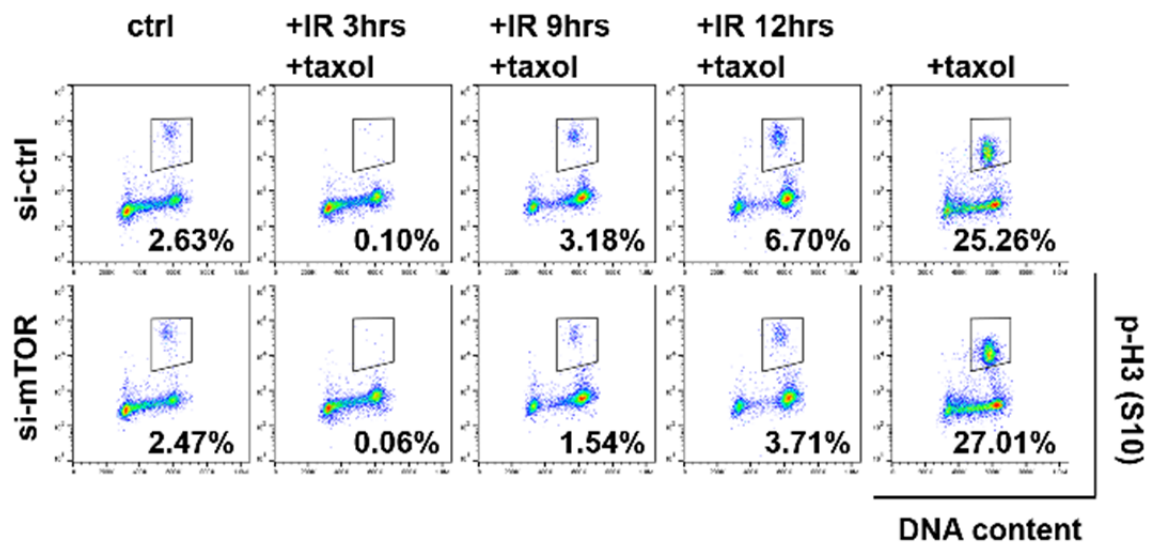


Figure 14 The function of mTOR in G2/M checkpoint recovery is not cell-type specific

We depleted mTOR by either shRNA or siRNA in HCT116 cells and treated cells with IR (7Gy) plus 2 μ M paclitaxel for mitotic entry analysis and immunoblot. si-ctrl and si-mTOR: cells transfected with non-target control siRNA and mTOR siRNA; ctrl: control; error bars represent mean \pm SEM; n = 3 independent experiments; * p<0.05

3.3 The mTORC1 kinase activity is required for mitotic entry after irradiation

We further tested whether mTOR in mitotic entry regulation after IR required the integrity of the mTOR complex and the kinase activity. First, we treated U2OS cells with rapamycin (mTORC1 inhibition) or KU0063794 (mTORC1/mTORC2 dual inhibition) before irradiation and paclitaxel. The percentages of mitotic cells in both drug-treated groups were less than the percentage in the DMSO group, but the difference was more dramatic during checkpoint recovery (Fig. 15). The result suggested that the function of mTOR in checkpoint recovery was through the complex and its kinase activity.

To clarify the role of the mTOR kinase activity in checkpoint recovery, we used D2338A-cKI HCT116 cells with knock-in of kinase-dead mutation (D2338A) in one allele and conditional knock-in of mutation in the other allele. After Cre-Lox recombination (+Cre), D2338A-cKI cells produced only kinase-dead mTOR (Fig. 16). We treated the cells with IR and paclitaxel as we did before. The percentage of mitotic cells and the levels of PLK1, Cyclin B1 and p-H3 during checkpoint recovery were positively correlated with the mTOR kinase activity (Fig. 17). It suggested that mTOR kinase activity was important for cell cycle recovery regulation.

We next depleted Raptor and Rictor by siRNA oligos in U2OS cells to see whether mTORC1 or mTORC2 involved in the recovery process. Raptor-depleted cells showed similar recovery defects to mTOR-depleted cells. The percentage of p-H3 positive cells during recovery from irradiation decreased in cells with Raptor or mTOR depletion, but not in cells with Rictor depletion. Reduced levels of PLK1 and p-H3 were only shown in Raptor-depleted cells during the recovery process (Fig. 18). The results

indicated that mTORC1 but not mTORC2 was required in the recovery process of cellular response to irradiation.

We further confirmed the results by depletion of amino acid which controls the activation of mTORC1. In cells without IR treatment, amino acids withdrawal from 10% to 0.01% decreased mitotic cell population. After IR and paclitaxel treatment, the percentages of mitotic cells in the condition of amino acids withdrawal dropped more compared to cells without IR treatment (Fig. 19). The results suggested that amino acids mediated the mitotic entry possibly through the kinase activity of mTORC1.

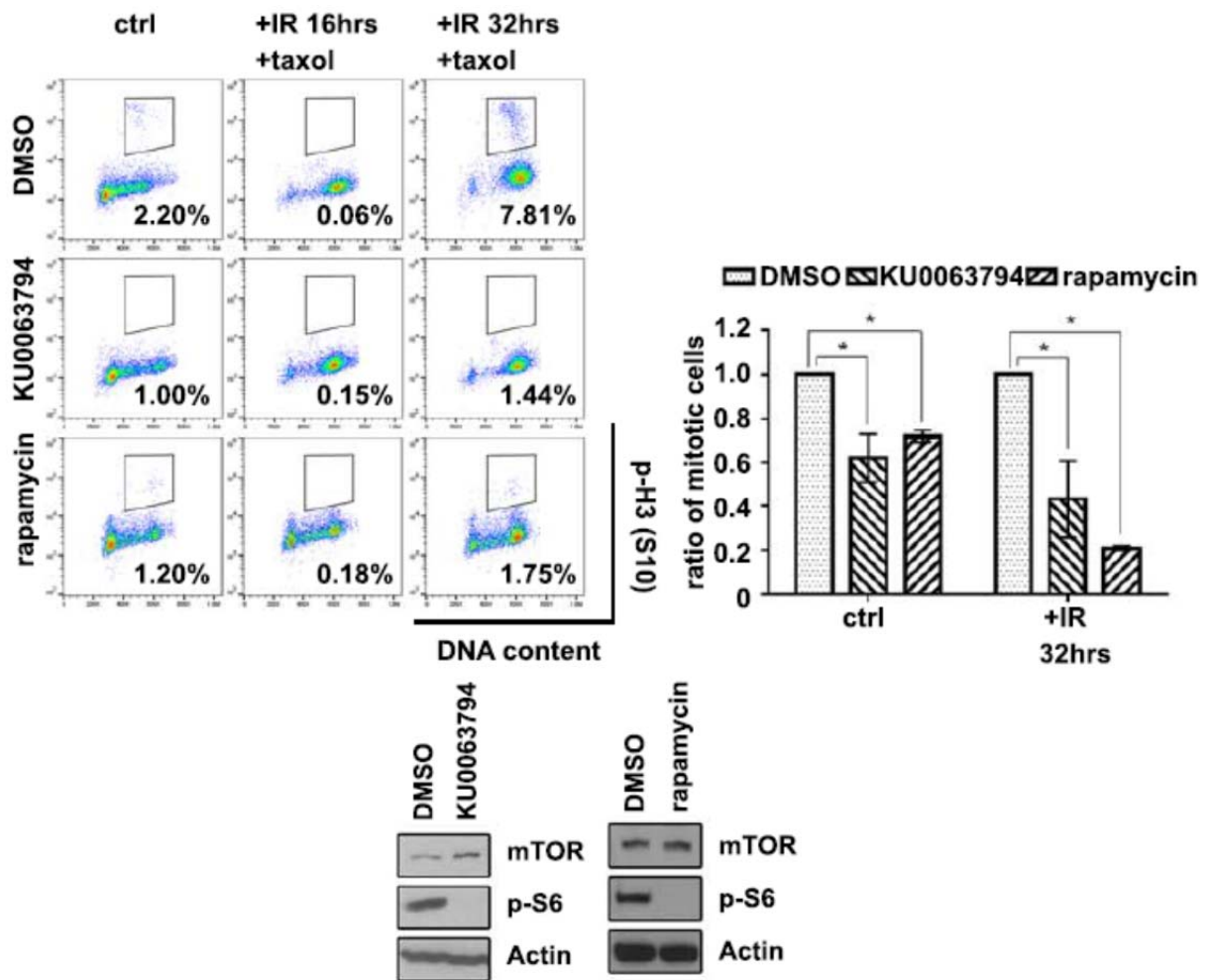


Figure 15 The mTOR activity is required for recovery from IR-induced G2 arrest

U2OS cells were incubated with DMSO, 20nM rapamycin or 1μM KU0063794 for 12 hours before exposed to IR (7Gy) and 2μM paclitaxel. We stained cells with PI and p-H3 for mitotic entry analysis. The numbers indicated the percentages of positive p-H3 stained cells detected by flow cytometry. The ratio of mitotic cells in rapamycin or KU0063794 groups was normalized to mitotic cells (%) in DMSO group at each time point. Efficiency of mTOR inhibition by rapamycin or KU0063794 was detected by western blot. ctrl: control; error bars represent mean \pm SEM; n = 3 independent experiments; * p<0.05

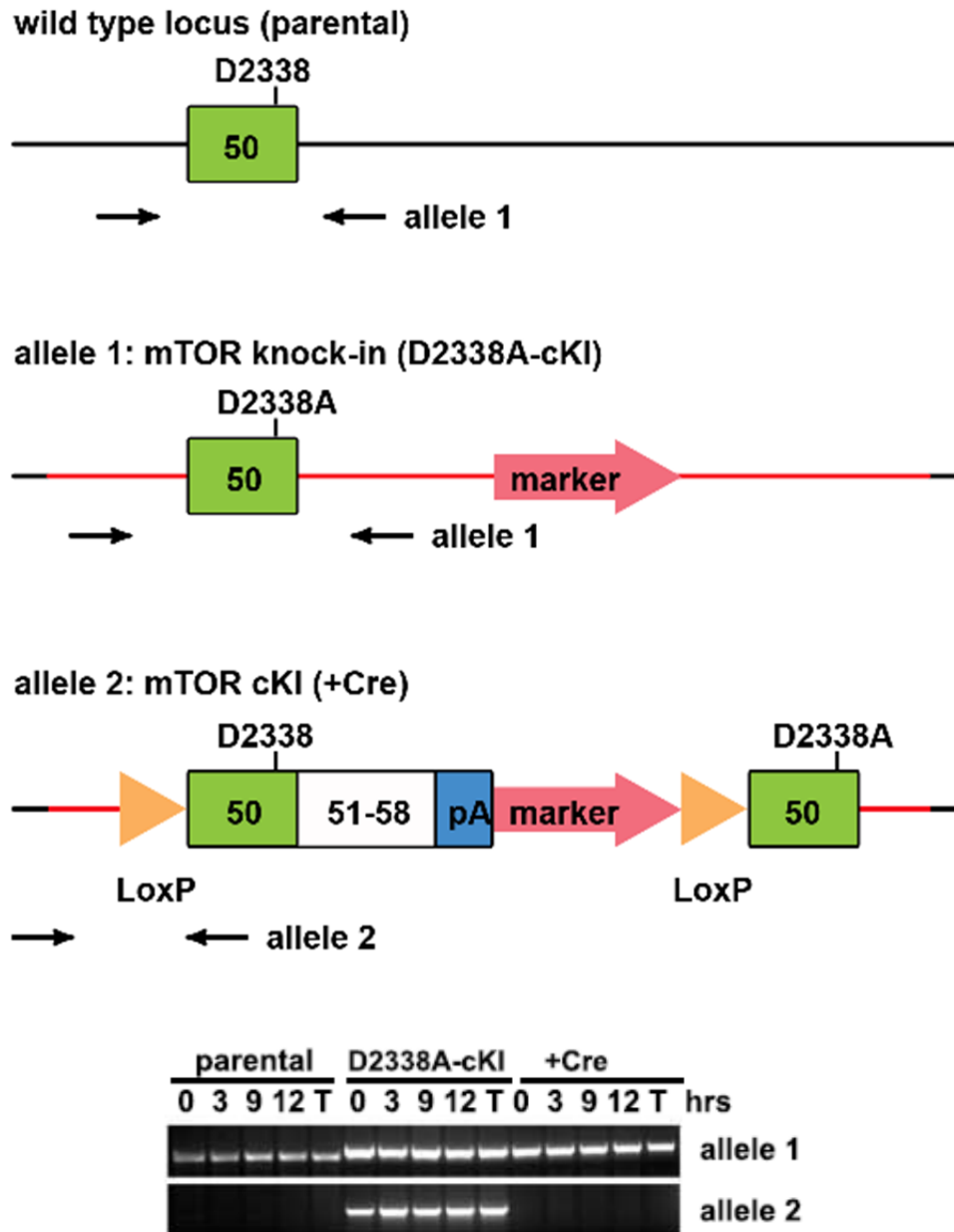


Figure 16 The structure and the test of mTOR conditional knock-in cell line

The graphs illustrated genomic structures of mTOR conditional knock-in cell line (D2338A-cKI) and primers (black arrows) identifying allele 1 and cre-excised allele 2. We followed the manufacturer's instruction to generate cells with mTOR kinase-dead mutation (D2338A) using cre-lox recombination system. PCR products on the agarose gel indicated efficiency of Cre recombinase.

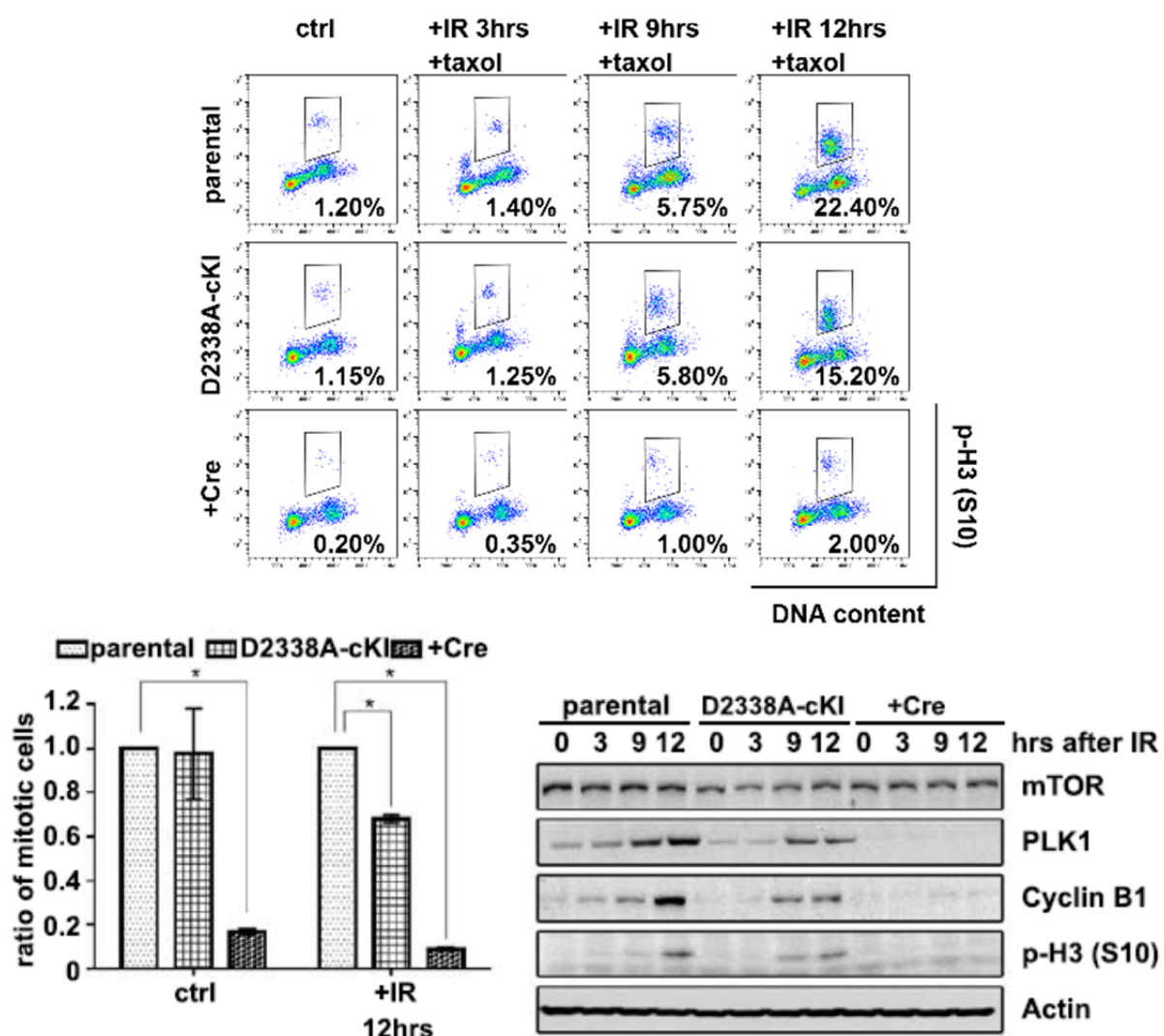


Figure 17 The mTOR kinase activity is required for the recovery from IR-induced G2 arrest

mTOR kinase-dead conditional knock-in HCT116 cells (D2338A-cKI) were stabilized after infected by Ad5-CMV-empty or Ad5-CMV-Cre virus particles (Vector Development Laboratory). Stabilized cells were collected 3, 9 and 12 hours after IR (7Gy) and 2μM paclitaxel treatment for mitotic entry analysis and western blot. The graph presented the ratio of mitotic cells normalized to the parental cell line (wild-type HCT116) at different time points. Error bars represent mean ± SD; n = 3 independent experiments;

* p<0.05

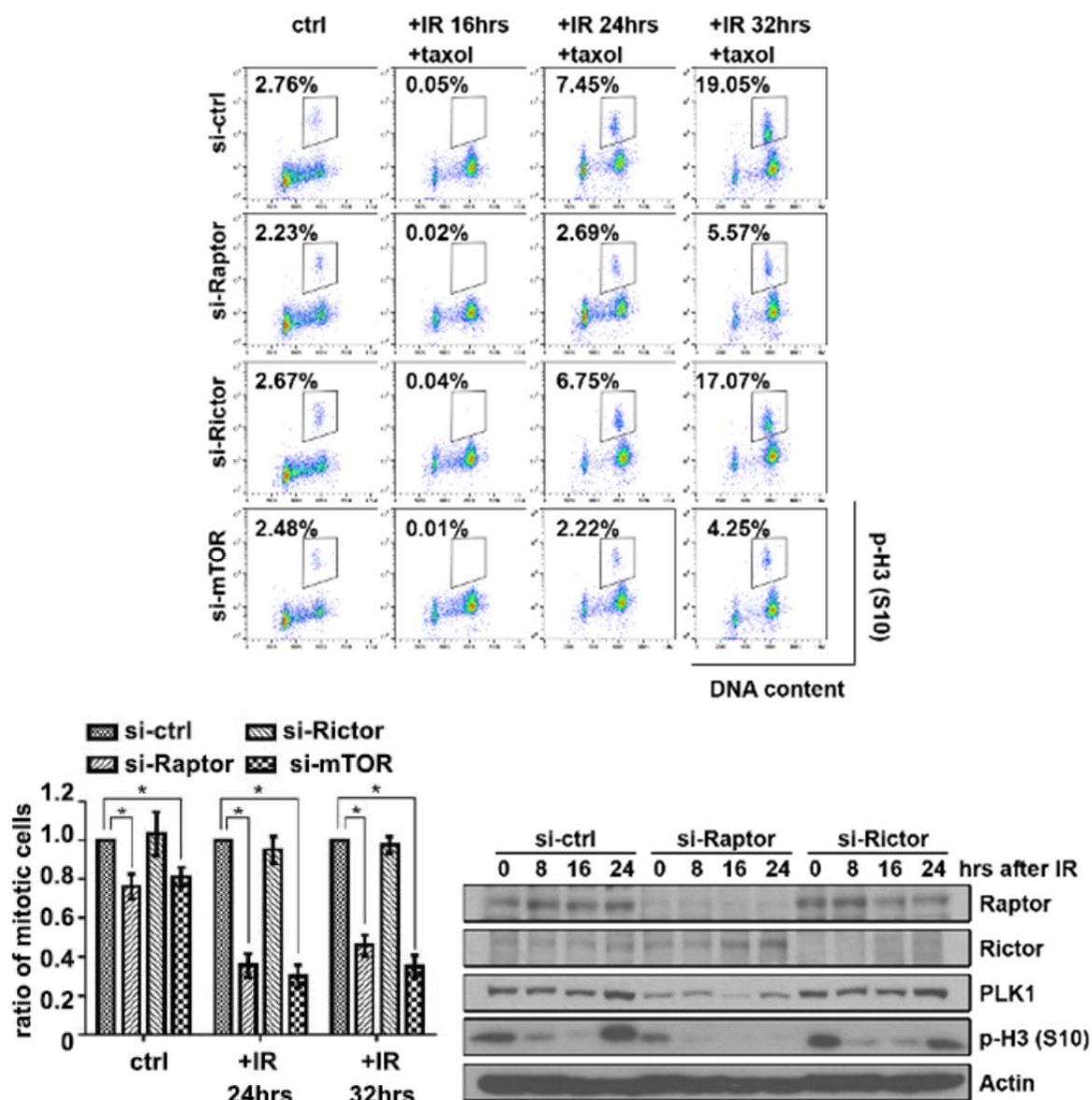


Figure 18 The mTORC1 kinase activity is required for the recovery from IR-induced G2 arrest

U2OS cells with control, Raptor, Rictor, or mTOR siRNA (si-ctrl, si-Raptor, si-Rictor, or si-mTOR) were exposed to IR (7Gy) plus 2 μ M paclitaxel for mitotic entry analysis and western blot. The numbers shown in flow cytometry graphs were the percentages of p-H3 (+) cells. The analysis is similar to previous description. Error bars represent mean \pm SEM; n = 3 independent experiments; * p<0.05

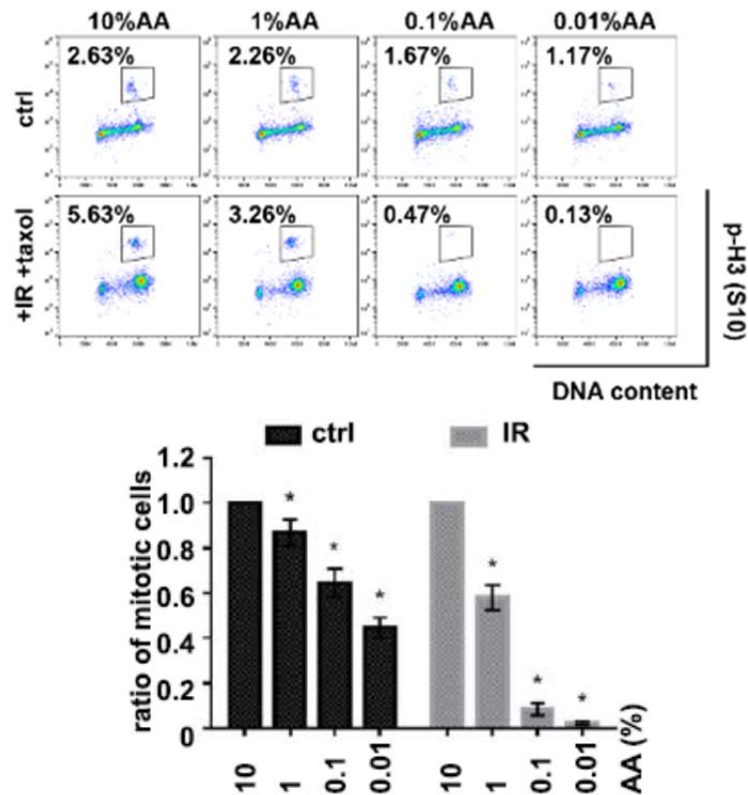


Figure 19 The amino acid withdrawal experiment confirmed that mTORC1 is required for G2/M checkpoint recovery

U2OS cells were incubated with different low concentrations of amino acids (AA, the regular medium contains 100%AA) for 28 hours, and these amino-acid-starved cells were treated with IR (7Gy) and 2 μ M paclitaxel for mitotic entry analysis. The ratio of mitotic cells in the bar graph was relative to the mitotic cell percentage of the 10% AA medium group (set as 1). ctrl: control; error bars represent mean \pm SD; n = 3 independent experiments; * p<0.05

3.4 mTORC1 functions as positive transcription regulator of *CCNB1* and *PLK1*

To understand how mTORC1 controls expression of cell cycle regulators, including Cyclin B1 and PLK1, we measured the mRNA levels of *CCNB1* and *PLK1* (encoding protein Cyclin B1 and PLK1) in U2OS cells. Both *CCNB1* and *PLK1* mRNA levels decreased first and then increased after IR treatment. In mTOR-depleted cells, the basal mRNA levels of *CCNB1* and *PLK1* were lower but the increase of mRNA expression after IR was even less compared to control cells (Fig. 20). The change of *CCNB1* and *PLK1* mRNA levels in Raptor-depleted cells was similar to the changes in mTOR-depleted cells, but not in Rictor-depleted cells (Fig. 21). The results supported that mTORC1 regulated *CCNB1* and *PLK1* expression at the transcription level.

We further performed the dual luciferase assay to validate the function of mTOR in *CCNB1* and *PLK1* transcription regulation. The luciferase activities driven by *CCNB1* and *PLK1* promoters (*CCNB1*-luciferase, *PLK1*-luciferase) were lower in mTOR-depleted cells (Fig. 22). On the other hand, *PLK1*-luciferase activities were higher in cells overexpressing wild-type mTOR compared to cells overexpressing empty vector or catalytic-dead mTOR (Fig. 23). The results indicated that the mTOR kinase activity was involved in transcriptional regulation of cell cycle proteins.

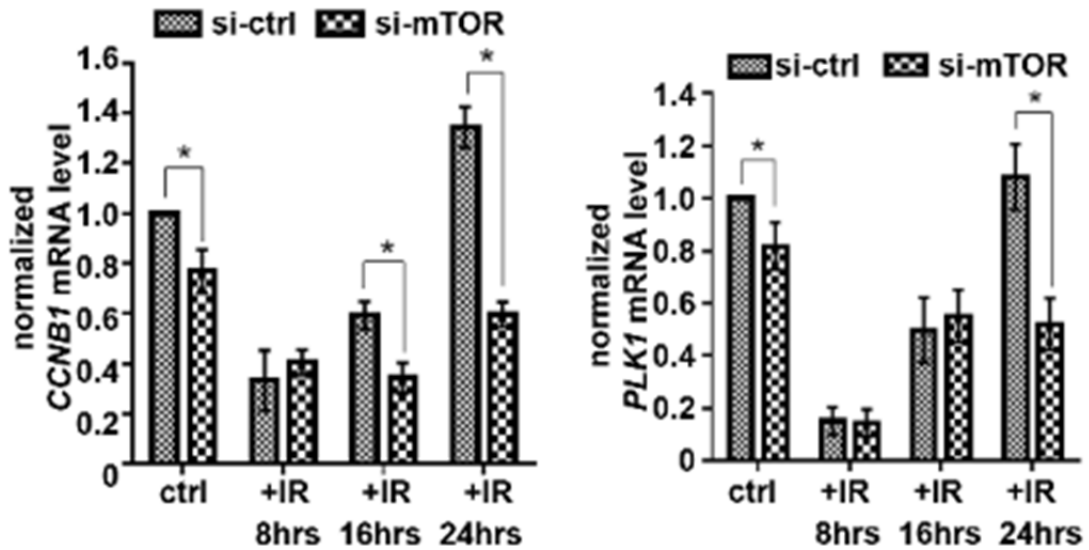


Figure 20 The mTOR expression level was associated with *CCNB1* and *PLK1* transcription

U2OS cells transfected with siRNAs were collected at different time points after IR (7Gy) and 2 μ M paclitaxel treatment. *CCNB1* and *PLK1* mRNA levels were measured by qPCR and normalized by *actin*. In the bar graphs, each normalized mRNA level of *CCNB1* or *PLK1* was relative to the level in the si-ctrl group without treatment (ctrl in si-ctrl, set as 1). si-ctrl and si-mTOR: cells transfected with non-target control siRNA and mTOR siRNA; ctrl: control; error bars represent mean \pm SD; n = 3 independent experiments; * p<0.05

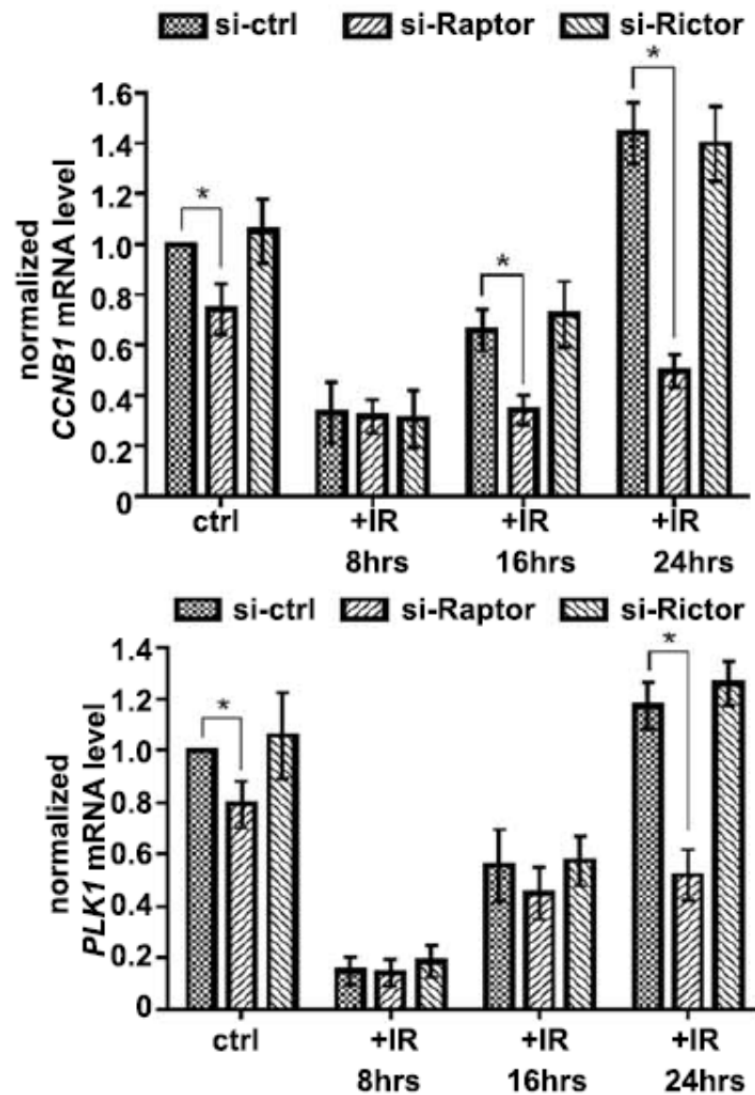


Figure 21 The Raptor expression level was associated with *CCNB1* and *PLK1* transcription

The experiments were exactly the same with Figure 20, but U2OS cells were transfected with different siRNAs. si-ctrl, si-Raptor, and si-Rictor: cells transfected with non-target control siRNA, Raptor, and Rictor siRNA; ctrl: control; error bars represent mean \pm SD; n = 3 independent experiments; * p < 0.05

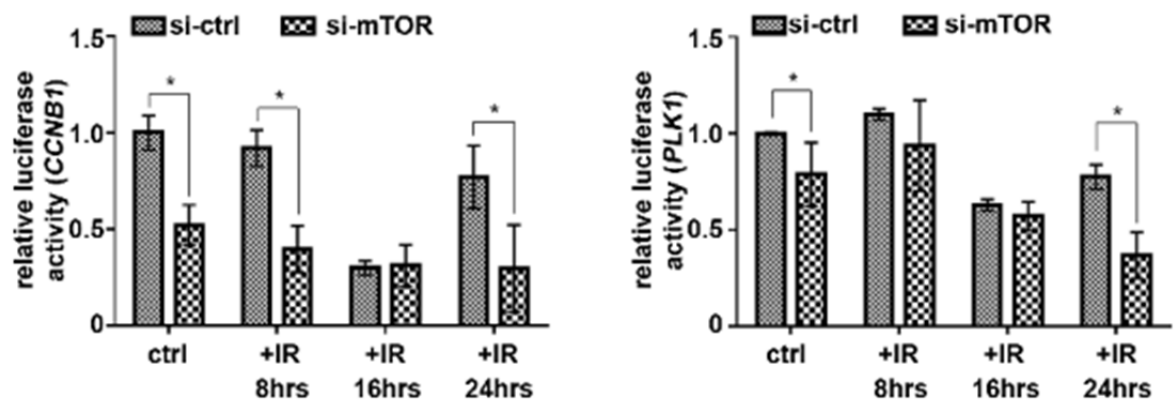


Figure 22 The dual luciferase assay showed the requirement of mTOR in *CCNB1* and *PLK1* transcription regulation.

The dual-luciferase reporter assay was conducted in U2OS cells with control or mTOR siRNA. The value of firefly-luciferase driven by the *CCNB1* or *PLK1* promoter was normalized with the value of renilla-luciferase. In the bar graph, normalized values at different time points were relative to the value in the si-ctrl group without IR treatment. si-ctrl and si-mTOR: cells transfected with non-target control siRNA and mTOR siRNA; ctrl: control; error bars represent mean \pm SD; n = 3 independent experiments; * p<0.05

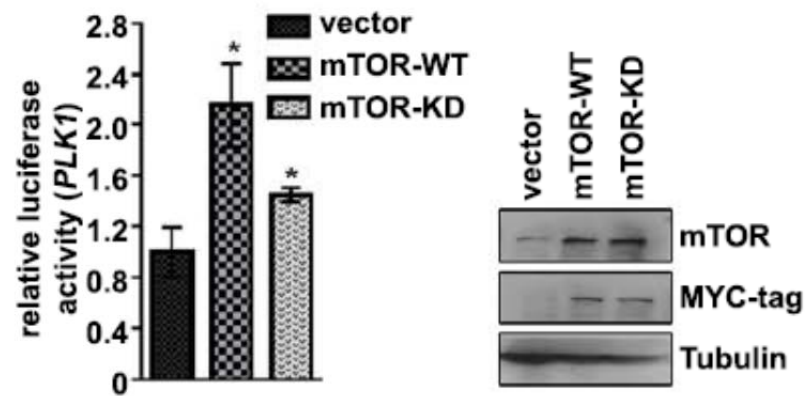


Figure 23 The dual luciferase assay confirmed the function of mTOR in *CCNB1* and *PLK1* transcription regulation through mTOR over-expression.

We also used dual-luciferase reporter assay in U2OS cells expressing control vector (vector), wild-type mTOR (mTOR-WT) or kinase-dead mTOR (mTOR-KD) construct. The normalized value in the vector group was set as 1. Error bars represent mean \pm SD; n = 3 independent experiments; * p<0.05

3.5 mTOR controls transcription of *CCNB1* and *PLK1* through KDM4B

It is known that histone lysine demethylase 4B (KDM4B) activates transcription of Myb-related protein B (B-myb)-regulated genes, such as *CCNB1* and *PLK1* (77). We depleted either mTOR or KDM4B and treated U2OS cells with IR and paclitaxel. We found that Cyclin B1 levels decreased during checkpoint recovery in KDM4B-depleted cells and mTOR-depleted cells. KDM4B level decreased in mTOR-depleted cells but mTOR level remained the same in KDM4B-depleted cells. The decrease of KDM4B in mTOR-depleted cells was more dramatic during checkpoint recovery (Fig. 24). The phenomenon was repeatable in HCT116 cells (Fig. 25). Cells treated with rapamycin also decreased expression of KDM4B, but KDM4B level had no change when we treated cells with AKT inhibitor, MK2206 (Fig. 26). It indicated that mTORC1 was the major complex which controlled KDM4B expression. Next we depleted KDM4B and the percentage of mitotic cells decreased after IR and paclitaxel treatment (Fig. 27). The results suggested KDM4B could be a potential link between mTOR and transcriptional control.

We then performed the ChIP-pPCR assay. The results showed that KDM4B was associated with the 5'-untranslated region (5'-UTR) of *CCNB1* close to the promoter region, and the association was stronger 4 hours after IR treatment, which is earlier than the increase of Cyclin B1 expression (Fig. 28). In the control group, the increased association of KDM4B, the decreased association of H3K9me3, and the increased association of B-myb with *CCNB1* gene during G2/M checkpoint recovery suggested that KDM4B epigenetically controlled expression of *CCNB1*. In the mTOR-depleted group, the decrease of KDM4B, the increase of H3K9me3, and the decrease of B-myb in downstream of *CCNB1* promoter region suggested that decreased expression of

KDM4B in mTOR-depleted cells affected the transcription of *CCNB1* (Fig. 29). We then treated cells with MG132, the proteasome inhibitor, and found that mTOR may regulate KDM4B stability through proteasome (Fig. 30).

In mTOR-depleted cells, we did not observe the increase of IR-induced DNA damage through comet assay (Fig. 31). The activations of ATM and ATR pathways were also intact (Fig. 32). Protein expression of KDM4B, PLK1 and Cyclin B1 in ATM-depleted cells were relatively the same as expression in control cells (Fig. 33). The results indicated that the function of mTOR in checkpoint recovery was independent to DNA damage pathways which also controlled checkpoints.

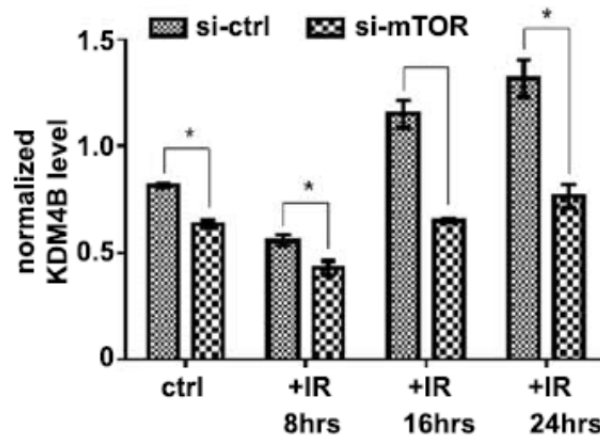
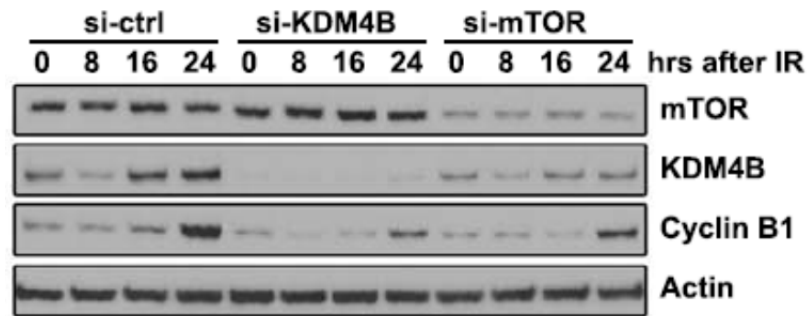


Figure 24 KDM4B linked mTOR to Cyclin B expression

U2OS cells transfected with siRNAs were collected at different time points after IR (7Gy) and 2 μ M paclitaxel treatment for western blot. The bar graph showed the normalized KDM4B protein expression level by Actin (the internal control) in each group. si-ctrl, si-KDM4B and si-mTOR: cells transfected with non-target control siRNA, KDM4B and mTOR siRNA; ctrl: control; error bars represent mean \pm SD; n = 3 independent experiments; * p<0.05

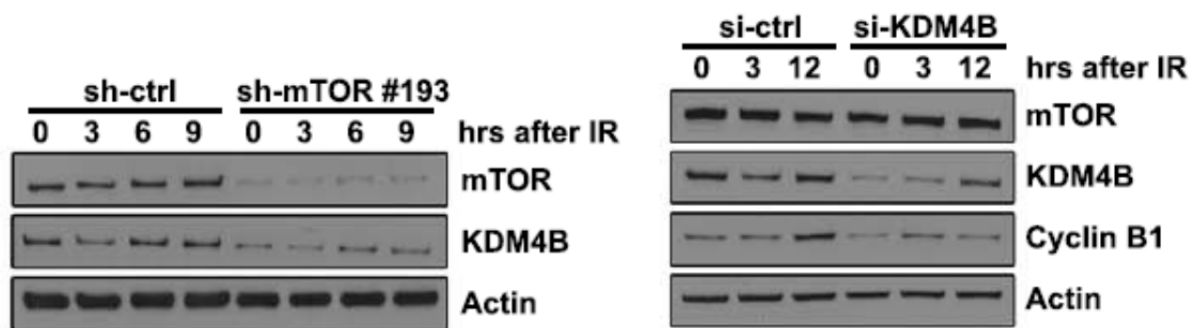


Figure 25 Regulation of KDM4B expression by mTOR was not U2OS cell-specific

We depleted mTOR by an individual shRNA (sh-mTOR #193) or depleted KDM4B by siRNA in HCT116 cells and treated cells with IR (7Gy) plus 2 μ M paclitaxel for western blot.

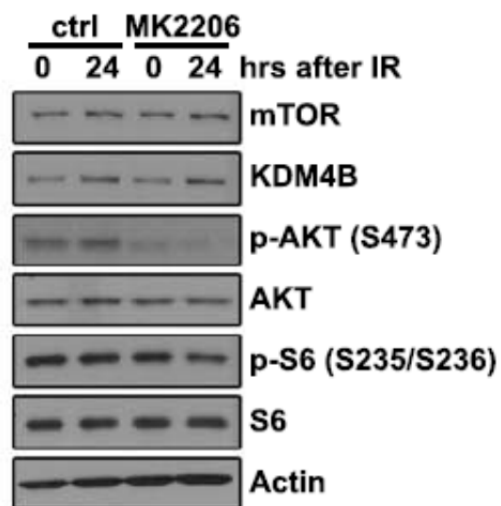


Figure 26 KDM4B expression was not affected by the AKT inhibitor

U2OS cells were pretreated with the AKT inhibitor MK2206 followed by IR (7Gy) and 2 μ M paclitaxel for immunoblot. ctrl: control

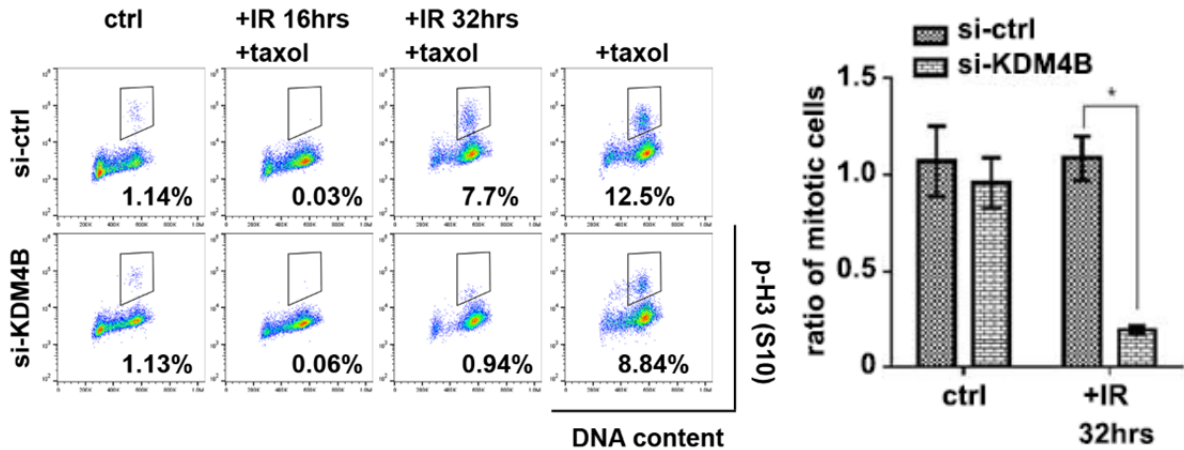


Figure 27 KDM4B was required for mitotic entry after irradiation

U2OS cells with control or KDM4B siRNAs were exposed to IR (7Gy) and 2 μ M paclitaxel for different periods of time. We stained cells with PI and p-H3 for mitotic entry analysis. The numbers in flow cytometry representative graphs indicated the percentages of positive p-H3 stained cells. In the bar graph, the percentages of mitotic cells in the KDM4B-depletion group at each time point were normalized to the percentages of mitotic cells in the control group. si-ctrl and si-KDM4B: cells transfected with non-target control siRNA and KDM4B siRNA; ctrl: control; error bars represent mean \pm SD; n = 3 independent experiments; * p<0.05

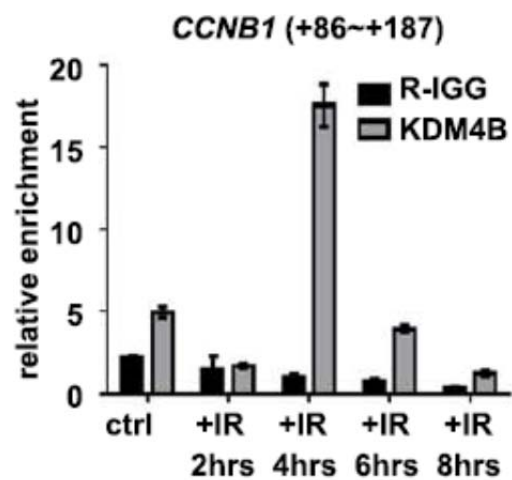


Figure 28 KDM4B was associated with *CCNB1* gene

Quantitative ChIP in the 5'-untranslated region (5'-UTR) close to the *CCNB1* promoter region was performed at different time points after irradiation. R-IGG: rabbit immunoglobulin G; ctrl: control; error bars represent mean \pm SD; n = 3 independent experiments

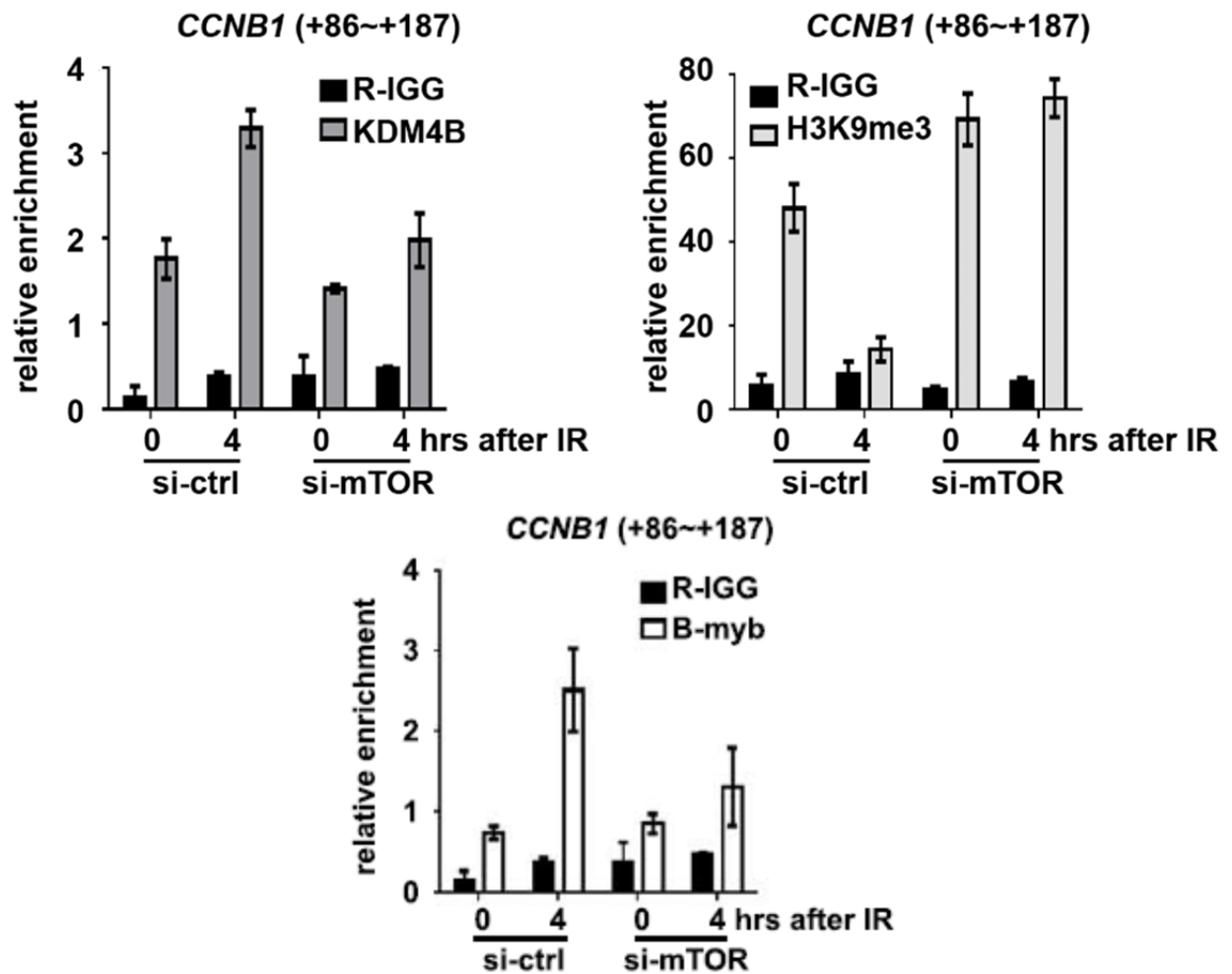


Figure 29 KDM4B links mTORC1 to transcriptional control of *CCNB1*

U2OS cells treated with IR (7Gy) were collected for ChIP analysis using anti-KDM4B, anti-H3K9me3 or anti-B-myb antibody. The immunoprecipitated DNA fragments were amplified with the primer to *CCNB1* gene (+86 to +187). The bar graphs represented the amount of precipitated DNA normalized to total input chromatin. si-ctrl and si-mTOR: cells transfected with non-target control siRNA and mTOR siRNA; ctrl: control; error bars represent mean \pm SD; n = 3 independent experiments; * p < 0.05

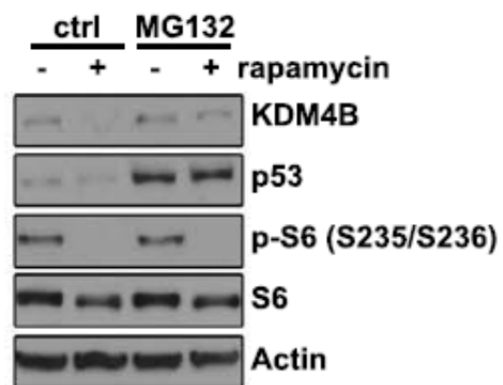


Figure 30 Regulation of KDM4B expression by mTOR was probably through proteasome degradation

U2OS cells were pretreated with the proteasome inhibitor MG132 followed by IR (7Gy) and 2 μ M paclitaxel for immunoblot.

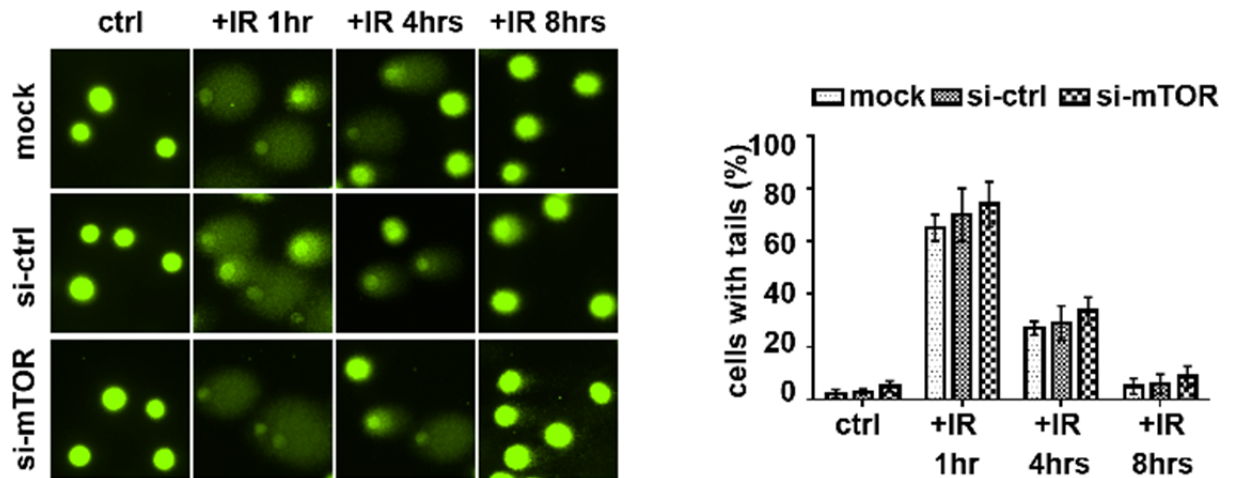


Figure 31 mTOR depletion did not affect IR-induced DNA breaks and repairs

U2OS cells were transfected with control siRNA, mTOR siRNA, or without siRNA, and were collected at different time points after IR (7Gy) for Comet assay. Representative images showed the changes of comet tails after IR treatment. We counted 50 cells in each group and statistical analysis was performed as the percentage of damaged cells in each group. Mock: cells incubated with only the transfection reagent; si-ctrl and si-mTOR: cells transfected with non-target control siRNA and mTOR siRNA; ctrl: control; error bars represent mean \pm SD; n = 3 independent experiments

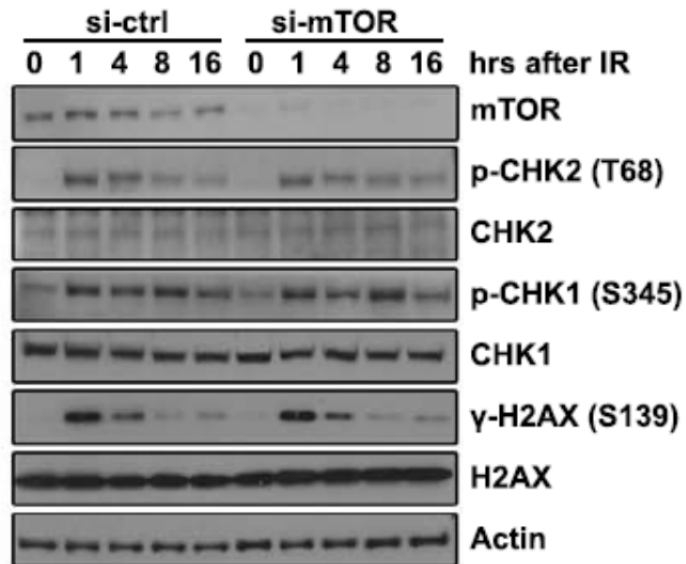


Figure 32 mTOR depletion did not affect IR-induced DNA damage response

U2OS cells were transfected with control siRNA or mTOR siRNA. The immunoblot showed the kinetics of the DNA damage response signaling after IR (7Gy). si-ctrl and si-mTOR: cells transfected with non-target control siRNA or mTOR siRNA

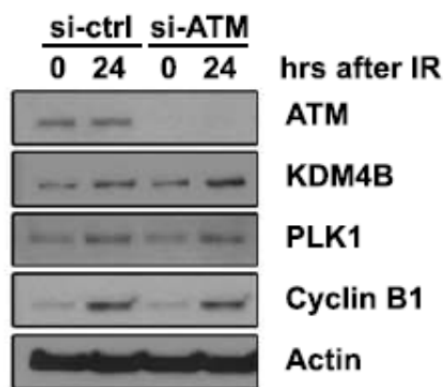


Figure 33 ATM depletion did not change expression of mitosis-related proteins

U2OS cells with control or ATM siRNAs were collected after IR (7Gy) and 2 μ M paclitaxel treatment for western blot. Mock: cells incubated with only the transfection reagent; si-ctrl and si-ATM: cells transfected with non-target control siRNA and ATM siRNA

3.6 The high mTOR kinase activity in TSC2-depleted cells promotes recovery from irradiation-induced G2 arrest

TSC2 negatively regulates mTOR signaling, especially the mTORC1 complex(78). In order to test mitotic entry after irradiation in the condition of high mTOR kinase activity, we treated TSC2-depleted (TSC2^{-/-}) and TSC2-wild type (TSC2^{+/+}) MEF cells with IR and paclitaxel. The TSC2^{-/-} group showed higher percentage of mitotic cells after IR compared to the TSC2^{+/+} group and the difference were greater in the longer period of time (Fig. 34). KDM4B, PLK1, and Cyclin B1 protein levels were higher after IR treatment in TSC2^{-/-} MEF cells (Fig. 35), and KDM4B was mostly located in the nucleus (Fig. 36). The results were the same when we depleted TSC2 in U2OS cells (Fig. 37). In conclusion, the balance of the mTOR kinase activity affects recovery from IR-induced cell cycle arrest.

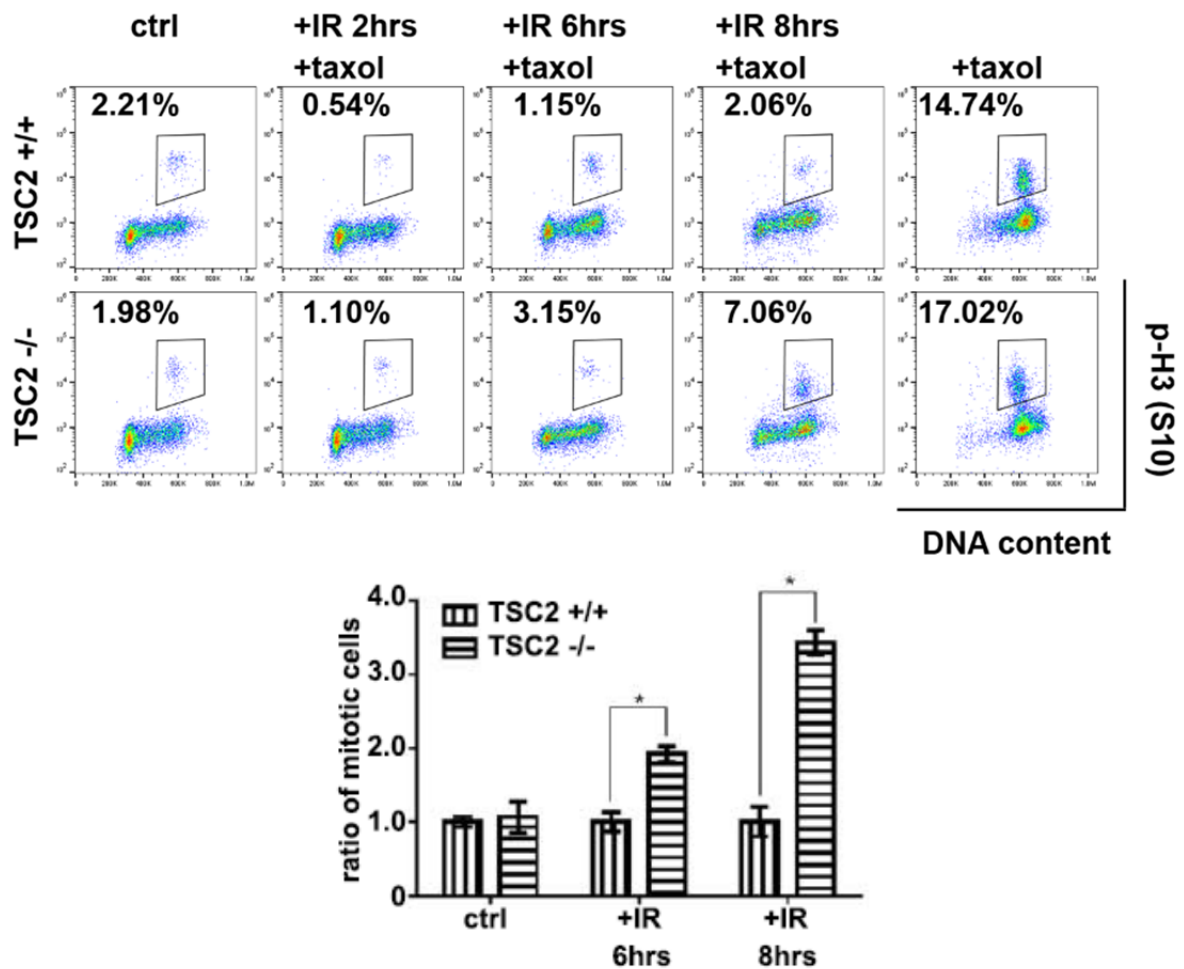


Figure 34 TSC2 depletion facilitates G2/M checkpoint recovery-mitotic entry analysis

Wild-type (TSC2 +/+) and *Tsc2*^{-/-} (TSC2 -/-) MEFs were irradiated with 15Gy followed by 2μM paclitaxel immediately at the time points indicated. Cells treated with paclitaxel alone (“+taxol” group) were collected after 8-hour treatment. Cells entered the mitosis phase were stained with p-H3 and detected by flow cytometer. The numbers in the graphs indicated the percentages of p-H3 (+) cells. The ratio of mitotic cells at each time point in the bar graph was normalized with the percentages of mitotic cells in wild-type MEFs (set as 1). ctrl: control; error bars represent mean ± SEM; n = 3 independent experiments; * p<0.05

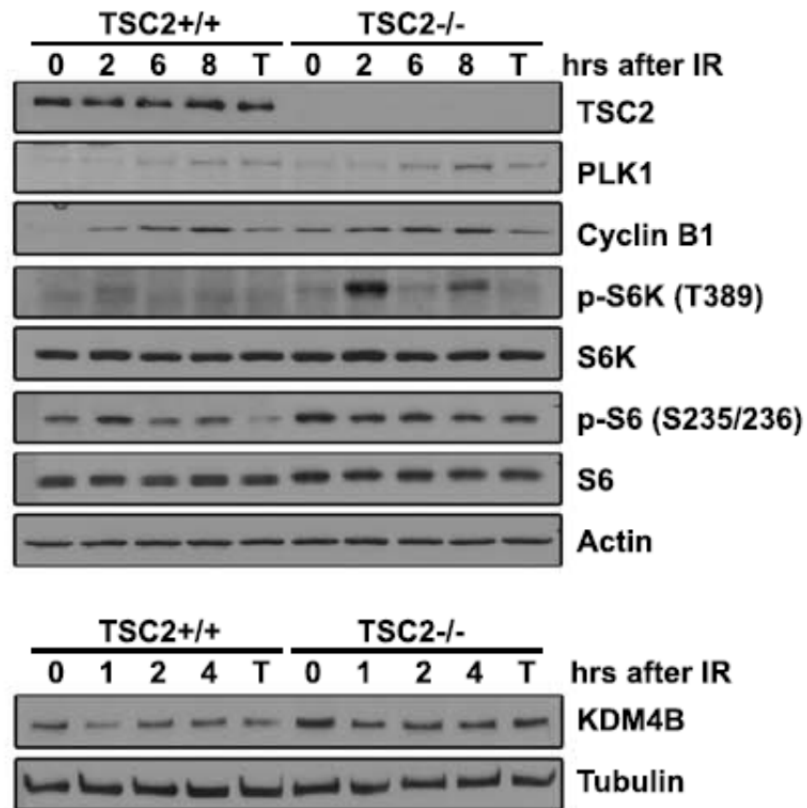


Figure 35 TSC2 depletion facilitates G2/M checkpoint recovery-western blot

Wild-type (TSC2 ^{+/+}) and *Tsc2*^{-/-} (TSC2 ^{-/-}) MEFs were irradiated with 15Gy followed by 2μM paclitaxel and collected at different time points for western blot. Actin and Tubulin were the loading control. T: paclitaxel;

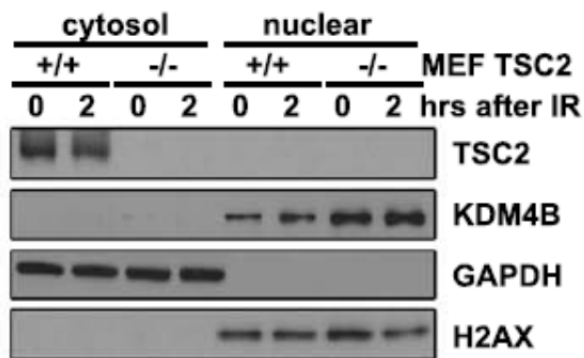


Figure 36 The change of KDM4B expression was mainly in nuclei

Wild-type (TSC2 +/+) and *Tsc2*^{-/-} (TSC2 -/-) MEFs treated with IR plus paclitaxel for two hours were separated into nuclear and non-nuclear fractions by Dounce homogenizer. GAPDH was used as the loading control in the non-nuclear fraction and H2AX was the loading control of the nuclear fraction.

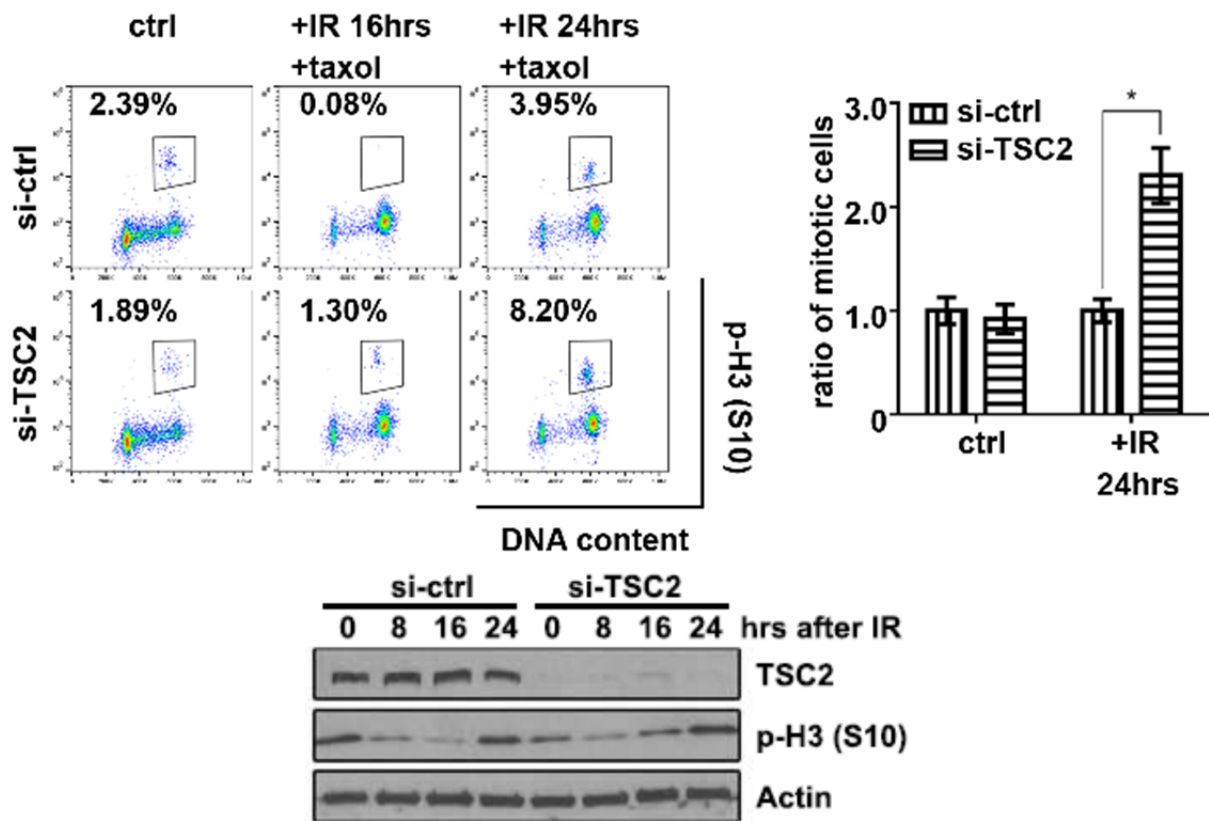


Figure 37 TSC2 depletion promotes mitotic entry after IR-induced G2 arrest

We transfected either non-target control siRNA (si-ctrl) or TSC2 siRNA pool (si-TSC2) oligos in U2OS cells and then treated cells with IR (7Gy) plus 2 μ M paclitaxel for a period of time as the graphs indicated. Mitotic cells were defined as p-H3 (+) cells which were detected by flow cytometer and the percentage in each sample was shown in graphs. The ratio of mitotic cells in each group in the bar graph was normalized using the same method as previous description. The level of p-H3 was also detected by western blot. ctrl: control; error bars represent mean \pm SEM; n = 3 independent experiments; * p<0.05

3.7 WEE1 inhibition is a therapeutic strategy for tuberous sclerosis complex

Tuberous sclerosis complex (TSC) is a disease caused by inactivating mutations in TSC2 which leads to constitutive mTORC1 activation (78). Given TSC2-depleted cells with faster G2/M checkpoint recovery, we treated TSC2^{-/-} and TSC2^{+/+} MEF cells [TSC2-knock out (TSC2^{-/-}) vs. TSC2-wild type (TSC2^{+/+}); TSC2-knock out with the empty vector (TSC2 KO) vs. TSC2-knock out with reconstituted TSC2 (TSC2 KO+ rescue)] with the WEE1 inhibitor MK1775 to accelerate premature mitotic entry of cells (79). Compared to TSC2^{+/+} MEF cells, TSC2^{-/-} MEF cells were more sensitive to MK1775 in MTT cell proliferation assay and the drug sensitivity was not due to WEE1 expression (Fig. 38). We also treated MEF cells with 0.2μM MK1775 after cells formed 3-dimensional structures in Matrigel and MK1775 caused stronger inhibition of cell proliferation in TSC2^{-/-} cells (Fig. 39). More rapid cell cycle progression (Fig. 40) with persisted γ-H2AX (Fig. 41) in TSC2^{-/-} MEF cells treated with 0.2μM MK1775 indicated that cells bypassed the checkpoint with continuous activation of DNA damage signaling pathways. In order to increase MK1775 effects, we combined MK1775 with a PARP inhibitor BMN 673, which caused DNA damage. TSC2^{-/-} MEF cells were more sensitive to the drug combination and the combination effect was better than any single drug (Fig. 42). More apoptotic cells were found in TSC2^{-/-} MEF cells treated with two drugs by Annexin V assay and Cytochrome c immunofluorescence staining (Fig. 43 and Fig. 44). The result was similar when we combined MK1775 with another PARP inhibitor olaparib (Fig. 45). Moreover, drug combination induced more multipolar mitosis and multinucleated cells in TSC2^{-/-} cells, which were the evidences of mitotic catastrophe (Fig. 46). Due to all DNA damage-related drugs with carcinogenic effects, the treatment with MK1775 plus BMN673 probably should be applied as the second line in TSC

patients. We generated rapamycin-resistant line in rat ELT3 TSC2^{-/-} cells (ELT3 V3 became ELT3 V3R, R as resistant) and treated cells with MK1775 or BMN 673. ELT3 V3R cells were still sensitive to the drug combination (Fig. 47). Those evidences supported that WEE1 and PARP1 inhibition could be a potential treatment for TSC2 patients.

To further evaluate the drug effect *in vivo*, we inoculated either rat ELT3-V3 (TSC2 null) or ELT3-T3 (with re-constitutive TSC2) cells with luciferase in bilateral posterior flanks of mice. Five weeks later we started treating mice until the average tumor size of any group reached the maximum allowable size in the animal facility. The body weight was monitored to evaluate the toxicity throughout the experiment. Although the tumor weights in both ELT3-V3 and ELT3-T3 groups did not show any significant changes after MK1775 treatment, tumor volumes and bioluminescence levels were significantly decreased after MK1775 treatment in the ELT3-V3 group but not in the ELT3-T3 group (Fig. 48). Therefore, WEE1 inhibition could be a potential strategy for TSC treatment.

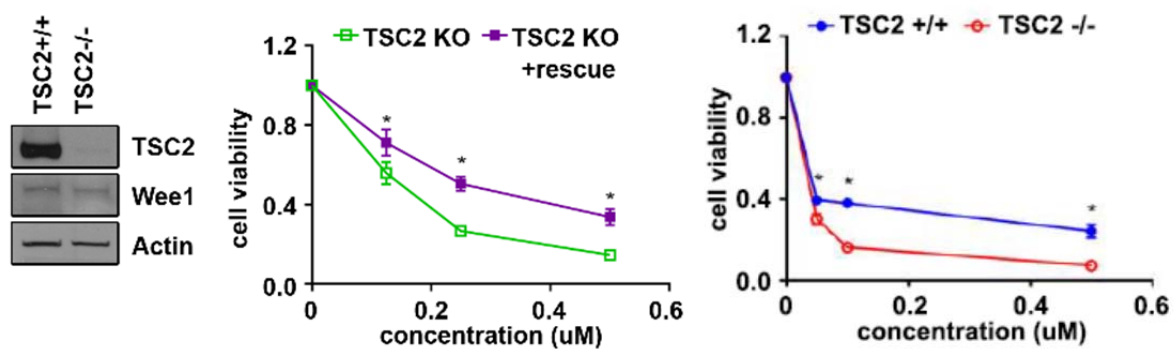


Figure 38 TSC2-null cells were more sensitive to the WEE1 inhibitor-MTT assay

The basal levels of WEE1 in TSC2 wild-type and TSC2-null MEFs were relatively the same. MEFs were treated with different concentrations of MK1775 in 96-well plates for 4 days and cell viability was measured by MTT assay. MK1775 sensitivity was presented as the ratio to the untreated group in each cell line (set as 1). TSC2 +/+ : *Tsc2*^{+/+}, *Tsc2* wild-type; TSC2 -/- and TSC2 KO: *Tsc2*^{-/-}, *Tsc2* null; TSC2 KO + rescue: *Tsc2* null cells with re-constitutive *Tsc2*; error bars represent mean \pm SD; n = 3 independent experiments; * p<0.05

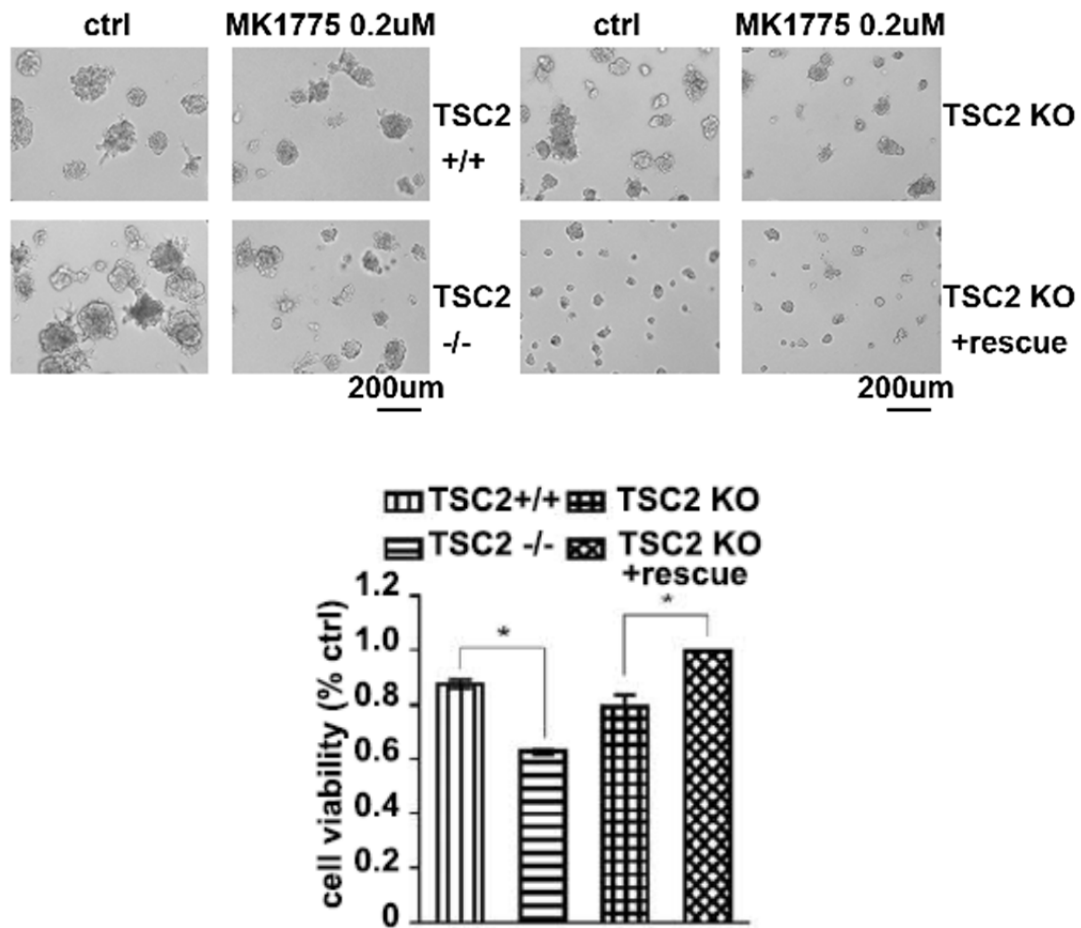


Figure 39 TSC2-null cells were more sensitive to the WEE1 inhibitor-3D culture

MEFs were embedded in Matrigel (Day 0) and started to treat with 0.2μM MK1775 from Day 3. The medium with or without MK1775 was changed every three days. The representative photos were taken on Day 10. The fluorescence value was measured by adding 10μl of PrestoBlue in 96-well plates. The graph showed the ratio of treated to untreated groups in each cell line. TSC2 +/+ : *Tsc2*^{+/+}, *Tsc2* wild-type; TSC2 -/- and TSC2 KO: *Tsc2*^{-/-}, *Tsc2* null; TSC2 KO + rescue: *Tsc2* null cells with re-constitutive *Tsc2*; error bars represent mean ± SD; n = 3 independent experiments; * p<0.05

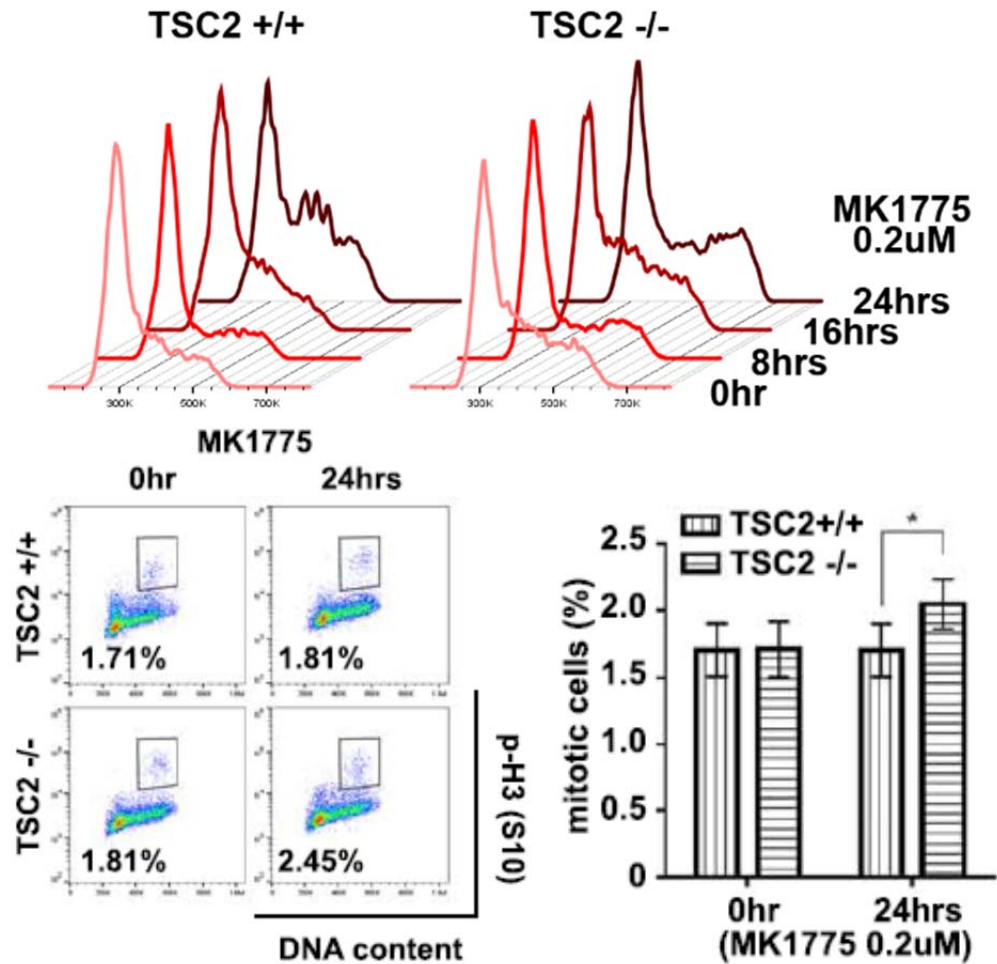


Figure 40 TSC2-null cells with WEE1 inhibition showed faster cell cycle progression into mitosis

MEFs treated with 0.2 μ M MK1775 were collected at different time points for cell cycle analysis and mitotic entry analysis. Percentages of mitotic cells were shown in representative graphs. TSC2 $+/+$: *Tsc2*^{+/+}, *Tsc2* wild-type; TSC2 $-/-$: *Tsc2*^{-/-}, *Tsc2* null; error bars represent mean \pm SD; n = 3 independent experiments; * p<0.05

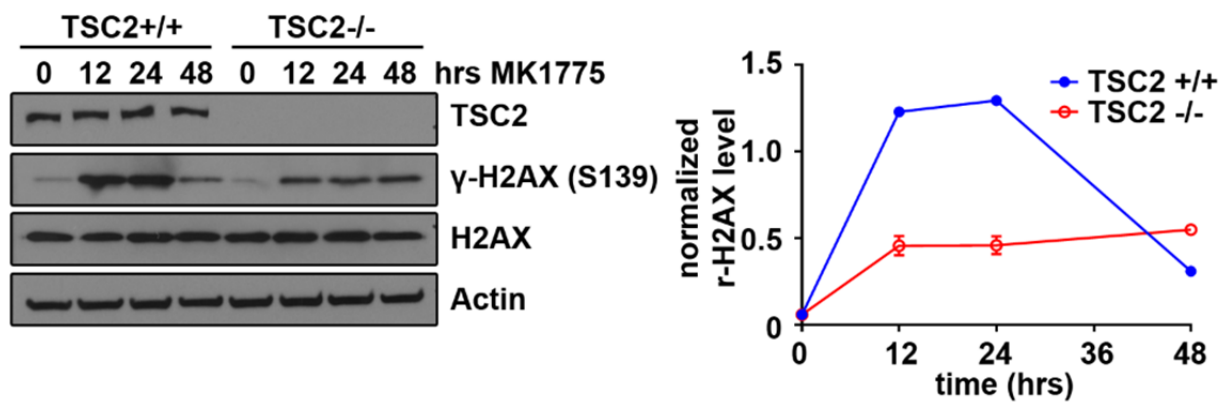


Figure 41 Prolonged WEE1 inhibition induced persistent DNA damage in TSC2-null cells

MEFs treated with 0.2μM MK1775 were collected at different time points for western blot. The graph indicated expression of γ-H2AX normalized by Actin in each group. TSC2^{+/+}: *Tsc2*^{+/+}, *Tsc2* wild-type; TSC2^{-/-}: *Tsc2*^{-/-}, *Tsc2* null; error bars represent mean ± SD; n = 3 independent experiments

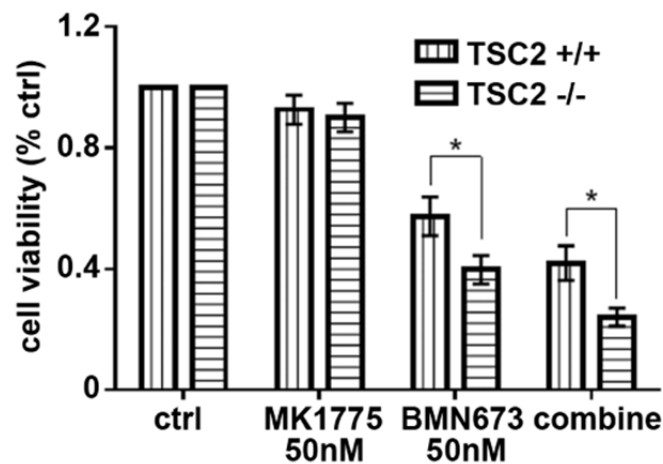


Figure 42 TSC2-null cells were more sensitive to the WEE1 inhibitor combined with the PARP inhibitor BMN 673-MTT assay

We treated MEFs with 50nM MK1775 and 50nM BMN 673 for 4 days for MTT assay. Cell viability was defined as the ratio to the untreated group. TSC2 +/+ : *Tsc2*^{+/+}, *Tsc2* wild-type; TSC2 -/- : *Tsc2*^{-/-}, *Tsc2* null; error bars represent mean ± SD; n = 3 independent experiments; * p<0.05

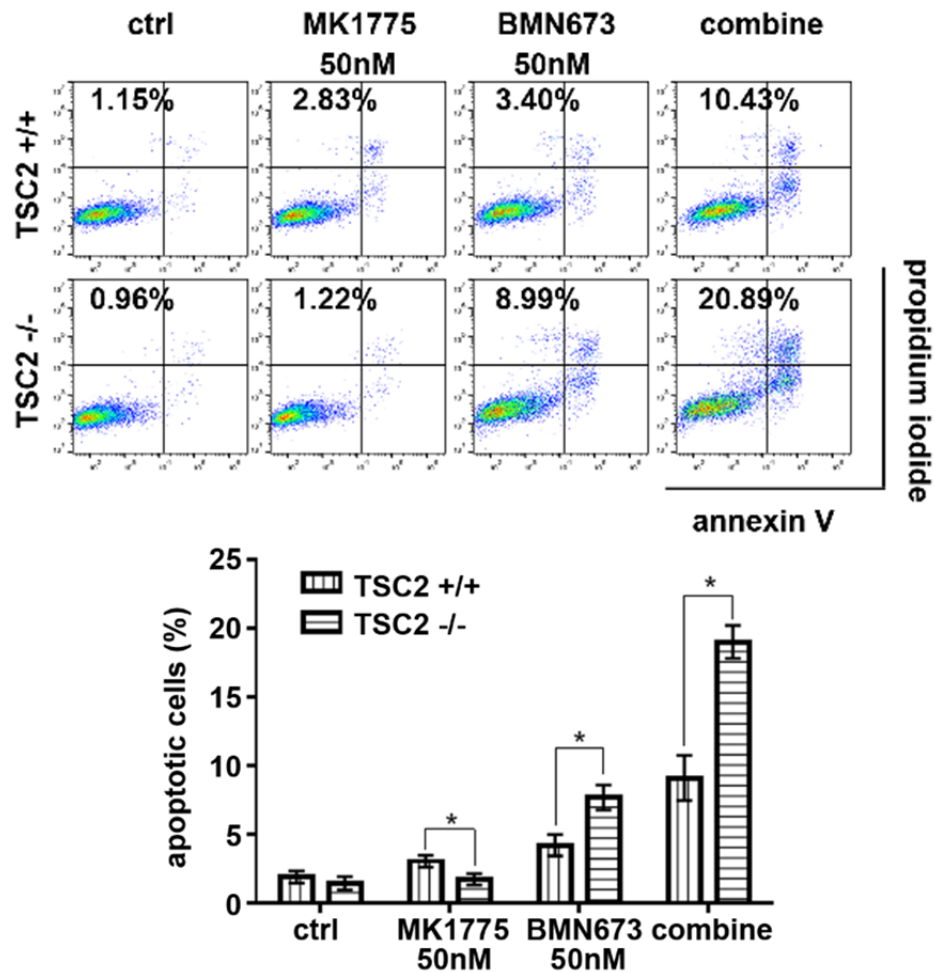


Figure 43 TSC2-null cells were more sensitive to the WEE1 inhibitor combined with the PARP inhibitor BMN 673-apoptosis assay

MEFs were incubated with 50nM MK1775 or/and 50nM BMN 673 for 48 hours and stained with annexin V and PI. Apoptotic cells were defined as annexin V positive cells. TSC2 ^{+/+}: *Tsc2*^{+/+}, *Tsc2* wild-type; TSC2 ^{-/-}: *Tsc2*^{-/-}, *Tsc2* null; error bars represent mean \pm SD; n = 3 independent experiments; * p<0.05

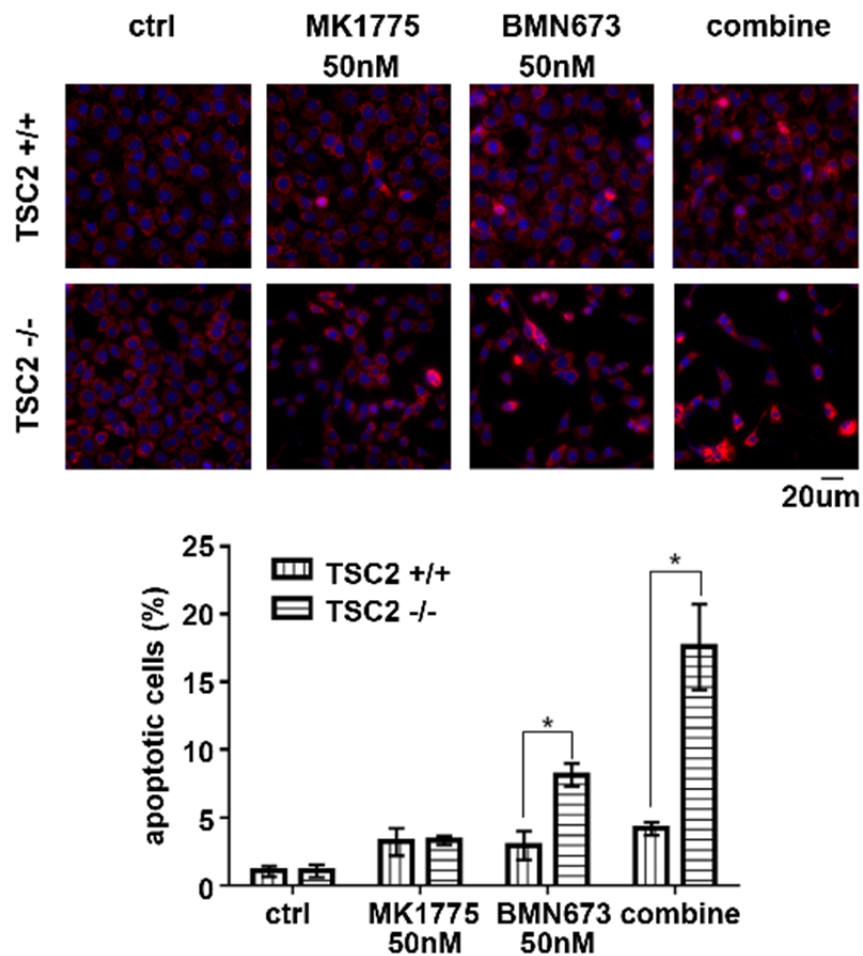


Figure 44 TSC2-null cells were more sensitive to the WEE1 inhibitor combined with the PARP inhibitor BMN 673-Cytochrome c staining

MEFs were incubated with 50nM MK1775 or/and 50nM BMN 673 for 48 hours and stained with Cytochrome c. The percentages of apoptotic cells were calculated based on the positive staining of Cytochrome c and nucleus morphology. TSC2^{+/+}: *Tsc2*^{+/+}, *Tsc2* wild-type; TSC2^{-/-}: *Tsc2*^{-/-}, *Tsc2* null; error bars represent mean \pm SD; n = 3 independent experiments; * p<0.05

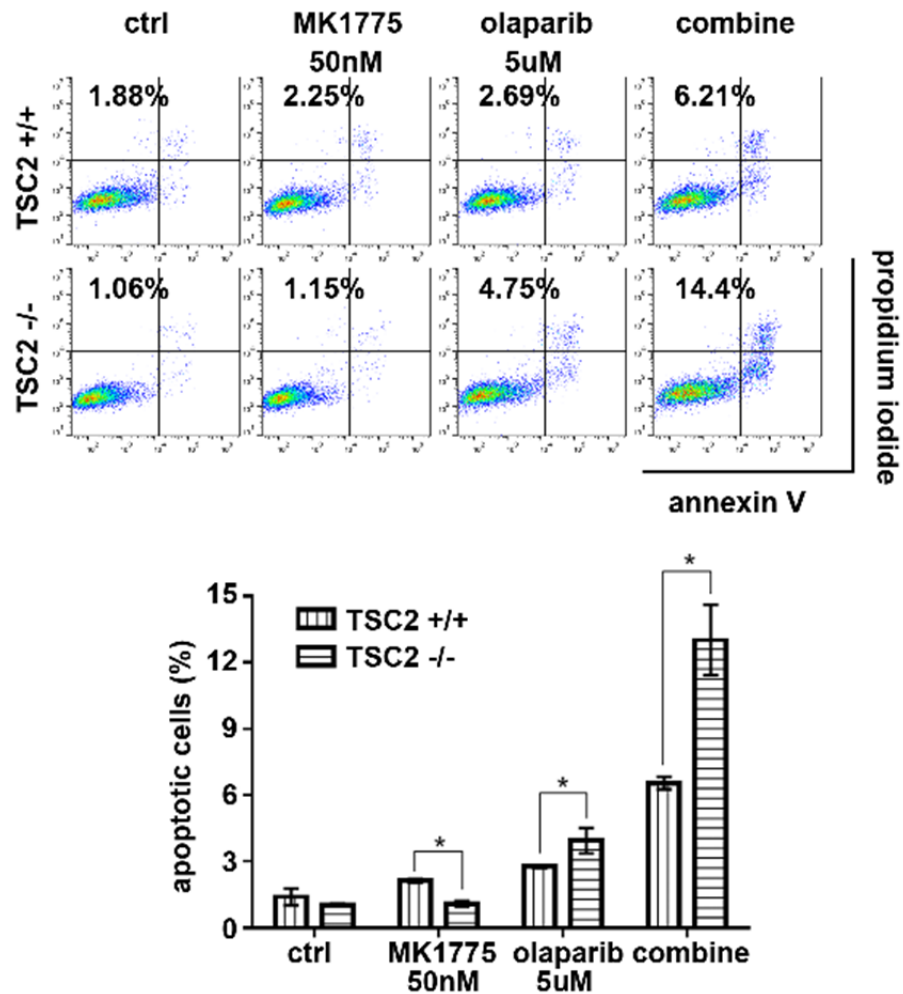


Figure 45 TSC2-null cells were more sensitive to the WEE1 inhibitor combined with the PARP inhibitor olaparib-apoptosis assay

MEFs were incubated with 50nM MK1775 or/and 5uM olaparib for 48 hours for apoptosis assay. TSC2 ^{+/+}: *Tsc2*^{+/+}, *Tsc2* wild-type; TSC2 ^{-/-}: *Tsc2*^{-/-}, *Tsc2* null; error bars represent mean ± SD; n = 3 independent experiments; * p<0.05

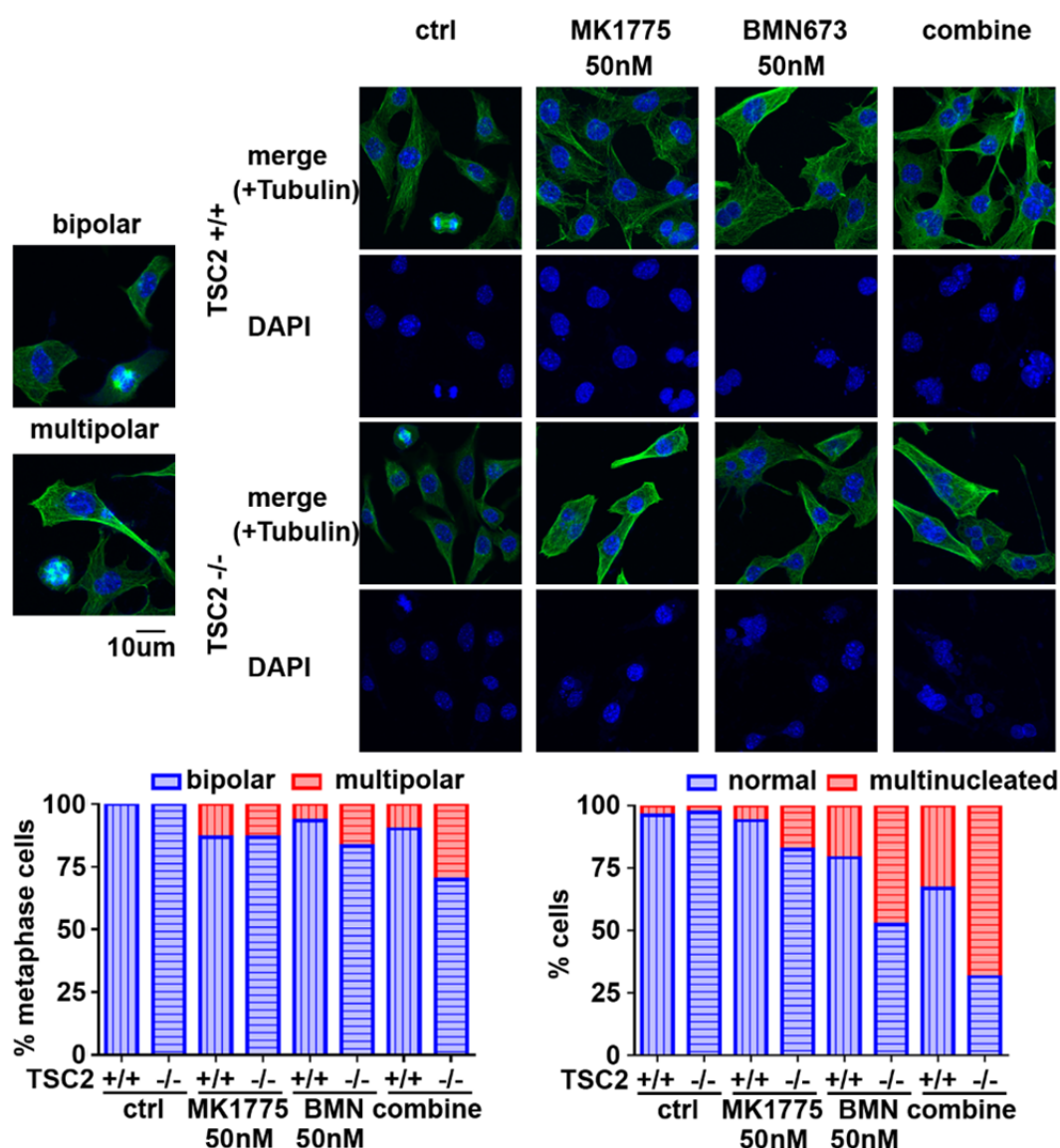


Figure 46 The WEE1 inhibitor MK1775 combined with the PARP inhibitor BMN 673 induced stronger mitotic catastrophe in TSC2-null cells

MEFs were treated with 50nM MK1775 and 50nM BMN 673 for 48 hours and were stained with α -Tubulin and DAPI. The numbers of centrosomes and nuclei in one cell were calculated. The bar graphs showed the percentage of bipolar/multipolar cells and the percentage of normal/multinucleated cells in each group. TSC2 +/+ : *Tsc2*^{+/+}, *Tsc2* wild-type; TSC2 -/- : *Tsc2*^{-/-}, *Tsc2* null; error bars represent mean \pm SD; n = 3 independent experiments; * p<0.05

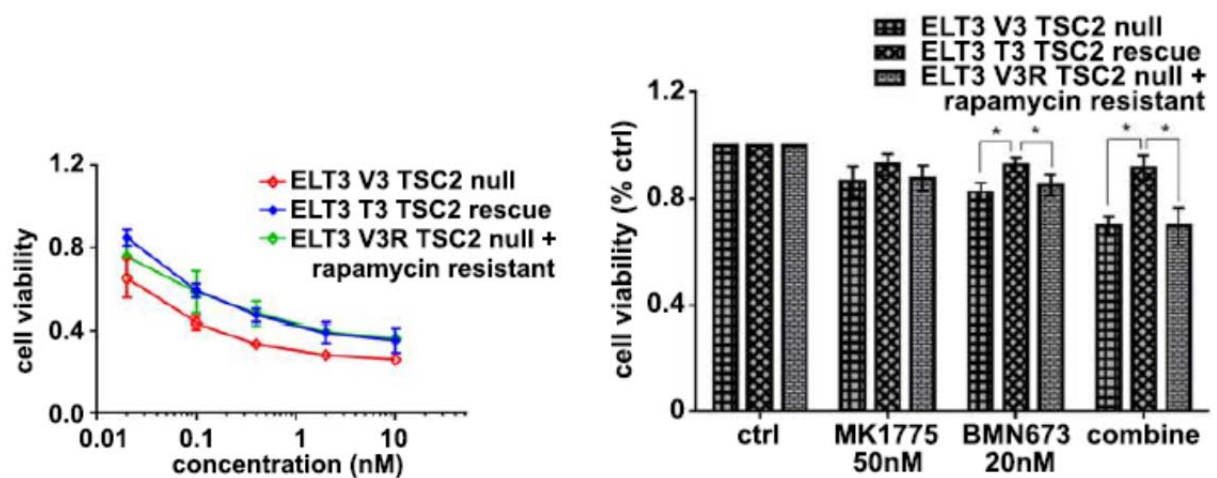


Figure 47 The combination effect was relatively similar in rapamycin-sensitive and rapamycin-resistant TSC2-null cells

We treated rat ELT3 V3 (*Tsc2* null, rapamycin sensitive), ELT3 T3 (re-expressing *Tsc2*), and ELT3 V3R (*Tsc2* null but rapamycin resistant) cells with 50nM MK1775 or 20nM BMN673 for 4 days. Cell viability was measured by MTT assay and was defined as the ratio to the untreated group in each cell line. Error bars represent mean \pm SD; $n = 3$ independent experiments; * $p < 0.05$

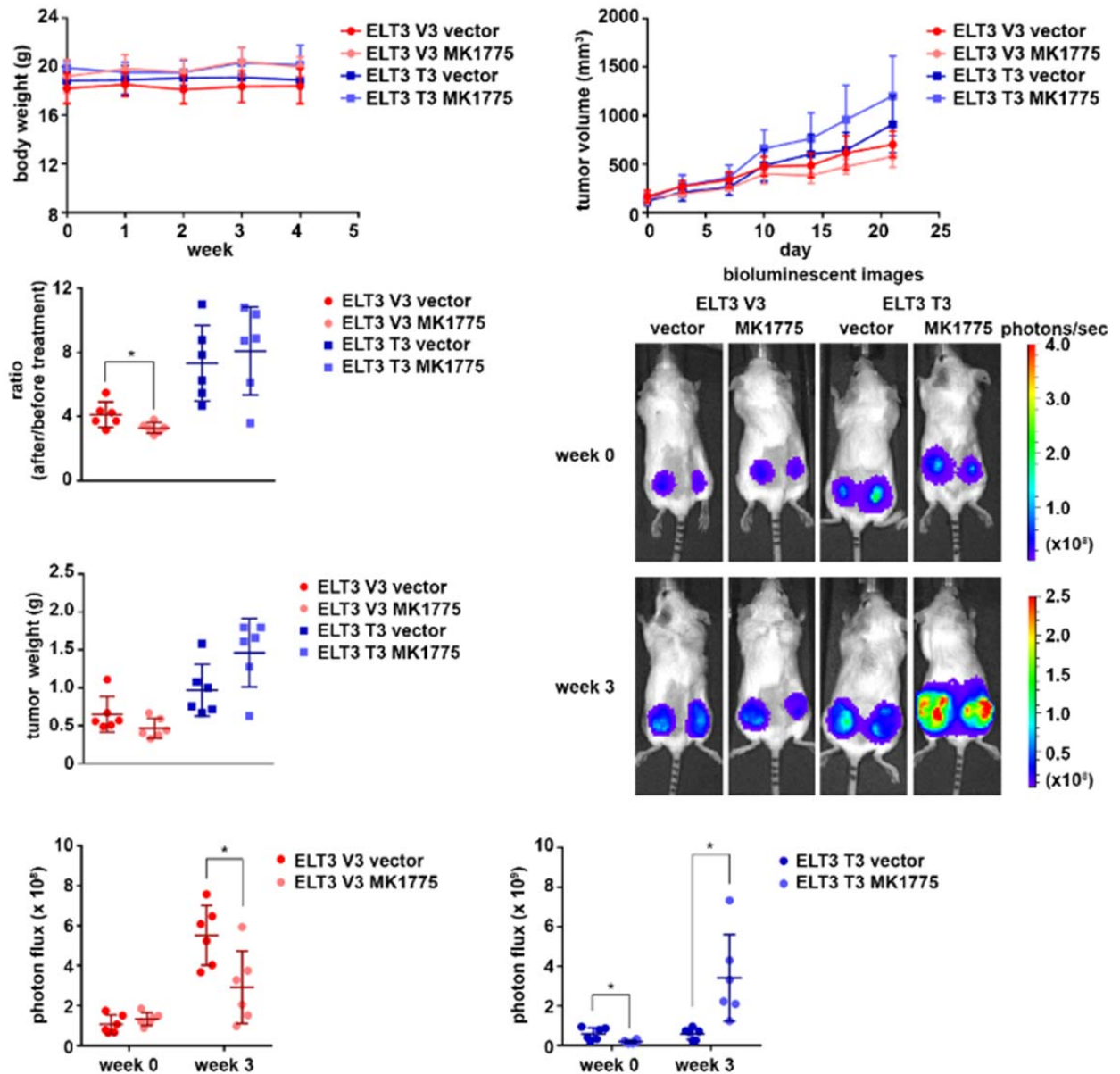


Figure 48 TSC2-null tumors were more sensitive to the WEE1 inhibitor *in vivo*

ELT3-V3/T3-luciferase cells were injected into mice. Five weeks later, mice were treated with the vehicle or 60mg/kg MK1775 once every two days for three weeks. Body weights, tumor volumes using the formula $(\text{length} \times \text{width}^2)/2$, tumor weights, and bioluminescence levels were monitored regularly. ELT3 V3: *Tsc2* null; ELT3 T3: ELT3 V3 re-expressing *Tsc2*; error bars represent mean \pm SD; n=6; * p<0.05

CHAPTER 4

Discussion, Conclusions and Perspectives

We have utilized a multidisciplinary approach to identify potential molecules that regulate checkpoint recovery from irradiation (Fig. 6). It includes a high-throughput protein array, systemic protein network analysis and an appropriate mathematical model. The reverse phase protein array (RPPA) provides a set of total protein and posttranslationally modified protein expression data in a time series across different types of cells (80). The problem is that existing RPPA data processing platforms provide limited systematic tools to identify novel molecule pathways after quantification and normalization. For example, MIRACLE is a biologist-friendly web interface but it does not provide network analysis (81). RPPApipe, which is also a web-based pipeline, only focuses on existing pathway analysis (82). In order to identify new upstream targets which may not change their expression dramatically but control the dynamics of the checkpoint recovery network in our RPPA data, we first screened possible candidates through the linear regression model written in R (Fig. 8) and generated an IPA causal network containing all of our candidates (Fig. 10). Although IPA also provides algorithms to identify upstream regulatory molecules, the downstream molecules are usually not specific (83). Here we try to identify important regulators which specifically control cell-cycle related proteins, including Cyclin B1 and Cyclin D1. The process is similar to the way we solve maximum flow problems in mathematics. It involves finding a maximum flow (signaling cascade) through a flow network (signaling

network) with a source (upstream molecule) and a sink (downstream molecule). The method we chose is the Ford-Fulkerson algorithm, which repeatedly finds augmenting paths in the network and improves the total amount of flow until the flow reaches the maximum (Fig. 7-10. Detail explanations are in MATLAB files). The advantage of the algorithm is that the sink (downstream molecule) can be either specific or non-specific. Based on our needs, we applied the algorithm and identified that mTOR has the maximum signaling cascade to both Cyclin B1 and Cyclin D1 (Fig. 10).

mTOR regulates cell growth and cell division in response to growth factors, energy status, nutrients, and stress, and mTORC1 is the main complex that couples the environment cues, especially the abundance of amino acids, to G1 cell cycle progression (21, 31). The G2 phase is also a period related to cell growth and protein synthesis. Usually it is relatively short compared to the G1 phase because cells in the G2 phase only synthesize basic needs for mitosis and for cell survival after mitosis. In fission yeast, it has been studied that the activities of Cell division cycle 25 (Cdc25) and Wee1 are correlated with cell size and nutrition status in the control of the Cyclin-dependent kinase 1 (Cdk1)-cyclin B complex at G2/M transition (84-86). It is not surprising that we have confirmed our RPPA data and showed that mTORC1, the nutrient sensor, regulated G2/M checkpoint recovery through the control of Cyclin B1 and PLK1 expression (Fig. 11-19).

Activation of the CDK1-Cyclin B1 complex triggers mitosis and it is regulated by the CDK1 activity and the Cyclin B1 level in the nucleus. CDK1 is activated through its phosphorylation by CDC25 and is inhibited through its phosphorylation by WEE1/MYT1 (47). PLK1 controls both CDC25 and WEE1 and functions as a positive regulator of CDK1. The level of Cyclin B1 is regulated by protein ubiquitination and the transcription

activity. Cyclin B1 expression gradually reaches the peak when cells enter mitosis and drops in the end of mitosis (87-88). In response to IR-induced DNA damage, ATM/ATR signaling pathways inhibit CDK1 activity mainly through *PLK1* gene transcription repression and CDC25 degradation (44). DNA damage pathways also arrest cells in the G2 phase through the decrease of *CCNB1* (encoding Cyclin B1) mRNA level and the decrease of nuclear Cyclin B1 (34). Once damage is repaired, cell cycle progresses again. PLK1 and Cyclin B1 level should increase as well. In our studies, mTOR depletion did not affect checkpoint activation, but checkpoint recovery. Recovery of *PLK1* and *CCNB1* transcription through mTORC1 regulation was observed in mitotic reentry after irradiation, and the dynamics matched the increase of mitotic populations (Fig. 20-23).

mTOR also regulated expression of KDM4B, a histone demethylase selectively demethylates H3K9me2/me3 to H3K9me1/me2 (Fig. 24-30). KDM4B (JMJD2B) belongs to the Jumonji C domain (JMJD) family, which is comprised of at least thirty members based on the presence of the JmjC (Jumonji C) domain and demethylates tri- (me3), di- (me2) and mono- (me1) methylated histone H3 lysine 4 (H3K4), H3K9, H3K27, H3K36 or H4K20 through a dioxygenase reaction mechanism requiring Fe^{2+} , O_2 and 2-oxoglutarate (α -ketoglutarate, a Krebs' cycle intermediate) (89). The location of histone lysine methylation determines the binding specificity of JMJD demethylases. Histone lysine methylation at different sites of the gene also affect gene transcription activity (90). Thus, epigenetic control by histone lysine demethylase is a sophisticated process and is usually cell type specific. KDM4B is only over-expressed in some types of cancers, such as gastric, colorectal, lung, and bladder cancers, and the expression level is correlated with the tumor size and the clinical stage. In gastric cancer, KDM4B

depletion induces apoptosis with increased levels of p53 and p21. In colorectal cancer, depletion of KDM4B causes DNA damage, cell cycle arrest and apoptosis. KDM4B also promotes G1/S transition and cell growth in lung cancer (91). The increased level of KDM4B in DNA damage contributes to radioresistance in certain types of cells, and the involvement of KDM4B in DNA damage appears evolutionary conserved (92). Therefore, KDM4B at least shows its importance in specific types of cancer and it is related to DNA damage response. Previous studies have shown that the stability of KDM4 family regulated by E3 ubiquitin ligases involves in key cellular process including transcription, DNA damage response, and cell cycle progression (93-96). Here, mTOR controlled transcription activities of *CCNB1* and *PLK1* during checkpoint recovery through the increased association of KDM4B, decreased association of H3K9me3 and increased association of the transcription factor B-myb with *CCNB1* gene during checkpoint recovery (Fig. 29). KDM4B expression regulated by mTOR was probably through ubiquitin-dependent proteasomal degradation (Fig. 30) and more detail mechanisms need to be done.

Another interesting point between KDM4B and mTOR is the energy status. The function of the histone demethylase JMJD family, including KDM4B, requires 2-oxoglutarate (α -ketoglutarate) (90). α -ketoglutarate is the intermediate in the Krebs cycle, a series of oxidation-reduction reactions in mitochondria to eventually generate ATP. The abundance of ATP controls mTORC1 activity and promote cell growth. That is probably the reason that both KDM4B and mTOR are related to G1/S transition. Since cells also synthesize proteins in the G2 phase, especially after DNA damage, the energy status may affect G2/M checkpoint recovery through mTORC1 and KDM4B.

In some of our results, mTOR seemed to control G2/M transition without any stimulants but the effects were not as dramatic as effects when we treated cells with irradiation. The limit is that we couldn't exactly tell the phenomenon was due to late G1 cell cycle arrest in amino acids deprivation and mTORC1 inhibition (97), or it was due to the function of mTOR directly in mitotic entry in physiological conditions. In cell cycle analysis (data not shown), G1 arrest in mTOR-depleted cells was not as obvious as in rapamycin-treated cells, but both conditions cause delayed mitotic entry during recovery from irradiation and paclitaxel treatment. Cells treated with only paclitaxel had relatively similar mitotic populations in control and mTOR-depleted cells, which indicated that G1 arrest was not the main cause of delayed checkpoint recovery in mTOR-depleted cells (Fig.11-14). KDM4B depletion itself did not cause the change of basal cell cycle profile (data not shown), but affect mitotic entry after irradiation and paclitaxel, which demonstrated the function of KDM4B in G2/M transition (Fig. 27). These evidences strongly suggested that mTOR had its role at least in G2/M checkpoint recovery after irradiation.

The severity of DNA damage and the activities of ATM/ATR signaling pathways also control the G2/M checkpoint following irradiation (34, 98). Although it has been known that mTOR inhibitors suppress homologous recombination (99), we did not observe significant increase of DNA damage after IR in mTOR-depleted cells (Fig. 31). It might be due to less sensitivity of comet assay, relatively low dosage of IR or the existence of other repair mechanisms. Depletion of mTOR did not affect activation of ATM/ATR pathways and the G2/M checkpoint, and depletion of ATM did not show the changes of KDM4B, PLK1 and Cyclin B1. These evidences suggested that mTOR depletion controlled checkpoint recovery instead of causing checkpoint adaptation, and

also indicated that the function of mTOR in checkpoint recovery was ATM/ATR independent (Fig. 32-33).

Tuberous sclerosis complex (TSC) is a rare genetic disease. Mutations in either *TSC1* or *TSC2* are found in 85% of TSC patients, and the majority of patients have *TSC2* mutations (100). Patients with TSC usually have benign tumors during childhood in many parts of bodies, including brain, kidney, and lung. More than 80% of TSC patients have central nervous system complications, such as seizures, mental retardation, and autism. Renal tumors cause the most lethal complications for TSC patients. Around 80% of TSC patients develop bilateral renal angiomyolipoma, hamartoma or cysts, leading to end-stage renal failure, massive bleeding or infection. Few *TSC2* patients, especially women, develop chronic obstructive pulmonary disease due to pulmonary lymphangiomyomatosis (78). The treatment for TSC patients is either surgery or symptomatic treatment. Inhibition of mTOR activity by rapalogs is one of few strategies to control tumor growth in TSC patients. Everolimus has been approved by FDA for only two indications. One indication is that adult TSC patients with renal angiomyolipoma who are at risk of complications but do not require surgery. The other indication is that any patients with subependymal giant cell astrocytomas who require treatment but are unable to do surgery. However, rapalogs may cause severe adverse reactions, such as the increased infection risk. It is a need to develop new treatment for TSC patients (78, 100).

As previous description, WEE1 phosphorylates CDK1 and inhibits G2/M transition. Inhibition of WEE1 by MK1775 (AZD1775) abrogates G2/M arrest resulting in premature mitotic entry and mitotic catastrophe (55-56). Currently many studies combine MK1775 with radiation therapy or different DNA damaging drugs, such as

cisplatin and carboplatin, for cancer treatment. The effect is more pronounced in p53-deficient cancers which have the G1 checkpoint defect and strongly depend on the G2 checkpoint to prevent cell cycle progression before damages are repaired (101-103). In TSC2-depleted cells, the persistent high mTORC1 activity promotes G1/S transition and may also facilitate G2/M checkpoint recovery after irradiation even under nutrient and energy deprivation, the common condition in cancer (104). Thus, TSC2-depleted tumors with faster G2/M checkpoint recovery are candidates for MK1775 treatment (Fig. 34-37). In our study, TSC2-depleted cells were more sensitive to MK1775 *in vitro*. TSC2-depleted cells showed faster cell cycle progression and persistent DNA damage after MK1775 treatment (Fig. 38-41). We combined MK1775 with the PARP inhibitor (BMN673 or olaparib) which cause DNA damage, and the combination treatment worked better compared to any single agent in TSC2-depleted cells. Although mitotic catastrophe is the mechanism how cells maintain genome integrity, all DNA damage and cell cycle-related reagents still have risks of developing cancer. We proposed that MK1775 combined with PARP inhibitors were applied as the second-line treatment for TSC patients, and so we generated rapamycin-resistant TSC2-depleted cells to test the drug effects. In rapamycin-resistant TSC2-depleted cells, the sensitivity to combination treatment was similar to parental TSC2-depleted cells, but the mechanisms could be even more complicated (Fig. 42-47). We further tested drug combination in the mouse model. Only MK1775 alone and BMN 673 alone (105) showed the therapeutic effect in mice with TSC2-depleted tumors (Fig. 48, data only showed the MK1775 part). The possible reason could be the way we combined these two drugs. We treated mice with the PARP inhibitor and the WEE1 inhibitor simultaneously. Because TSC2-depleted cells have relatively intact DNA repair machineries compared to other cancer cells, the

way we apply drug combination probably should be the PARP inhibitor followed by the WEE1 inhibitor. The PARP inhibitor is given first to accumulate sufficient DNA damage, and then the WEE1 inhibitor releases the G2/M checkpoint to cause mitotic catastrophe. Furthermore, the timing, the dosage, and the treatment course should also be tested, since tuberous sclerosis complex forms benign tumors instead of cancers. Therefore, more animal experiments may need to be done.

In conclusion, we have combined several disciplines to identify a novel mechanism of mTOR signaling in regulating a transcriptional program required for G2/M checkpoint recovery after DNA damage. It is one step forward to link environmental cues outside the cell, signaling cascades in the cytoplasm, and genome integrity in the nucleus together. This mechanism also provides a new therapeutic approach for TSC patients using the WEE1 inhibitor, which has potential to be translated into clinical trials (Fig. 49).

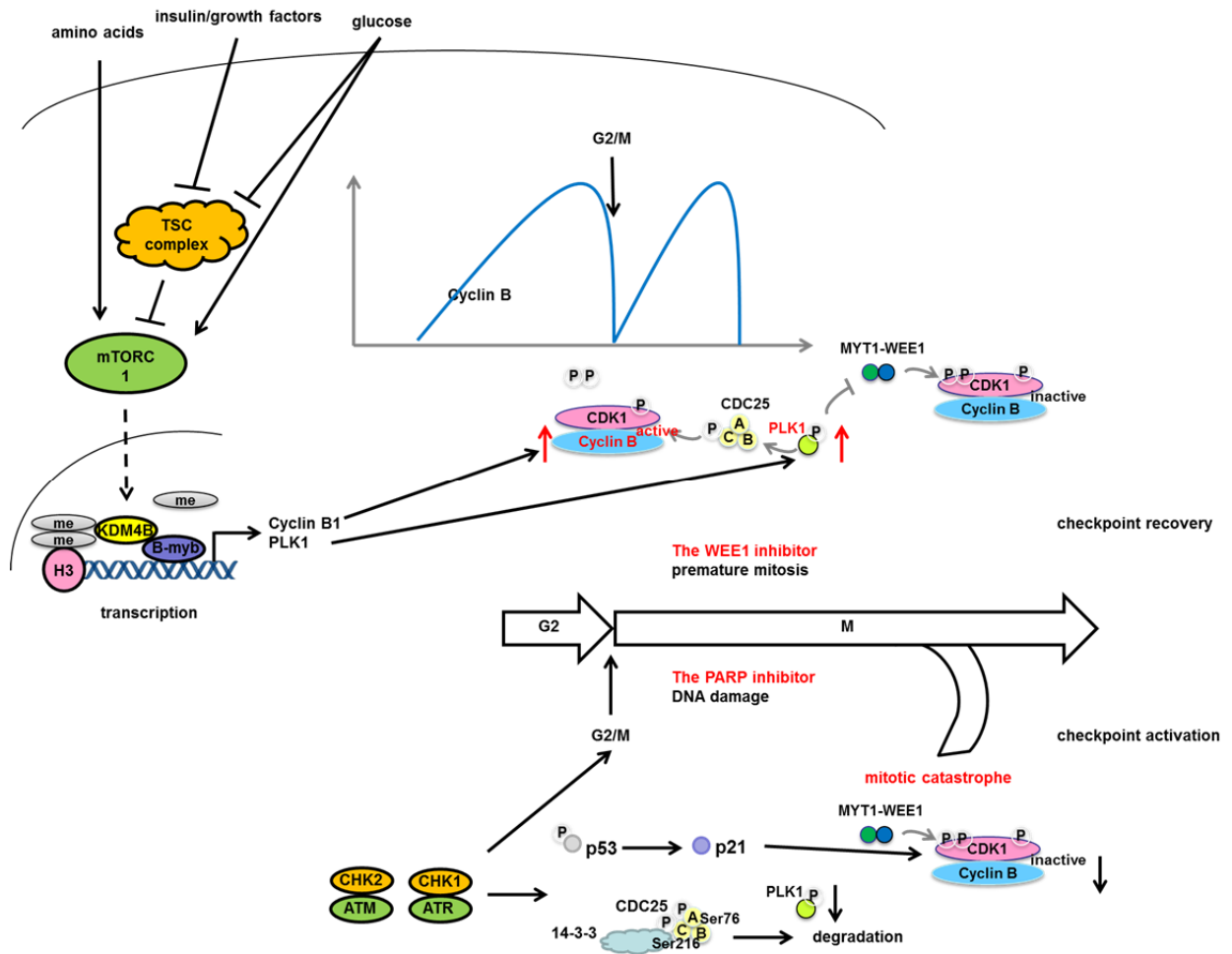


Figure 49 The summary of the study

BIBLIOGRAPHY

1. Laplante M, Sabatini DM. 2009. mTOR signaling at a glance. *J Cell Sci* 122: 3589-94
2. Sabatini DM. 2006. mTOR and cancer: insights into a complex relationship. *Nat Rev Cancer* 6: 729-34
3. Hiom K. 2005. DNA repair: how to PIKK a partner. *Curr Biol* 15: R473-5
4. Lovejoy CA, Cortez D. 2009. Common mechanisms of PIKK regulation. *DNA Repair (Amst)* 8: 1004-8
5. Jewell JL, Guan KL. 2013. Nutrient signaling to mTOR and cell growth. *Trends Biochem Sci* 38: 233-42
6. Weber AM, Ryan AJ. 2015. ATM and ATR as therapeutic targets in cancer. *Pharmacol Ther* 149: 124-38
7. Kakumoto K, Ikeda J, Okada M, Morii E, Oneyama C. 2015. mLST8 Promotes mTOR-Mediated Tumor Progression. *PLoS One* 10: e0119015
8. Gao D, Inuzuka H, Tan MK, Fukushima H, Locasale JW, Liu P, Wan L, Zhai B, Chin YR, Shaik S, Lyssiotis CA, Gygi SP, Toker A, Cantley LC, Asara JM, Harper JW, Wei W. 2011. mTOR drives its own activation via SCF(betaTrCP)-dependent degradation of the mTOR inhibitor DEPTOR. *Mol Cell* 44: 290-303
9. Wiza C, Nascimento EB, Ouwers DM. 2012. Role of PRAS40 in Akt and mTOR signaling in health and disease. *Am J Physiol Endocrinol Metab* 302: E1453-60
10. Ekim B, Magnuson B, Acosta-Jaquez HA, Keller JA, Feener EP, Fingar DC. 2011. mTOR kinase domain phosphorylation promotes mTORC1 signaling, cell growth, and cell cycle progression. *Mol Cell Biol* 31: 2787-801
11. Yip CK, Murata K, Walz T, Sabatini DM, Kang SA. 2010. Structure of the human mTOR complex I and its implications for rapamycin inhibition. *Mol Cell* 38: 768-74
12. De P, Miskimins K, Dey N, Leyland-Jones B. 2013. Promise of rapalogues versus mTOR kinase inhibitors in subset specific breast cancer: old targets new hope. *Cancer Treat Rev* 39: 403-12
13. Dibble CC, Asara JM, Manning BD. 2009. Characterization of Rictor phosphorylation sites reveals direct regulation of mTOR complex 2 by S6K1. *Mol Cell Biol* 29: 5657-70
14. Pignochino Y, Dell'Aglio C, Basirico M, Capozzi F, Soster M, Marchio S, Bruno S, Gammaitoni L, Sangiolo D, Torchiario E, D'Ambrosio L, Fagioli F, Ferrari S, Alberghini M, Picci P, Aglietta M, Grignani G. 2013. The Combination of Sorafenib and Everolimus Abrogates mTORC1 and mTORC2 upregulation in osteosarcoma preclinical models. *Clin Cancer Res* 19: 2117-31
15. Dibble CC, Elis W, Menon S, Qin W, Klekota J, Asara JM, Finan PM, Kwiatkowski DJ, Murphy LO, Manning BD. 2012. TBC1D7 is a third subunit of the TSC1-TSC2 complex upstream of mTORC1. *Mol Cell* 47: 535-46
16. Zhou X, Clister TL, Lowry PR, Seldin MM, Wong GW, Zhang J. 2015. Dynamic Visualization of mTORC1 Activity in Living Cells. *Cell Rep*
17. Zoncu R, Efeyan A, Sabatini DM. 2011. mTOR: from growth signal integration to cancer, diabetes and ageing. *Nat Rev Mol Cell Biol* 12: 21-35
18. Sancak Y, Bar-Peled L, Zoncu R, Markhard AL, Nada S, Sabatini DM. 2010. Ragulator-Rag complex targets mTORC1 to the lysosomal surface and is necessary for its activation by amino acids. *Cell* 141: 290-303

19. Lim CY, Zoncu R. 2016. The lysosome as a command-and-control center for cellular metabolism. *J Cell Biol* 214: 653-64
20. Menon S, Dibble CC, Talbott G, Hoxhaj G, Valvezan AJ, Takahashi H, Cantley LC, Manning BD. 2014. Spatial control of the TSC complex integrates insulin and nutrient regulation of mTORC1 at the lysosome. *Cell* 156: 771-85
21. Jewell JL, Russell RC, Guan KL. 2013. Amino acid signalling upstream of mTOR. *Nat Rev Mol Cell Biol* 14: 133-9
22. Chaveroux C, Eichner LJ, Dufour CR, Shatnawi A, Khoutorsky A, Bourque G, Sonenberg N, Giguere V. 2013. Molecular and genetic crosstalks between mTOR and ERalpha are key determinants of rapamycin-induced nonalcoholic fatty liver. *Cell Metab* 17: 586-98
23. Avalos Y, Canales J, Bravo-Sagua R, Criollo A, Lavandero S, Quest AF. 2014. Tumor suppression and promotion by autophagy. *Biomed Res Int* 2014: 603980
24. Magnuson B, Ekim B, Fingar DC. 2012. Regulation and function of ribosomal protein S6 kinase (S6K) within mTOR signalling networks. *Biochem J* 441: 1-21
25. Rozengurt E, Soares HP, Sinnett-Smith J. 2014. Suppression of feedback loops mediated by PI3K/mTOR induces multiple overactivation of compensatory pathways: an unintended consequence leading to drug resistance. *Mol Cancer Ther* 13: 2477-88
26. Shaw RJ, Cantley LC. 2006. Ras, PI(3)K and mTOR signalling controls tumour cell growth. *Nature* 441: 424-30
27. Oshiro N, Yoshino K, Hidayat S, Tokunaga C, Hara K, Eguchi S, Avruch J, Yonezawa K. 2004. Dissociation of raptor from mTOR is a mechanism of rapamycin-induced inhibition of mTOR function. *Genes Cells* 9: 359-66
28. Vemulapalli S, Mita A, Alvarado Y, Sankhala K, Mita M. 2011. The emerging role of mammalian target of rapamycin inhibitors in the treatment of sarcomas. *Target Oncol* 6: 29-39
29. Yao JC, Pavel M, Lombard-Bohas C, Van Cutsem E, Voi M, Brandt U, He W, Chen D, Capdevila J, de Vries EG, Tomassetti P, Hobday T, Pommier R, Oberg K. 2016. Everolimus for the Treatment of Advanced Pancreatic Neuroendocrine Tumors: Overall Survival and Circulating Biomarkers From the Randomized, Phase III RADIANT-3 Study. *J Clin Oncol*
30. Zheng Y, Jiang Y. 2015. mTOR Inhibitors at a Glance. *Mol Cell Pharmacol* 7: 15-20
31. Foster DA, Yellen P, Xu L, Saqcena M. 2010. Regulation of G1 Cell Cycle Progression: Distinguishing the Restriction Point from a Nutrient-Sensing Cell Growth Checkpoint(s). *Genes Cancer* 1: 1124-31
32. Averous J, Fonseca BD, Proud CG. 2008. Regulation of cyclin D1 expression by mTORC1 signaling requires eukaryotic initiation factor 4E-binding protein 1. *Oncogene* 27: 1106-13
33. Aarts M, Sharpe R, Garcia-Murillas I, Gevensleben H, Hurd MS, Shumway SD, Toniatti C, Ashworth A, Turner NC. 2012. Forced mitotic entry of S-phase cells as a therapeutic strategy induced by inhibition of WEE1. *Cancer Discov* 2: 524-39
34. Iliakis G, Wang Y, Guan J, Wang H. 2003. DNA damage checkpoint control in cells exposed to ionizing radiation. *Oncogene* 22: 5834-47
35. Lens SM, Voest EE, Medema RH. 2010. Shared and separate functions of polo-like kinases and aurora kinases in cancer. *Nat Rev Cancer* 10: 825-41
36. Martin Y, Dominguez-Kelly R, Freire R. 2011. Novel insights into maintaining genomic integrity: Wee1 regulating Mus81/Eme1. *Cell Div* 6: 21
37. Musacchio A, Salmon ED. 2007. The spindle-assembly checkpoint in space and time. *Nat Rev Mol Cell Biol* 8: 379-93
38. Leung-Pineda V, Ryan CE, Piwnicka-Worms H. 2006. Phosphorylation of Chk1 by ATR is antagonized by a Chk1-regulated protein phosphatase 2A circuit. *Mol Cell Biol* 26: 7529-38
39. Abbas T, Dutta A. 2009. p21 in cancer: intricate networks and multiple activities. *Nat Rev Cancer* 9: 400-14

40. Karimian A, Ahmadi Y, Yousefi B. 2016. Multiple functions of p21 in cell cycle, apoptosis and transcriptional regulation after DNA damage. *DNA Repair (Amst)* 42: 63-71
41. Nghiem P, Park PK, Kim Y, Vaziri C, Schreiber SL. 2001. ATR inhibition selectively sensitizes G1 checkpoint-deficient cells to lethal premature chromatin condensation. *Proc Natl Acad Sci U S A* 98: 9092-7
42. Sorensen CS, Syljuasen RG. 2012. Safeguarding genome integrity: the checkpoint kinases ATR, CHK1 and WEE1 restrain CDK activity during normal DNA replication. *Nucleic Acids Res* 40: 477-86
43. Lopez-Contreras AJ, Fernandez-Capetillo O. 2010. The ATR barrier to replication-born DNA damage. *DNA Repair (Amst)* 9: 1249-55
44. Ree AH, Bratland A, Nome RV, Stokke T, Fodstad O. 2003. Repression of mRNA for the PLK cell cycle gene after DNA damage requires BRCA1. *Oncogene* 22: 8952-5
45. Zuazua-Villar P, Rodriguez R, Gagou ME, Eysers PA, Meuth M. 2014. DNA replication stress in CHK1-depleted tumour cells triggers premature (S-phase) mitosis through inappropriate activation of Aurora kinase B. *Cell Death Dis* 5: e1253
46. Dobbstein M, Sorensen CS. 2015. Exploiting replicative stress to treat cancer. *Nat Rev Drug Discov* 14: 405-23
47. Hsieh HJ, Peng G. 2017. Cellular responses to replication stress: Implications in cancer biology and therapy. *DNA Repair (Amst)* 49: 9-20
48. Marechal A, Zou L. 2013. DNA damage sensing by the ATM and ATR kinases. *Cold Spring Harb Perspect Biol* 5
49. Katsuno Y, Suzuki A, Sugimura K, Okumura K, Zineldeen DH, Shimada M, Niida H, Mizuno T, Hanaoka F, Nakanishi M. 2009. Cyclin A-Cdk1 regulates the origin firing program in mammalian cells. *Proc Natl Acad Sci U S A* 106: 3184-9
50. Bartek J, Lukas J. 2007. DNA damage checkpoints: from initiation to recovery or adaptation. *Curr Opin Cell Biol* 19: 238-45
51. Medema RH, Macurek L. 2011. Checkpoint recovery in cells: how a molecular understanding can help in the fight against cancer. *F1000 Biol Rep* 3: 10
52. van Vugt MA, Gardino AK, Linding R, Ostheimer GJ, Reinhardt HC, Ong SE, Tan CS, Miao H, Keezer SM, Li J, Pawson T, Lewis TA, Carr SA, Smerdon SJ, Brummelkamp TR, Yaffe MB. 2010. A mitotic phosphorylation feedback network connects Cdk1, Plk1, 53BP1, and Chk2 to inactivate the G(2)/M DNA damage checkpoint. *PLoS Biol* 8: e1000287
53. Wang H, Zhang X, Teng L, Legerski RJ. 2015. DNA damage checkpoint recovery and cancer development. *Experimental Cell Research* 334: 350-8
54. Syljuasen RG, Jensen S, Bartek J, Lukas J. 2006. Adaptation to the ionizing radiation-induced G2 checkpoint occurs in human cells and depends on checkpoint kinase 1 and Polo-like kinase 1 kinases. *Cancer Res* 66: 10253-7
55. Vakifahmetoglu H, Olsson M, Zhivotovsky B. 2008. Death through a tragedy: mitotic catastrophe. *Cell Death Differ* 15: 1153-62
56. Vitale I, Galluzzi L, Castedo M, Kroemer G. 2011. Mitotic catastrophe: a mechanism for avoiding genomic instability. *Nat Rev Mol Cell Biol* 12: 385-92
57. Vakifahmetoglu H, Olsson M, Tamm C, Heidari N, Orrenius S, Zhivotovsky B. 2008. DNA damage induces two distinct modes of cell death in ovarian carcinomas. *Cell Death Differ* 15: 555-66
58. Bekier ME, Fischbach R, Lee J, Taylor WR. 2009. Length of mitotic arrest induced by microtubule-stabilizing drugs determines cell death after mitotic exit. *Mol Cancer Ther* 8: 1646-54
59. Elmore S. 2007. Apoptosis: a review of programmed cell death. *Toxicol Pathol* 35: 495-516
60. Vandenabeele P, Galluzzi L, Vanden Berghe T, Kroemer G. 2010. Molecular mechanisms of necroptosis: an ordered cellular explosion. *Nat Rev Mol Cell Biol* 11: 700-14

61. Shah RB, Thompson R, Sidi S. 2016. A mitosis-sensing caspase activation platform? New insights into the PIDDosome. *Mol Cell Oncol* 3: e1059921
62. Kim M, Murphy K, Liu F, Parker SE, Dowling ML, Baff W, Kao GD. 2005. Caspase-mediated specific cleavage of BubR1 is a determinant of mitotic progression. *Mol Cell Biol* 25: 9232-48
63. Parrish AB, Freel CD, Kornbluth S. 2013. Cellular mechanisms controlling caspase activation and function. *Cold Spring Harb Perspect Biol* 5
64. Blagosklonny MV. 2007. Mitotic arrest and cell fate: why and how mitotic inhibition of transcription drives mutually exclusive events. *Cell Cycle* 6: 70-4
65. Livraghi L, Garber JE. 2015. PARP inhibitors in the management of breast cancer: current data and future prospects. *BMC Med* 13: 188
66. Bunting SF, Callen E, Wong N, Chen HT, Polato F, Gunn A, Bothmer A, Feldhahn N, Fernandez-Capetillo O, Cao L, Xu X, Deng CX, Finkel T, Nussenzweig M, Stark JM, Nussenzweig A. 2010. 53BP1 inhibits homologous recombination in Brca1-deficient cells by blocking resection of DNA breaks. *Cell* 141: 243-54
67. Shen Y, Rehman FL, Feng Y, Boshuizen J, Bajrami I, Elliott R, Wang B, Lord CJ, Post LE, Ashworth A. 2013. BMN 673, a novel and highly potent PARP1/2 inhibitor for the treatment of human cancers with DNA repair deficiency. *Clin Cancer Res* 19: 5003-15
68. Murai J, Huang SY, Renaud A, Zhang Y, Ji J, Takeda S, Morris J, Teicher B, Doroshow JH, Pommier Y. 2014. Stereospecific PARP trapping by BMN 673 and comparison with olaparib and rucaparib. *Mol Cancer Ther* 13: 433-43
69. Murai J, Huang SY, Das BB, Renaud A, Zhang Y, Doroshow JH, Ji J, Takeda S, Pommier Y. 2012. Trapping of PARP1 and PARP2 by Clinical PARP Inhibitors. *Cancer Res* 72: 5588-99
70. Sarbassov DD, Guertin DA, Ali SM, Sabatini DM. 2005. Phosphorylation and regulation of Akt/PKB by the rictor-mTOR complex. *Science* 307: 1098-101
71. Azar R, Alard A, Susini C, Bousquet C, Pyronnet S. 2009. 4E-BP1 is a target of Smad4 essential for TGFbeta-mediated inhibition of cell proliferation. *EMBO J* 28: 3514-22
72. Fujimura K, Sasaki AT, Anderson P. 2012. Selenite targets eIF4E-binding protein-1 to inhibit translation initiation and induce the assembly of non-canonical stress granules. *Nucleic Acids Res* 40: 8099-110
73. Ip CK, Cheung AN, Ngan HY, Wong AS. 2011. p70 S6 kinase in the control of actin cytoskeleton dynamics and directed migration of ovarian cancer cells. *Oncogene* 30: 2420-32
74. Li C, Lee PS, Sun Y, Gu X, Zhang E, Guo Y, Wu CL, Auricchio N, Priolo C, Li J, Csibi A, Parkhitko A, Morrison T, Planaguma A, Kazani S, Israel E, Xu KF, Henske EP, Blenis J, Levy BD, Kwiatkowski D, Yu JJ. 2014. Estradiol and mTORC2 cooperate to enhance prostaglandin biosynthesis and tumorigenesis in TSC2-deficient LAM cells. *J Exp Med* 211: 15-28
75. Guertin AD, Li J, Liu Y, Hurd MS, Schuller AG, Long B, Hirsch HA, Feldman I, Benita Y, Toniatti C, Zawel L, Fawell SE, Gilliland DG, Shumway SD. 2013. Preclinical evaluation of the WEE1 inhibitor MK-1775 as single-agent anticancer therapy. *Mol Cancer Ther* 12: 1442-52
76. Huang YJ, Frazier ML, Zhang N, Liu Q, Wei C. 2014. Reverse-phase protein array analysis to identify biomarker proteins in human pancreatic cancer. *Dig Dis Sci* 59: 968-75
77. Duan L, Rai G, Roggero C, Zhang QJ, Wei Q, Ma SH, Zhou Y, Santoyo J, Martinez ED, Xiao G, Raj GV, Jadhav A, Simeonov A, Maloney DJ, Rizo J, Hsieh JT, Liu ZP. 2015. KDM4/JMJD2 Histone Demethylase Inhibitors Block Prostate Tumor Growth by Suppressing the Expression of AR and BMYB-Regulated Genes. *Chem Biol* 22: 1185-96
78. Inoki K, Guan KL. 2009. Tuberous sclerosis complex, implication from a rare genetic disease to common cancer treatment. *Hum Mol Genet* 18: R94-100
79. Do K, Doroshow JH, Kummar S. 2013. Wee1 kinase as a target for cancer therapy. *Cell Cycle* 12: 3159-64
80. Creighton CJ, Huang S. 2015. Reverse phase protein arrays in signaling pathways: a data integration perspective. *Drug Des Devel Ther* 9: 3519-27

81. List M, Block I, Pedersen ML, Christiansen H, Schmidt S, Thomassen M, Tan Q, Baumbach J, Mollenhauer J. 2014. Microarray R-based analysis of complex lysate experiments with MIRACLE. *Bioinformatics* 30: i631-8
82. Eichner J, Heubach Y, Ruff M, Kohlhof H, Strobl S, Mayer B, Pawlak M, Templin MF, Zell A. 2014. RPPApipe: a pipeline for the analysis of reverse-phase protein array data. *Biosystems* 122: 19-24
83. Kramer A, Green J, Pollard J, Jr., Tugendreich S. 2014. Causal analysis approaches in Ingenuity Pathway Analysis. *Bioinformatics* 30: 523-30
84. Barnum KJ, O'Connell MJ. 2014. Cell cycle regulation by checkpoints. *Methods Mol Biol* 1170: 29-40
85. Turner JJ, Ewald JC, Skotheim JM. 2012. Cell size control in yeast. *Curr Biol* 22: R350-9
86. Wood E, Nurse P. 2015. Sizing up to divide: mitotic cell-size control in fission yeast. *Annu Rev Cell Dev Biol* 31: 11-29
87. Krause K, Wasner M, Reinhard W, Haugwitz U, Dohna CL, Mossner J, Engeland K. 2000. The tumour suppressor protein p53 can repress transcription of cyclin B. *Nucleic Acids Res* 28: 4410-8
88. Lindqvist A, Rodriguez-Bravo V, Medema RH. 2009. The decision to enter mitosis: feedback and redundancy in the mitotic entry network. *J Cell Biol* 185: 193-202
89. Shi YG, Tsukada Y. 2013. The discovery of histone demethylases. *Cold Spring Harb Perspect Biol* 5
90. Berry WL, Janknecht R. 2013. KDM4/JMJD2 histone demethylases: epigenetic regulators in cancer cells. *Cancer Res* 73: 2936-42
91. Toyokawa G, Cho HS, Iwai Y, Yoshimatsu M, Takawa M, Hayami S, Maejima K, Shimizu N, Tanaka H, Tsunoda T, Field HI, Kelly JD, Neal DE, Ponder BA, Maehara Y, Nakamura Y, Hamamoto R. 2011. The histone demethylase JMJD2B plays an essential role in human carcinogenesis through positive regulation of cyclin-dependent kinase 6. *Cancer Prev Res (Phila)* 4: 2051-61
92. Soini Y, Kosma VM, Pirinen R. 2015. KDM4A, KDM4B and KDM4C in non-small cell lung cancer. *Int J Clin Exp Pathol* 8: 12922-8
93. Ipenberg I, Guttmann-Raviv N, Khoury HP, Kupershmit I, Ayoub N. 2013. Heat shock protein 90 (Hsp90) selectively regulates the stability of KDM4B/JMJD2B histone demethylase. *J Biol Chem* 288: 14681-7
94. Young LC, McDonald DW, Hendzel MJ. 2013. Kdm4b histone demethylase is a DNA damage response protein and confers a survival advantage following gamma-irradiation. *J Biol Chem* 288: 21376-88
95. Mallette FA, Mattioli F, Cui G, Young LC, Hendzel MJ, Mer G, Sixma TK, Richard S. 2012. RNF8- and RNF168-dependent degradation of KDM4A/JMJD2A triggers 53BP1 recruitment to DNA damage sites. *EMBO J* 31: 1865-78
96. Tan MK, Lim HJ, Harper JW. 2011. SCF(FBXO22) regulates histone H3 lysine 9 and 36 methylation levels by targeting histone demethylase KDM4A for ubiquitin-mediated proteasomal degradation. *Mol Cell Biol* 31: 3687-99
97. Saqcena M, Menon D, Patel D, Mukhopadhyay S, Chow V, Foster DA. 2013. Amino acids and mTOR mediate distinct metabolic checkpoints in mammalian G1 cell cycle. *PLoS One* 8: e74157
98. Xu B, Kim ST, Lim DS, Kastan MB. 2002. Two molecularly distinct G(2)/M checkpoints are induced by ionizing irradiation. *Mol Cell Biol* 22: 1049-59
99. Mo W, Liu Q, Lin CC, Dai H, Peng Y, Liang Y, Peng G, Meric-Bernstam F, Mills GB, Li K, Lin SY. 2016. mTOR Inhibitors Suppress Homologous Recombination Repair and Synergize with PARP Inhibitors via Regulating SUV39H1 in BRCA-Proficient Triple-Negative Breast Cancer. *Clin Cancer Res* 22: 1699-712

100. Switon K, Kotulska K, Janusz-Kaminska A, Zmorzynska J, Jaworski J. 2016. Tuberous sclerosis complex: From molecular biology to novel therapeutic approaches. *IUBMB Life* 68: 955-62
101. Bridges KA, Hirai H, Buser CA, Brooks C, Liu H, Buchholz TA, Molkentine JM, Mason KA, Meyn RE. 2011. MK-1775, a novel Wee1 kinase inhibitor, radiosensitizes p53-defective human tumor cells. *Clin Cancer Res* 17: 5638-48
102. Moser R, Xu C, Kao M, Annis J, Lerma LA, Schaupp CM, Gurley KE, Jang IS, Biktasova A, Yarbrough WG, Margolin AA, Grandori C, Kemp CJ, Mendez E. 2014. Functional kinomics identifies candidate therapeutic targets in head and neck cancer. *Clin Cancer Res* 20: 4274-88
103. Mueller S, Haas-Kogan DA. 2015. WEE1 Kinase As a Target for Cancer Therapy. *J Clin Oncol* 33: 3485-7
104. Soucek T, Pusch O, Wienecke R, DeClue JE, Hengstschlager M. 1997. Role of the tuberous sclerosis gene-2 product in cell cycle control. Loss of the tuberous sclerosis gene-2 induces quiescent cells to enter S phase. *J Biol Chem* 272: 29301-8
105. Sun Y, Gallacchi D, Zhang EY, Reynolds SB, Robinson L, Malinowska IA, Chiou TT, Pereira AM, Li C, Kwiatkowski DJ, Lee PS, Yu JJ. 2014. Rapamycin-resistant poly (ADP-ribose) polymerase-1 overexpression is a potential therapeutic target in lymphangioleiomyomatosis. *Am J Respir Cell Mol Biol* 51: 738-49

VITA

Hui-Ju Hsieh was born in Kaohsiung City, Taiwan on April 19, 1981, the daughter of Shen-Chie Hsieh and Shuie-Chuan Chen. After completing her work at Kaohsiung Girls' Senior High School, Kaohsiung, Taiwan in 1999, she entered Kaohsiung Medical University in Kaohsiung, Taiwan. She received the Doctor of Medicine with a major in medicine from Kaohsiung Medical School in September, 2006. For the next four years, she worked as a clinical residency in the Department of Internal Medicine at Kaohsiung Medical University Hospital and as a research assistant in the Department of Anatomy at Kaohsiung Medical University. In August 2010 she entered The University of Texas MD Anderson Cancer Center UTHealth Graduate School of Biomedical Sciences.

Permanent address:

35, Lin-De Street, 5F-2

Kaohsiung City, 802, Taiwan